

1. Report No. SWUTC/05/167245-1		2. Government Accession No.		3. Recipient's Catalog No.	
4. Title and Subtitle Evaluation of the Joint Effect of Wheel Load and Tire Pressure on Pavement Performance			5. Report Date January 2005		
			6. Performing Organization Code		
7. Author(s) Rong Luo and Jorge A. Prozzi			8. Performing Organization Report No. Report 167245-1		
9. Performing Organization Name and Address Center for Transportation Research University of Texas at Austin 3208 Red River, Suite 200 Austin, Texas 78705-2650			10. Work Unit No. (TRAIS)		
			11. Contract or Grant No. 10727		
12. Sponsoring Agency Name and Address Southwest Region University Transportation Center Texas Transportation Institute Texas A&M University System College Station, Texas 77843-3135			13. Type of Report and Period Covered		
			14. Sponsoring Agency Code		
15. Supplementary Notes Supported by general revenues from the State of Texas.					
16. Abstract Most pavement design and analysis procedures predict performance based on the expected damage of the pavement structure under the traffic loads expected during the entire design life. Some failure criteria are primarily dependent on wheel loads and almost independent of contact stresses. Other failure criteria, however, are primarily dependent on normal and shear stresses, not on the load magnitude. The effect of contact stresses is currently indirectly accounted by using wheel load as a proxy for tire pressure. In most pavement design methods, the tire-pavement contact stress is assumed to be equal to the tire inflation pressure and uniformly distributed over a circular area. A methodology that explicitly accounts for the effect of tire inflation pressure and the corresponding contact stresses on pavement response and performance is currently lacking. This research evaluates the pavement responses of typical pavement structures under the combined actions of variable wheel loads and tire pressure. A multi-layer linear-elastic computer program, CIRCLY, was used to estimate the pavement responses under uniform constant stress and actual contact stress distributions. Three critical pavement responses were evaluated, including longitudinal and transverse tensile strains and compressive strains on the top of the subgrade. The differences of the strains estimated by the two models were statistically analyzed to quantify the effect of the assumption of uniform stress over a circular shape in most traditional pavement design approaches. The traditional model proved to be reliable for estimating the compressive strains on the top of the subgrade. The tensile strains at the bottom of the asphalt layer under actual contact stress, however, are quite different from those under uniform constant stress. Contrary to initial expectation, for the cases evaluated in this research, the assumption of uniform stresses is a conservative approach.					
17. Key Words Mechanistic-Empirical Design, Wheel Load, Tire Pressure, Pavement Response, Performance			18. Distribution Statement No restrictions. This document is available to the public through NTIS: National Technical Information Service 5285 Port Royal Road Springfield, Virginia 22161		
19. Security Classif.(of this report) Unclassified		20. Security Classif.(of this page) Unclassified		21. No. of Pages 188	22. Price

**Evaluation of the Joint Effect of Wheel Load and Tire Pressure
on Pavement Performance**

By
Rong Luo
and
Jorge A. Prozzi

Research Report SWUTC/05/167245-1

Southwest Region University Transportation Center
Center for Transportation Research
University of Texas at Austin
Austin, Texas 78712

January 2005

DISCLAIMER

The contents of this report reflect the views of the authors, who are responsible for the facts and the accuracy of the information presented herein. This document is disseminated under the sponsorship of the Department of Transportation, University Transportation Centers Program, in the interest of information exchange. Mention of trade names or commercial products does not constitute endorsement or recommendation for use.

ABSTRACT

Most pavement design and analysis procedures predict performance based on the expected damage of the pavement structure under the traffic loads expected during the entire design life. Some failure criteria are primarily dependent on wheel loads and almost independent of contact stresses. Other failure criteria, however, are primarily dependent on normal and shear stresses, not on the load magnitude. The effect of contact stresses is currently indirectly accounted by using wheel load as a proxy for tire pressure. In most pavement design methods, the tire-pavement contact stress is assumed to be equal to the tire inflation pressure and uniformly distributed over a circular area. A methodology that explicitly accounts for the effect of tire inflation pressure and the corresponding contact stresses on pavement response and performance is currently lacking. This research evaluates the pavement responses of typical pavement structures under the combined actions of variable wheel loads and tire pressure. A multi-layer linear-elastic computer program, CIRCLY, was used to estimate the pavement responses under uniform constant stress and actual contact stress distributions. Three critical pavement responses were evaluated, including longitudinal and transverse tensile strains and compressive strains on the top of the subgrade. The differences of the strains estimated by the two models were statistically analyzed to quantify the effect of the assumption of uniform stress over a circular shape in most traditional pavement design approaches. The traditional model was proved to be reliable for estimating the compressive strains on the top of the subgrade. The tensile strains at the bottom of the asphalt layer under actual contact stress, however, are quite different from those under uniform constant stress. Contrary to initial expectation, for the cases evaluated in this research, the assumption of uniform stresses is a conservative approach.

ACKNOWLEDGEMENTS

The authors recognize that support for this research was provided by a grant from the U.S. Department of Transportation, University Transportation Centers Program to the Southwest Region University Transportation Center which is funded 50 percent with general revenue funds from the State of Texas.

EXECUTIVE SUMMARY

Introduction

Most pavement design and analysis procedures predict performance based on the expected damage of the pavement structure under the traffic loads expected during the entire design life. Two approaches are used to account for highway traffic loads. The first approach consists of converting all expected traffic axle configurations and wheel loads into the number of Equivalent Single Axle Loads (ESALs). Most recent methodologies use the expected axle load spectra (frequency distribution of axle loads) to estimate performance, thus avoiding the conversion of traffic into ESALs and eliminating the uncertainty that is introduced by doing so. No current method considers tire pressure spectra.

The most comprehensive mechanistic-empirical design and analysis tool developed to-date is the National Cooperative Highway Research Program (NCHRP) Project 1-37A, "Development of the 2002 Guide for the Design of New and Rehabilitated Pavement Structures: Phase II." The advantages of the new guide are the use of multiple failure criteria and the consideration of axle load spectra. However, the effect of traffic on pavement performance is estimated based on the effect of wheel loads alone without accounting for the effect of tire inflation pressure or contact stress. Only one value of average tire pressure is used in the analysis.

Some failure criteria, such as bottom-up fatigue cracking, are primarily dependent on wheel loads and almost independent of contact stresses. Other failure criteria, such as asphalt rutting, are primarily dependent on vertical and horizontal contact stresses, almost independent of load magnitude. Although rutting is governed by the intensity of normal and shear stresses, not by load levels, axle load is the variable currently used to estimate rutting performance. Recent evidence suggests that the same applies to failure due to top-down fatigue cracking.

Currently, the effect of contact stresses is indirectly accounted for by using wheel load as a proxy for tire pressure. Although a positive correlation between wheel load and tire pressure exists, this correlation does not properly account for the effect of contact stress distribution. Thus, a

methodology that explicitly accounts for the effect of tire inflation pressure and the corresponding contact stresses on pavement response and performance is desirable.

Background

Empirical data has traditionally been used in pavement design to determine and predict the relationship between pavement design variables and response and performance. It has been determined that the relationships between pavement loading, response (in terms of stress and strain), and the influence of the environment on material properties are complex. Although pavement loading (3-dimensional) state of stress transferred from a vehicle tire to the pavement surface) has been recently quantified more accurately and finite element analysis has been applied to quantify pavement response as a result of loading and changing material properties, simplifying assumptions are still made in practice when pavements are designed. Some of these assumptions include:

1. the tire-pavement contact area has a circular shape,
2. contact stress is uniformly distributed, and
3. the contact stress is equivalent to the tire inflation pressure

As a result, the contact area is assumed to be the ratio of wheel load to tire inflation pressure.

The quantification of pavement loading and response is not as accurate as it could be and not yet clearly understood. Loading characteristics and material properties are influenced by numerous factors (many of which are difficult to quantify) and are consequently not accurately defined. In addition, there is a large inherent variability in these variables due to the effects of time and the environment.

However, as loading and pavement response are quantified more accurately, the relationships including the quantification of material characteristics are becoming more complex and often perceived as less cost effective to apply in practice. Relatively small accuracy improvements are attained as a result of significant cost increases, especially in terms of testing and computational time.

Research Tasks and Report Outline

Ideally, the numerous variables need to be quantified and relationships defined to such an extent that a clear understanding of these factors and their relationship can lead to simplified design procedures that can be cost effectively applied in practice. This research considers the use of simple models to assess these complex relationships and to quantify the differences created as a result of the simplifications adopted. The first task of this research, a literature review, was conducted to:

1. search for existing measurements of actual tire pavement contact stress distributions,
2. critically evaluate the measurements in terms of accuracy, usefulness, and limitations, and
3. identify the need for further research.

Chapter 2 provides a summary of the literature review.

With the data gathered during the literature review, pavement modeling and response analyses were performed by means of a multi-layer linear-elastic computer program (CIRCLY), which is briefly introduced in Chapter 3. CIRCLY was used to model pavement structure and estimate pavement response as a result of a circular uniform tire pavement contact stress distribution, and an approximation of the best actual measured tire pavement stress distribution. Based on the simulation results, pavement responses were calculated in terms of critical stresses, strains and displacements. The experimental design, pavement modeling and response estimations are detailed in Chapter 3.

Chapter 4 discusses the difference between pavement strains calculated by the models discussed in Chapter 3. The pavement strains studied in this research are tensile strains in the x -direction at the bottom of the asphalt layer, tensile strains in the y -direction at the bottom of the asphalt layer, and compressive strains on the top of the subgrade. Two types of difference, including absolute difference and relative difference, are computed and analyzed by statistical regression to study the effect of load, pavement structure and tire inflation pressure on the strain difference. Regression results and mathematical analysis are presented.

Chapter 5, Conclusions and Recommendations, includes the motivation, experimental design, statistical analysis and final results.

Major Findings and Recommendations

Most of the traditional pavement design methods assume that tire-pavement contact stresses are uniformly distributed on a circular area. Actual measurements, however, showed that the contact stresses are not uniform and the contact area is not a circular shape. To study the actual pavement response and evaluate the adequacy of a traditional pavement design model, the experiment-measured actual tire-pavement contact stresses are employed to calculate the pavement responses by the computer program CIRCLY. The traditional model with uniform contact stress over a circular shape was also used to compute the pavement responses at pavement interfaces. Pavement strains calculated by these two models were compared and the differences between them were analyzed.

Four pavement structures, three tire inflation pressure levels and three wheel loads comprised a factorial experiment to quantify the effect of the three parameters on the strain difference between the two modes. The four pavement structures selected had the same base, subbase, subgrade, and asphalt material. The only difference among them was the thickness of the asphalt layer, which varied from 40–130 mm, respectively, for each pavement structure. Tire inflation pressure levels were 586 kPa, 690 kPa, and 793 kPa, and the target wheel loading levels were 24 kN, 27.5 kN, and 31.1 kN.

The new model, which used the actual measured contact stresses, divided the contact area into a number of small circles, each with a radius of 8.5mm, and was regarded as a load component with an assigned value of contact stress. Each circular load produced pavement responses. Pavement strains produced by each load were superimposed to obtain the total strains at specific locations studied. The pavement responses considered are the tensile strains at the bottom of the asphalt layer, which is related to pavement fatigue cracking, and the compressive strains on the top of the subgrade, which controls pavement rutting. Three types of pavement strains were studied in this research, including compressive strains on the top of the subgrade, and tensile strains at the bottom of the asphalt layer in the x -direction and in the y -direction.

Both absolute difference and relative difference were studied between the two models by statistical regression analysis. Most of the strains calculated by the traditional model were greater than those computed by the new model, which indicated an over-estimation of pavement strains. The difference was significant — up to 23 percent. Wheel loading exhibited the most important effect on both absolute and relative difference of tensile strains in the x -direction. When the effect of wheel load was relatively low, the traditional model overestimated the tensile strains in the x -direction. As the wheel load increased, the difference between the two models decreased gradually to zero, and the strains calculated by the traditional model became less than those computed by the new model. Results indicated the traditional model's underestimation of the tensile strains in the x -direction at the bottom of the asphalt layer. A combination of high load, low tire pressure and thin asphalt layer may lead to the underestimation by the traditional model on the tensile strains in the x -direction. Asphalt thickness and tire inflation pressure do not significantly affect both strain differences.

The traditional model overestimated the tensile strain difference in the y -direction in all the combinations studied. Variations of the relative differences were within a small range with a mean of 13.03 percent and a standard deviation of 3.8. The three parameters did not show a strong relationship with both absolute and relative strain differences.

For the compressive strains on the top of the subgrade, both absolute difference and relative difference were small and varied slightly with the change of asphalt thickness, wheel load and tire pressure. As a result, the traditional model could be considered adequate and reliable in calculating the compressive strains on the top of the subgrade, and therefore properly predicted pavement rutting.

Since pavement fatigue cracking is regarded to be determined by the tensile strains at the bottom of the asphalt layer, and pavement rutting is controlled by the compressive strains on the top of the subgrade, estimating pavement performance in terms of critical responses is an interesting area for further research. Based on the strain difference of the two models stated in this paper, the traditional pavement transfer functions may be adjusted for more accurate prediction on

pavement performance. The effect of the variables on pavement behavior may be quantified to assist with the process of pavement design and analysis. Guidelines and recommendations can be advanced to specifically address the differences between expected performance under uniform stress assumption and performance under actual tire-pavement contact stress distribution.

In summary, the findings of this research suggest that there are significant differences in critical pavement response when the uniform and actual contact stress distributions are compared. However, if wheel load and tire inflation pressure are known, this difference can be accounted for by means of relatively simple models as those developed in this research.

TABLE OF CONTENTS

CHAPTER 1. INTRODUCTION	1
1.1 Problem Statement.....	1
1.2 Background.....	2
1.3 Research Tasks and Report Outline.....	3
CHAPTER 2. LITERATURE REVIEW	5
2.1 Traditional Assumptions on Tire-Pavement Contact Characteristics.....	5
2.2 Studies on the Actual Characteristics of Tire-Pavement Contact Pressure.....	8
2.3 Effect of Tire Parameters on Pavement Responses.....	19
2.4 Current Truck Characteristics in Texas.....	27
2.5 Conclusions of Literature Review.....	28
2.6 Inspiration from Literature Review.....	29
CHAPTER 3. EXPERIMENTAL DESIGN ON PAVEMENT MODELING AND ESTIMATION OF PAVEMENT RESPONSE	31
3.1 A Brief Description of CIRCLY.....	31
3.2 Tire-Pavement Contact Stress Modeling.....	33
3.3 Pavement Responses Evaluated in the Two Models.....	40
CHAPTER 4. COMPARISON OF PAVEMENT STRAINS ESTIMATED BY DIFFERENT MODELS	45
4.1 Absolute Strain Difference between Two Models.....	45
4.2 Relative Strain Difference between Two Models.....	50
CHAPTER 5. CONCLUSIONS AND RECOMMENDATIONS	57
REFERENCES	61
APPENDIX 1. Strain Comparison in LTEX007 (L=23.5 kN, P=586 kPa)	65
APPENDIX 2. Strain Comparison in LTEX008 (L=24.3 kN, P=690 kPa)	77
APPENDIX 3. Strain Comparison in LTEX009 (L=23.2 kN, P=793 kPa)	89
APPENDIX 4. Strain Comparison in LTEX012 (L=28.4 kN, P=586 kPa)	101
APPENDIX 5. Strain Comparison in LTEX013 (L=26.3 kN, P=690 kPa)	113
APPENDIX 6. Strain Comparison in LTEX014 (L=28.3 kN, P=793 kPa)	125
APPENDIX 7. Strain Comparison in LTEX017 (L=30.4 kN, P=586 kPa)	137

APPENDIX 8. Strain Comparison in LTEX018 (L=31.8 kN, P=690 kPa)	149
APPENDIX 9. Strain Comparison in LTEX019 (L=31.1 kN, P=793 kPa)	161

LIST OF ILLUSTRATIONS

Figures

Figure 1.	Relationship between Contact Pressure and Tire Pressure	6
Figure 2.	Illustration of Boussinesq Equation	7
Figure 3.	Experimental Design of Tire-Pavement Contact Pressure Testing	9
Figure 4.	3-Dimensional Plots of Pressure Distribution	10
Figure 5.	Device Used to Measure Tire Contact Pressure Distribution in Japan	14
Figure 6.	Layout of the Vehicle-Road Surface Pressure Transducer Array (VRSPTA) System (System: SIM MK II) in South Africa	16
Figure 7.	Alternative Load Types Provided by CIRCLY	32
Figure 8.	Test Tire: Goodyear 11R24.5 G G159A	33
Figure 9.	Model of Actual Measured Contact Stresses (LTEX013) in CIRCLY	35
Figure 10.	Layout in a Line of Spaced Points in CIRCLY	36
Figure 11.	Pavement Horizontal Locations Studied in CIRCLY	37
Figure 12.	Traditional Model for LTEX013 in CIRCLY	39

Tables

Table 1.	Filename of the Nine Combinations Studied	33
Table 2.	Pavement Structures Analyzed in CIRCLY	34
Table 3.	Comparison of Tensile Strains in the x -Direction at the Bottom of the Asphalt Layer (ϵ_{txx}) in the Two Models	42
Table 4.	Comparison of Tensile Strains in the y -Direction at the Bottom of the Asphalt Layer (ϵ_{tyy}) in the Two Models	43
Table 5.	Comparison of Compressive Strains at the Top of the Subgrade (ϵ_{czz}) in the Two Models	44
Table 6.	Absolute Difference of Tensile Strains in the x -Direction at the Bottom of the Asphalt Layer (ϵ_{txx}) between the Two Models	46

Table 7.	Absolute Difference of Tensile Strains in the y -Direction at the Bottom of the Asphalt Layer (ϵ_{yy}) between the Two Models.....	47
Table 8.	Regression Statistics of Model on the Absolute Difference of Tensile Strains in x -Direction at the Bottom of the Asphalt Layer.....	48
Table 9.	Regression Statistics of Model on the Absolute Difference of Tensile Strains in y -Direction at the Bottom of the Asphalt Layer.....	48
Table 10.	Absolute Difference of Compressive Strains at the Top of the Subgrade (ϵ_{czz}) between the Two Models.....	49
Table 11.	Regression Statistics of Model on the Absolute Difference of Compressive Strains.....	50
Table 12.	Relative Difference of Tensile Strains in the x -Direction at the Bottom of the Asphalt Layer (ϵ_{txx}) between the Two Models.....	51
Table 13.	Relative Difference of Tensile Strains in the y -Direction at the Bottom of the Asphalt Layer (ϵ_{tyy}) between the Two Models.....	52
Table 14.	Regression Statistics of Model on the Relative Difference of Tensile Strains in x -Direction at the Bottom of the Asphalt Layer.....	54
Table 15.	Regression Statistics of Model on the Relative Difference of Tensile Strains in y -Direction at the Bottom of the Asphalt Layer.....	54
Table 16.	Relative Difference of Compressive Strains at the Top of the Subgrade (ϵ_{czz}) between the Two Models.....	55
Table 17.	Regression Statistics of the Model on the Relative Difference of Compressive Strains.....	55

Chapter 1. Introduction

1.1 Problem Statement

Most pavement design and analysis procedures predict performance based on the expected damage of the pavement structure under the traffic loads expected during the entire design life. Two approaches are used to account for highway traffic loads. The first approach consists of converting all expected traffic axle configurations and wheel loads into the number of Equivalent Single Axle Loads (ESALs). Most recent methodologies use the expected axle load spectra (frequency distribution of axle loads) to estimate performance, thus avoiding the conversion of traffic into ESALs and eliminating the uncertainty that is introduced by doing so. No current method considers tire pressure spectra.

The most comprehensive mechanistic-empirical design and analysis tool developed to-date is the National Cooperative Highway Research Program (NCHRP) Project 1-37A, "Development of the 2002 Guide for the Design of New and Rehabilitated Pavement Structures: Phase II." The advantages of the new guide are the use of multiple failure criteria and the consideration of axle load spectra. However, the effect of traffic on pavement performance is estimated based on the effect of wheel loads alone without accounting for the effect of tire inflation pressure or contact stress. Only one value of average tire pressure is used in the analysis.

Some failure criteria, such as bottom-up fatigue cracking, are primarily dependent on wheel loads and almost independent of contact stresses. Other failure criteria, such as asphalt rutting, are primarily dependent on vertical and horizontal contact stresses, almost independent of load magnitude. Although rutting is governed by the intensity of normal and shear stresses, not by load levels, axle load is the variable currently used to estimate rutting performance. Recent evidence suggests that the same applies to failure due to top-down fatigue cracking.

Currently, the effect of contact stresses is indirectly accounted for by using wheel load as a proxy for tire pressure. Although a positive correlation between wheel load and tire pressure exists, this correlation does not properly account for the effect of contact stress distribution. Thus, a

methodology that explicitly accounts for the effect of tire inflation pressure and the corresponding contact stresses on pavement response and performance is desirable.

1.2 Background

Empirical data has traditionally been used in pavement design to determine and predict the relationship between pavement design variables and response and performance. It has been determined that the relationships between pavement loading, response (in terms of stress and strain), and the influence of the environment on material properties are complex. Although pavement loading (3-dimensional) state of stress transferred from a vehicle tire to the pavement surface) has been recently quantified more accurately and finite element analysis has been applied to quantify pavement response as a result of loading and changing material properties, simplifying assumptions are still made in practice when pavements are designed. Some of these assumptions include:

4. the tire-pavement contact area has a circular shape,
5. contact stress is uniformly distributed, and
6. the contact stress is equivalent to the tire inflation pressure (8, 28).

As a result, the contact area is assumed to be the ratio of wheel load to tire inflation pressure.

The quantification of pavement loading and response is not as accurate as it could be and not yet clearly understood. Loading characteristics and material properties are influenced by numerous factors (many of which are difficult to quantify) and are consequently not accurately defined. In addition, there is a large inherent variability in these variables due to the effects of time and the environment.

However, as loading and pavement response are quantified more accurately, the relationships including the quantification of material characteristics are becoming more complex and often perceived as less cost effective to apply in practice. Relatively small accuracy improvements are attained as a result of significant cost increases, especially in terms of testing and computational time.

1.3 Research Tasks and Report Outline

Ideally, the numerous variables need to be quantified and relationships defined to such an extent that a clear understanding of these factors and their relationship can lead to simplified design procedures that can be cost effectively applied in practice. This research considers the use of simple models to assess these complex relationships and to quantify the differences created as a result of the simplifications adopted. The first task of this research, a literature review, was conducted to:

4. search for existing measurements of actual tire pavement contact stress distributions,
5. critically evaluate the measurements in terms of accuracy, usefulness, and limitations, and
6. identify the need for further research.

Chapter 2 provides a summary of the literature review.

With the data gathered during the literature review, pavement modeling and response analyses were performed by means of a multi-layer linear-elastic computer program (CIRCLY), which is briefly introduced in Chapter 3. CIRCLY was used to model pavement structure and estimate pavement response as a result of a circular uniform tire pavement contact stress distribution, and an approximation of the best actual measured tire pavement stress distribution. Based on the simulation results, pavement responses were calculated in terms of critical stresses, strains and displacements. The experimental design, pavement modeling and response estimations are detailed in Chapter 3.

Chapter 4 discusses the difference between pavement strains calculated by the models discussed in Chapter 3. The pavement strains studied in this research are tensile strains in the x -direction at the bottom of the asphalt layer, tensile strains in the y -direction at the bottom of the asphalt layer, and compressive strains on the top of the subgrade. Two types of difference, including absolute difference and relative difference, are computed and analyzed by statistical regression to study the effect of load, pavement structure and tire inflation pressure on the strain difference. Regression results and mathematical analysis are presented.

Chapter 5, Conclusions and Recommendations, includes the motivation, experimental design, statistical analysis and final results.

Chapter 2. Literature Review

2.1 Traditional Assumptions on Tire-Pavement Contact Characteristics

2.1.1 Literature Survey

Historically, three important assumptions are made about tire-pavement contact characteristics in pavement design procedures:

1. the tire-pavement contact area is in a circular shape;
2. contact pressure is uniformly distributed;
3. contact pressure is equal to the tire inflation pressure (8, 28).

As a result, the contact area is assumed to be the ratio of wheel load to tire inflation pressure given by

$$S = \frac{P}{p}$$

Equation 1

where S = tire-pavement contact area;
 P = wheel load; and
 p = tire inflation pressure.

The assumption of uniform pressure over a circular area was once regarded as “sufficient accuracy” for most analytical research work (28). Huang (8) described the relationship between contact pressure and tire pressure, as shown in Figure 1:

for low-pressure tires, the wall of the tires is compressed,

$$\text{Contact Pressure} = \text{Vertical Forces of Wall} + \text{Tire Pressure}$$

Equation 2

In this case, contact pressure is greater than tire inflation pressure.

for high-pressure tires, the wall of the tires is in tension,

$$\text{Contact Pressure} = \text{Tire Pressure} - \text{Vertical Forces of Wall}$$

Equation 3

In this case, contact pressure is lower than tire inflation pressure.

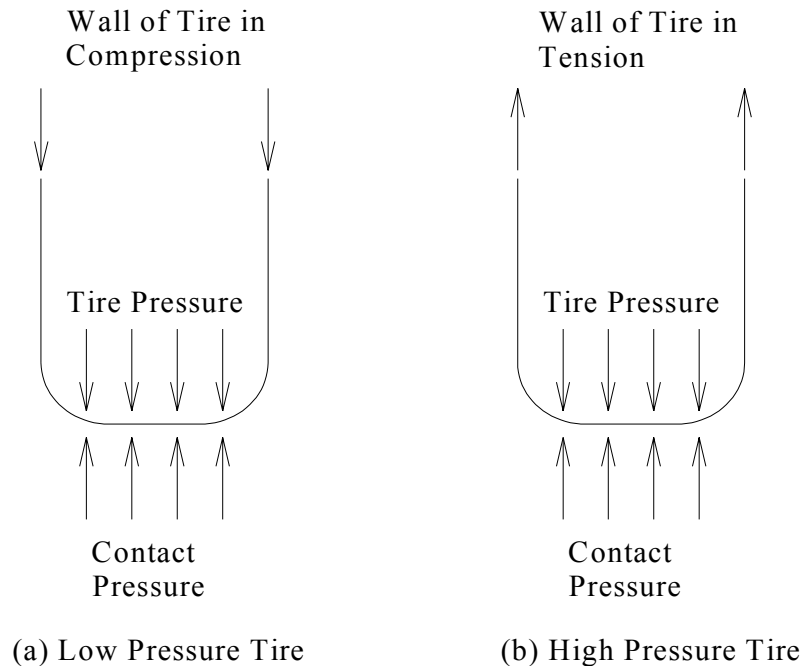


Figure 1. Relationship between Contact Pressure and Tire Pressure (8)

Since vehicles with heavy loads — which have a more destructive effect on pavements — have higher tire inflation pressure, the assumption that contact pressure equals tire pressure is safer for pavement design.

Based on the assumption stated at the beginning of this section, the Boussinesq Equation was modified to estimate vertical stresses under the center of the load in a flexible pavement at various depths. The original Boussinesq Equation (28), Equation 4, is applied for a semi-infinite elastic body to determine the stress at any point on a horizontal plane inside due to a concentrated load, as illustrated in Figure 2.

$$\sigma_z = \frac{3P}{2\pi z^2} \frac{1}{\left[1 + \left(\frac{r}{z}\right)^2\right]^{5/2}}$$

Equation 4

in which σ_z = vertical stress at point x in Figure 2;
 P = magnitude of concentrated load;
 z = the depth of point x below surface; and
 r = the radial distance from point x to the point of concentrated load applied.

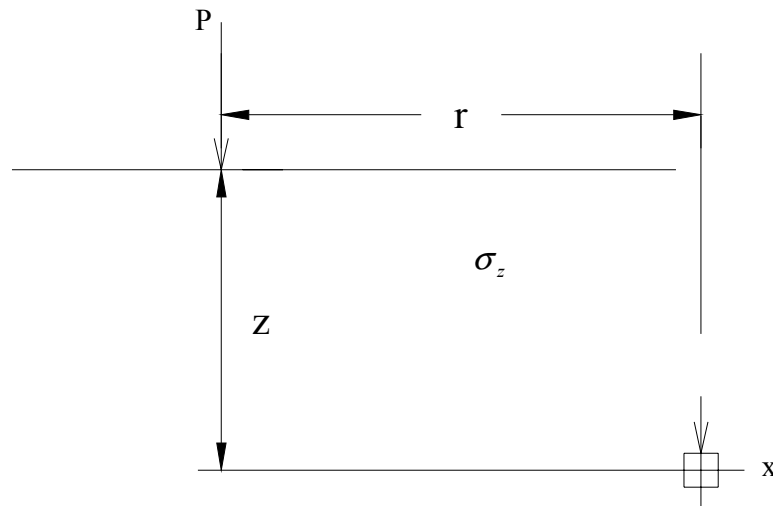


Figure 2 Illustration of Boussinesq Equation

The Boussinesq Equation was integrated to obtain the vertical stresses produced by a uniform load over a circular area, as follows in Equation 5. This equation is the basic approach used in past pavement design methods to estimate the vertical stresses under loading in flexible pavements.

$$\sigma_z = p \left[1 - \frac{z^3}{(a^2 + z^2)^{3/2}} \right]$$

Equation 5

where σ_z = vertical stress at z depth beneath the center of circular area;
 p = unit load over that contact area;
 z = the depth of point x below surface; and
 a = the radius of the circular area.

2.1.2 *Comments*

Tire-pavement contact pressure, as an important factor in pavement damage, had received little attention until the 1980s. Huang's analysis on the relationship between tire inflation pressure and contact pressure sounds reasonable, but it is only a general description and cannot quantitatively explain the problem in detail.

With the increase in fuel costs, the truck industry has attempted to improve truck gas mileage by increasing tire inflation pressure to reduce rolling resistance. Radial tires have been gradually replacing bias ply tires in Texas because radial tires can be inflated to a higher pressure (23, 24, 25, and 26). The increased tire inflation pressure has presumably accelerated pavement deterioration associated with an increase in rutting and fatigue failures, a fact that merits more consideration than so-called "sufficient accurate" assumptions on tire-pavement contact characteristics in new and rehabilitated pavement design. A better understanding of this topic will undoubtedly lead to significant progress in the analysis of pavement damage mechanisms and improved pavement design approaches.

2.2 Studies of Actual Characteristics of Tire-Pavement Contact Pressure

2.2.1 *Contact Pressure under Static Loading*

During the 1980s, researchers at The University of Texas at Austin (UT-Austin) conducted a series of experiments to investigate the effects of truck tire inflation pressure on pavement-tire contact area and pressure distribution (11, 16). Marshek et al. (11) used paper and printer's ink to capture the tire-pavement contact area and measured the area using a Grinnell Imaging System. Eight types of tires including Goodyear bias 10-20, Uniroyal bias 10-20, Goodyear bias 11-22.5, Bridgestone bias 11-22.5, Bridgestone bias 11-24.5, Goodyear radial 10R-20, Goodyear radial 11R-22.5, and Bridgestone radial 16.5R-22.5, were used in the experiment to study the effect of tire construction (bias ply or radial) and dimensions on the shape and size of the contact area. After being cleaned and inked, the truck tires were placed over a piece of paper, then statically loaded with a load frame. The load frame was mounted on a hydraulic ram, as shown in Figure 3. The inked print was obtained by a digitizing camera and stored by the data acquisition system.

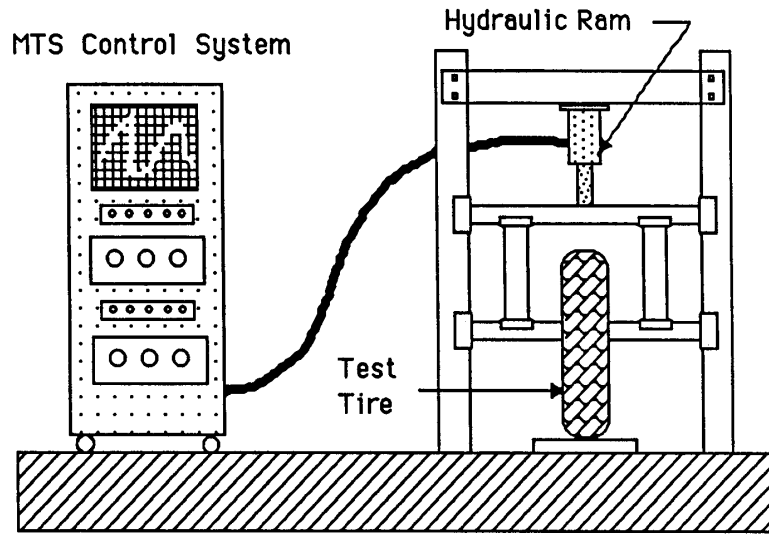


Figure 3. Experimental Design of Tire-Pavement Contact Pressure Testing

Results show that both tire inflation pressure and axle load significantly affect the contact area. Higher tire inflation pressure produces a smaller contact area: a 50 percent increase in tire inflation pressure results in a decrease of about 8–20 percent in the contact area. The greater the axle load, the larger the contact area: a 50 percent increase in axle load leads to an increase of about 30–35 percent in contact area. Tire construction also affects the contact area. It was found in the experiment that the contact area of radial tires was smaller than that of bias ply tires; however, a change in the size of the contact area due to the change of either tire inflation pressure or axle load was approximately the same for both types of tires.

The pressure distributions under statically loaded tires were captured by pressure sensitive film and were acquired by a densitometer and a data acquisition system. The experiments were conducted with both bald and treaded tires, three different tire inflation pressures (75 psi, 90 psi, and 110 psi), and two different axle loads (4500 lbf and 5400 lbf (a 20 percent overload)) to study the effect of tread pattern, inflation pressure, and axle load on the contact pressure distribution. Figure 4 summarizes different contact pressure distributions in given combinations of tread pattern, axle load and inflation pressure.

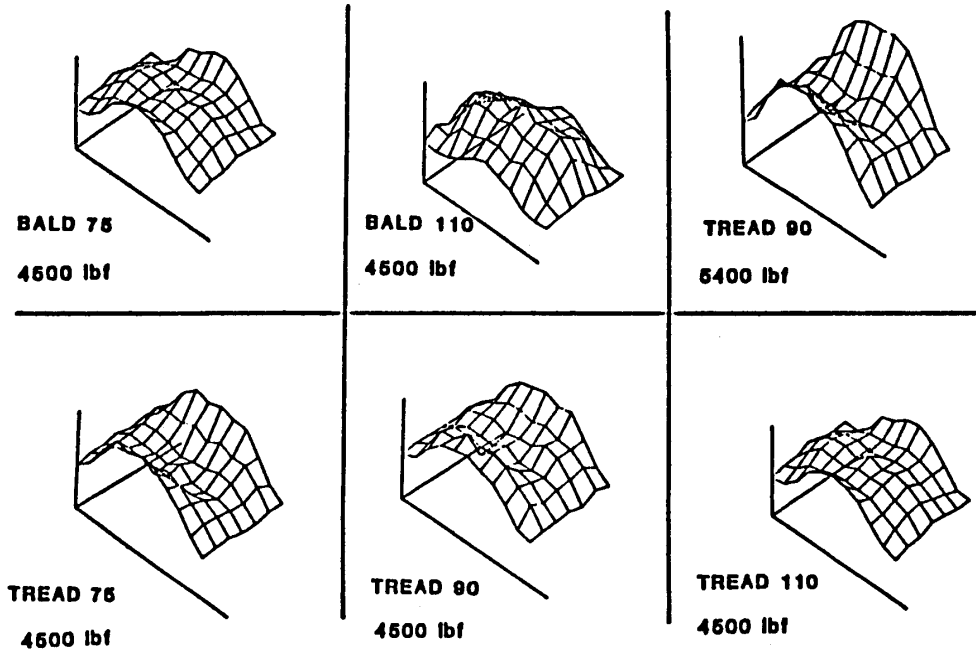


Figure 4. 3-Dimensional Plots of Pressure Distribution (10)

As shown in Figure 4, tread pattern dominates the shape of contact pressure distribution and significantly affects contact area size. Treaded tires developed a smaller contact area because of the presence of tread gaps, which reduce the contact points in the tire imprints. Pressure beneath bald tires was uniform with significant gradients only at the center and the shoulder region, while treaded tires had broken pressure distribution with zero pressure at the tread gaps, separating adjacent regions of sharply different pressure levels. Greater pressure was found in the region of tread-gap interface and tire shoulder. Marshek, et al. predicted an increase of contact area and a reduction of peak pressure near the tire shoulder with a more continuous pressure distribution as tire treads begin to wear.

Tire inflation pressure determined the location of high pressure regions in the contact area and the change rate of contact area, and it also influenced the axle load carried by tire shoulders. Low pressure tires produced a larger contact area (a 20 percent decrease in inflation pressure produced a 4 percent larger net contact area), and the high pressure region was at the tire shoulder. On the contrary, high pressure tires developed a vastly smaller contact area (a 20 percent increase in inflation pressure produced a 1 percent smaller contact area). In this case, the high pressure

region moved from the tire shoulder to the center, which reduced the peak loads carried by tire shoulders.

The axle load is also a parameter affecting the size of the contact area and the shape of the contact pressure distribution. For the Goodyear 10-20 bias ply truck tire in the test, an increase of 20 percent in axle load corresponded to an increase of 10 percent in contact area. Under an axle load of 4,500 lbf, peak loads were carried by the tire shoulders, while the pressures in the tire center region were close to the inflation pressure. When the axle load was increased by 20 percent to 5,400 lbf, pressure in the tire center changed little; however, pressure in the tire shoulders carried much higher peak pressure, between 160–220 psi.

Following the experiment, Pezo et al. (16), researchers at UT-Austin, conducted a further study on truck tire pavement contact pressure distribution characteristics. Four different types and sizes of tires, Goodyear bias 18-22.5, Michelin radial 275/80R/24.5, Michelin radial 255/70R/22.5, and Goodyear radial 11R24.5, were used in the experiment in contact with a steel plate to establish pressure distributions. Fuji and ink prints produced by tires were subjected to a number of combinations of tire, wheel load, and inflation pressure. The Fuji prints are pressure-sensitive by color intensity — higher pressure regions are indicated by darker pigmentation. Calibration squares were produced on the Fuji prints at different loads for the analysis and construction of “a calibration curve to relate color intensities with pressure values” (16). White paper covered the steel plate to record the imprint of inked tires with loading, and then a transparent grid paper was placed on the print to count the shaded squares to calculate the contact areas.

The measured contact areas enhanced the conclusion of the previous test: an increase in wheel load is associated with an increase in contact area, while an increase in inflation pressure produces a decrease in contact area. Different tire types have different contact area shapes. For radial tires, the contact area is rectangular, while the contact area of bias tires is oval. Since in pavement design approaches, the contact area is assumed to be the ratio of axle load to tire inflation pressure, this ratio was defined as a “Relative Area” to construct a statistical model describing the relationship of actual contact area with “Relative Area”, which is shown in Equation 6.

$$TCA = 0.28905 + 1.0627 (RA) - 0.00202 (RA)^2$$

Equation 6

in which TCA = the tire contact area in square inches; and
RA = the relative area in square inches.

When using a 95 percent confidence interval, this model has a high correlation factor of 94 percent irrespective of tire wear, tire brand, tire type and other factors. With this model, the actual contact area can be easily estimated with the obtainable tire inflation pressures and wheel loads. Comparison of this model with the traditional assumption that actual contact area equals “Relative Area”, Pezo et al. found that the traditional assumption meets the relative areas well below 50 square inches, while the increase of wheel load causes the decrease of assumption accuracy, and the increase of inflation pressure leads to the increase of assumption accuracy.

In addition, Pezo et al. considered the assumption of uniformly distributed contact pressure to be a “fallacy,” because their test results showed that mean contact pressures are generally higher than inflation pressures. High pressures were shown at the center and edge of the middle region of the tire imprints. Wheel loads and tire inflation pressure are two dominant parameters in contact pressure distribution. For a given wheel load, the higher pressure ranges increase with the rise in tire inflation pressure and decrease with the reduction of inflation pressure. For a given inflation pressure, the higher pressure ranges increase with heavier wheel loads and vice versa. However, different combinations of wheel loads and tire inflation pressure can produce the same contact pressure distribution. Based on the above analysis, Pezo et al. developed a model, Equation 7, to estimate an “equivalent contact pressure number (ECPN)” subjected to the change of static wheel load and tire inflation pressure. Specifically, this model incorporated the “Fourth Power Law” in the American Association of State Highway and Transportation Officials (AASHTO) pavement design method based on pavement fatigue theory.

$$ECPN = \frac{\sum_{i=1}^n f_i \cdot \overline{PR}_i^4}{P_r^4} \cdot \frac{TCA}{A_r}$$

Equation 7

in which $ECPN$ = the weighted number computed at each set of wheel load and tire inflation pressure;

f_i = the proportion of contact area at the pressure range i ;

\overline{PR}_i = the mean of the contact pressure range;

P_r = the chosen reference contact pressure ($P_r = 100$ psi was used, which is derived by the assumption that a wheel load of 10,000 pounds uniformly distributed over an area of 100 square inches);

TCA = the tire contact area; and

A_r = the chosen reference contact area ($A_r = 100$ square inches was used).

The model can be used to predict pavement damage resulting from a combination of wheel load and tire pressure with comparison to the damage caused by a wheel load of 10,000 pounds uniformly distributed over an area of 100 square inches. Compared to the “Fourth Power Law,” this model considers not only the effect of wheel load on pavement deterioration but the effect of tire inflation pressure.

Tire vertical stiffness, which is defined as the ratio of wheel load over the vertical deformation of the tire, was also measured in this experiment. Tire inflation pressure appeared to be in direct proportion to tire vertical stiffness and in inverse proportion to side tire movement. Equation 8 is a statistical model developed to estimate tire vertical stiffness.

$$TVS = 3.252 + 0.031 \cdot TCA - 0.000058 \cdot TCA^2$$

Equation 8

Where TVS = the tire vertical stiffness in kips/inch; and

TCA = the tire contact area in square inches.

2.2.2 Contact Pressure under Dynamic Loading

Himeno and Ikeda (7) used a device composed of piezo electric ceramics to measure tire-pavement contact pressure under dynamic loading. Two types of sensors in this device, as shown in Figure 5, are used to measure the moving speed of the tire and detect the loading weight on

each sensor. Contact pressure is obtained by dividing the loading weight by sensor area. An approach plate was placed in front of the device to reduce the effect of vertical move of the load on contact pressure distribution.

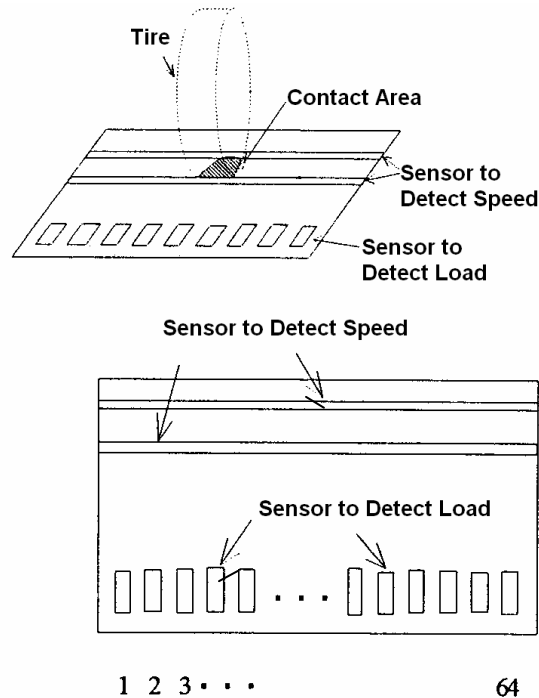


Figure 5. Device Used to Measure Tire Contact Pressure Distribution in Japan

A factorial experiment was conducted with varied vehicle load, tire inflation pressure, vehicle speed and tire tread. Four types of vehicles with four types of tire tread were used:

1. passenger car with pseudo-rib pattern,
2. passenger car with block pattern,
3. small truck with rug pattern,
4. large truck with pseudo-rib pattern,
5. and loading vehicle with purely rib pattern.

The tire inflation pressure was adjusted to standard, standard plus 20 percent, and standard minus 20 percent. The vehicle speed was controlled at 5 km/h, 30 km/h, and 60 km/h. The two dimensional contact pressure distributions under given combinations of conditions measured by the device indicate that none of the pressures are uniformly distributed on a circular shape. Each

distribution has its own specific characteristics. Generally, the discontinuous property of the distributions is probably due to gaps on the tire tread. For dual wheel, it was found that the contact pressure of outer tires was much greater than that of the inner tires. It was also found that neither the change in tire inflation pressure by ± 20 percent nor the change of vehicle speed by ± 30 km/h had much effect on the shape and magnitude of contact pressure distribution. However, wheel load and average contact pressure have a linear relationship, which is almost independent of tire inflation pressure and vehicle speed. The experiment results matched well with a regression equation developed by Ikeda in 1985, given in Equation 9, where gaps on the tire tread were included in the contact area.

$$c = 0.489L + 0.373p + 2.222$$

Equation 9

in which c = average contact pressure, in kgf/cm^2 ;
 L = wheel load, $\times 1000\text{kgf}$; and
 p = tire inflation pressure.

De Beer et al. (1, 4, 5) measured three-dimensional tire-pavement contact stresses under slow moving wheel loads (i.e. Stress-In-Motion [SIM]) by the Vehicle-Road Surface Pressure Transducer Array (VRSPTA) system, as shown in Figure 6. The system consists of an array of triaxial strain gauged steel pins fixed to a steel base plate, and data acquisition system. The speed of the moving wheel varies from 0.3–7 m/s and has vertical loads up to 200 kN and horizontal loads up to 20 kN. Since the effective friction between tires and pavements has a significant effect on the magnitude of horizontal stresses, the surface of the VRSPTA system was designed to represent an “average equivalent dry road surface” (5) to allow friction between the tire and VRSPTA surface to be close to maximum stresses. As a result, the real stresses in practice can be hardly underestimated by the VRSPTA system. Contact stresses in three directions — vertical, transverse, and longitudinal — was measured in the experiments.

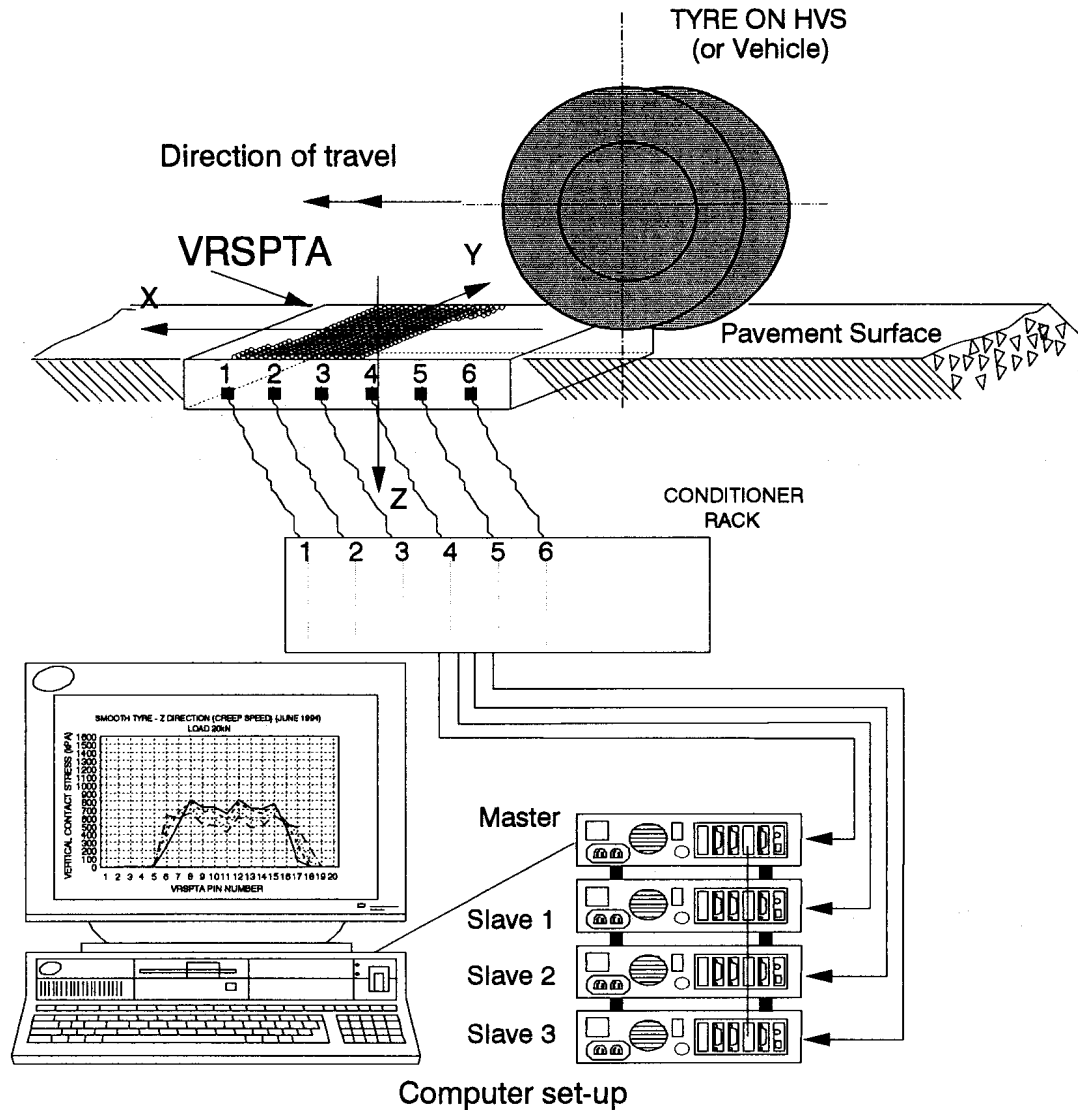


Figure 6. Layout of the Vehicle-Road Surface Pressure Transducer Array (VRSPTA) System (System: SIM MK II) in South Africa

Single bald bias-ply tyres were tested with different load combinations between 20–50 kN and tire inflation pressures from 420–720 kPa. It was found that both load magnitude and tire inflation pressures have a significant effect on the vertical contact stresses. An increase in load produces an increase of vertical stresses at tire edges, while an increase in tire inflation pressure results in the increase of vertical stresses at tire center. At constant load with varied tire inflation pressure, the change of tire inflation pressure had more affect on vertical stresses at tire center than at tire edges. The relationship between tire inflation pressure and the vertical stresses under the inner 60 percent of the tire width (tire center) was developed, as shown in Equation 10.

$$q_{60} = 0.86p + 175$$

Equation 10

in which q_{60} = average vertical contact stress at tire center area in kPa;

p = tire inflation pressure in kPa over a range of 420 kPa to 720 kPa, and a single wheel load range from 20 kN to 50 kN; and

$r^2 = 0.98$, standard error in $q_{60} = 20$ kPa.

However, at constant tire inflation pressure and varied load, the change of load strongly influenced vertical stresses at tire edges other than those at tire center. Equation 11 gives the relationship between wheel loading and edge contact stresses.

$$q_e = -0.53L^2 + 57.46L - 534.05$$

Equation 11

where q_e = vertical contact stress at the tire edges in kPa;

L = wheel load in kN, ranging between 20 kN and 50 kN; and

$r^2 = 0.97$, standard error in $q_e = 54$ kPa.

Since tire inflation pressure controls the contact stresses at tire center and wheel loading controls contact stresses at tire edges, relative overloading and under-inflation will produce contact pressure at tire edges up to 3–4 times the tire inflation pressure. The ratio of maximum stresses in three directions (vertical, transverse, and longitudinal) was found to be 10:3.6:1.4. The transverse ratio value can be increased from 3.6 to 4.5 or 5 if the effect of sideways shear is included in the above ratio because the VRSPTA test showed that sideways shear produced additional transverse stresses.

Following the tests on bald bias-ply tires, tread tires were also tested by the VRSPTA system. The contact stresses under treaded tires were vastly different from those under bald tires. The maximum vertical stresses occurred at tire center rib with a relatively low load, and moved toward the tire edge ribs as the load increased. Gaps in vertical stress distribution appeared between ribs on the tire tread. Since the ribs acted as bald tires, the tread pattern had the least effect on the longitudinal stresses. Similar to the results with bald tires, tire inflation pressure controlled contact stresses at tire center while wheel load controlled contact stresses at tire edges.

For both bias-ply and radial tires, the contact stresses were found to be much higher than the tire inflation pressure. Under given conditions, the contact stress can be twice that of tire inflation pressure. To predict relatively accurate maximum tire-pavement contact stresses, additional detailed analysis with seven types of tires, including three bias-ply tires and four radial tires was conducted with the VRSPTA system under “slow-moving free-rolling” conditions. The ratio of the maximum stresses in vertical, transverse and longitudinal directions is 10:1.6:1.3 for radial tires and 10:3:1.5 for bias-ply tires. A multiple linear regression analysis was conducted to relate the maximum contact stresses with both wheel load and inflation pressure. Equation 12 gives the general prediction form of tire-pavement contact stresses.

$$\text{Contact Stress} = K_1 + \{K_2 \cdot [\text{Inflation Pressure, P}]\} + \{K_3 \cdot [\text{Load, L}]\}$$

Equation 12

where Contact Stress in kPa;

Inflation Pressure, P in kPa;

Wheel load, L in kN, and

K_1 , K_2 and K_3 = the regression coefficients, which are different for each tire tested in the experiments.

2.2.3 Comments

Conclusions of the experiments on actual tire-pavement contact pressure showed that contact pressure is not uniformly distributed on a circular shaped area, the mean contact pressure is higher than the tire inflation pressure, and tire tread patterns affect contact pressure distribution. A dynamic loading measurement device is preferable to a static loading device because it more closely simulates actual roads. Experiments with tires on a steel plate may produce variances because the characteristics of the steel plate differ from those of flexible or rigid pavements. Himeno considered diverse possible variables in his experiment, such as vehicle speed, tire tread pattern, load magnitude, and tire inflation pressure, testing both single and dual tires. De Beer’s experiment seems to be the most in-depth, which includes dynamic loading, different types of tires, and contact stresses in three directions, from which a meaningful model of contact pressure estimation was developed. The result might be more reliable if dual tires were employed in the test because of the frequent use of dual tires on trucks.

2.3 Effects of Tire Parameters on Pavement Responses

2.3.1 Field Test

Roberts et al. (17), evaluating the effects of tire pressures on flexible pavements, based the field-collected data of truck tire inflation pressure and tire-pavement contact pressure on Texas highways. The field data collection was aided by the License and Weight Division of the Texas Department of Public Safety (DPS). A number of field sites were selected to collect information such as tire manufacturer, tire type (bias-ply or radial), tire size, inflation pressure, axle weight, and tread depth. Statistical analysis of the data shows that the mean tire pressure on Texas highways is greater than the value used in traditional pavement design procedures. Vehicle speed was found to have negligible effect on contact pressure distribution; therefore, for convenience, a standing tire model was studied instead of a free-rolling tire.

Sebaaly and Tabatabaee (19) investigated the effect of tire type and inflation pressure on response and load equivalency factors (LEFs) of flexible pavements by conducting full-scale tests on two flexible pavement sections having surface layers of 6 inches and 8 inches, respectively. Radial tires of different sizes — 11R22.5, 245/75R22.5, 425/65R22.5, and 385R/65R22.5 — were tested under two load levels (17,600 lb/axle and 21,700 lb/axle) and an adjusted temperature of 70°F (21°C). Based on the data from both single-axle and tandem-axle testing, 11R22.5 was found to be the least damaging tire, which was dealt with the standard tire type in the definition of three types of load equivalency factors for rutting rate, 10 percent fatigue cracking, and 45 percent fatigue cracking, respectively. Results show that tire inflation pressure has little effect on strains or deflections of the tested pavement sections, but tire type (single and dual), axle load, and axle configuration have a significant impact on pavement damage. Wide-single tires caused higher strains and deflections than dual tires, while smaller size dual tires produced higher strains and deflections than conventional duals. The tandem axle had higher rutting LEF than single axle, but lower fatigue LEF.

Huhtala et al. (9) used strain gauges developed by the Road and Traffic Laboratory of the Technical Research Center of Finland (VTT) to measure strains in the asphalt concrete (AC) surface layer under a combination of three axle loads (10 tons, 20 percent more, and 20 percent less), three tire inflation pressure levels (optimal as recommended by manufacturer, 20 percent

more, and 20 percent less), five tire types (12R22.5 dual, 265/70R19.5 dual, 445/65R22.5 wide base, 385/65R22.5 wide base, and 350/75R22.5 wide base). The tire-pavement contact pressure distribution was also measured in the laboratory under varied tire inflation pressure and axle load. Wide-base tires exhibited a larger destructive effect on pavements than dual tires by a factor of about 2.0. For dual tires, smaller size tires were more destructive than those of normal size by a factor of 1.5–2.0. For wide-base tires, wider tires were less destructive. An increase in tire inflation pressure caused an increase in pavement damage. The differences stated above were greater for thinner AC layers and lesser for thicker AC layers. The tire-pavement contact pressure appeared to be greatest at the center of truck tires and at the shoulder of passenger car tires.

Bonaquist et al. (2) studied the effect of tire inflation pressure on flexible pavement response and performance by analyzing data an Accelerated Loading Facility (ALF) test machine, two AC pavement lanes (each divided into four sections) with thicknesses of 5 and 7 inches respectively, and a computer-controlled data-acquisition system at the Federal Highway Administration (FHWA) Pavement Testing Facility. Surface deflection, surface strain, and strain at the bottom of the surface layer were measured under a combination of three load levels (9,400 lb, 14,100 lb, and 19,000 lb), three tire inflation pressures (76 psi, 108 psi, and 140 psi), and two tire types (radial and bias ply). The rutting and cracking of two pavement sections were evaluated under a constant load (19,000 lb) and two tire inflation pressures (100 psi and 140 psi). The analysis on pavement response indicated tire inflation pressure had minimal effect on the measured response for all the load levels. Double tire inflation pressure caused only 2–10 percent increase in surface strains and deflection. Rutting and cracking appeared more sensitive to tire inflation pressure on thinner AC surface layers with higher temperature.

Owende et al. (15) analyzed the effect of tire inflation pressure on pavement performance and advised the use of variable tire inflation pressure with respect to different vehicle speeds and wheel loads. Experimental tests on flexible pavement sections were conducted using a three-axle (one single and two tandem axles) timber truck with 10R20 tires. The factorial experiment tested four sets of inflation pressures (350, 490, 630, and 770 [recommended value by manufacturer] kPa) and three sets of loads on front, middle, and rear wheels, including the lowest values (28.4,

21.6, and 22.6 kN), medium values (31.6, 34.4, and 35.2 kN), and highest values (31.7, 44.6, and 44.1 kN). The lateral strain under the steering wheel appeared to determine the initiation of fatigue cracking in the surface layer, and the longitudinal strain largely affected the development of cracks. Since the longitudinal strain increased with tire inflation pressure, the lowest practical tire inflation pressure is recommended to increase pavement service life. For example, the potential pavement fatigue life would be increased by 200 percent due to a reduction of tire inflation pressure in the range of 770-350 kPa. Axle loads played a dominant role in subgrade distress which leads to rutting. Test data showed that load reduction decreased pavement rutting. However, cracking was regarded as more critical in soft soil foundations. As a result, lower tire inflation pressure with the application of a variable tire pressure system (inflating tires in proportion of axle loads) to truck operations may decrease pavement deterioration and increase the fatigue life of the surface layer.

Chatti et al. (3) tested the strains of an asphalt pavement section under an instrumented truck with three speeds (2.7, 32, and 64 km/hr) and three tire inflation pressures (620, 400, and 214 kPa) in the PACCAR Technical Center in Mount Vernon, Washington. The section was fitted with foil-type gauges to measure strains and had dense-graded asphalt concrete surface of 137 mm. Truck speed had a significant effect on surface response. Approximately 30–40 percent of the maximum longitudinal strain was reduced when the truck speed increased from creeping to 64 km/hr. Tire inflation pressure also affected pavement responses. A decrease of tire inflation pressure from 640 to 214 kPa reduced the longitudinal strain at the bottom of the surface course by 20–40 percent, while the pressure effect decreased at the top of the pavement surface. However, the effects of vehicle speed and tire inflation pressure may be decreased by each other at some values. Specifically, the speed effect on pavement response was reduced at a low value of tire inflation pressure, while the tire pressure effect was reduced at a high value of vehicle speed.

2.3.2 *Computer Simulation*

Based on the experiment on tire-pavement contact area and contact pressure distribution, Marshek et al. (12, 13) did further analysis on the effect of tire inflation pressure, wheel load, tire tread pattern, and friction on the stresses and strains in flexible and rigid pavement performance

with the computer program Bitumen Structures Analysis in Roads (BISAR) and a 3-dimensional finite element model, Texas Grain Analysis Program (TEXGAP-3D). In the analysis of flexible pavements, BISAR was used to deal with various experimental non-uniform concentric circular models for contact pressure distributions under either treaded tires or bald tires with different tire inflation pressures and axle loads. The axle load was found to be the dominant factor causing tensile strains at the bottom of the surface layer of flexible pavements. Tire inflation pressure causes the second most significant effect on tensile strains. Inflation pressure determines the magnitude of tensile strains and the location of maximum tensile strains, which was produced at the tire shoulder when under-inflated and moved toward the tire center with the increase of inflation pressure. High inflation pressure may cause a significant reduction in pavement life. The tire types slightly affected the tensile strains. Treaded tires produced a slightly higher tensile strain than that of bald tires, which indicated a decrease in tensile strain with the wearing of treaded tires. For compressive strains at the top of the subgrade, the axle load played the most significant role while tire inflation pressure had a negligible effect.

Because the non-uniform circular pressure model cannot simulate two strips of high pressure in the tire shoulder regions which appeared in the experimental results, TEXGAP-3D was used to investigate the effect of high tire inflation pressure and heavy load on the stress in flexible pavements instead of using a non-uniform circular pressure model. This model is more precise but time consuming. Results show that when the surface layer is less than 2 inches in depth, the tire inflation pressure has the greatest effect on the tensile strains at the bottom of the surface. As the tire inflation pressure increased by 47 percent, the tensile strains increased by 33 percent and pavement fatigue cracking life decreased by 60 percent. The axle load was also a significant factor on tensile stress. When the axle load increased by 20 percent, the tensile stress increased by 15 percent and the pavement fatigue cracking life was reduced by 36 percent. For compressive strains at the top of the subgrade, tire inflation pressure is an insignificant factor while the axle load does have a significant impact. When the axle load increased by 20 percent, subgrade compressive strain was increased by 19 percent and pavement life was reduced by approximately 50 percent.

Another finite element program, JSLAB, was used for rigid pavements to analyze the effect of contact pressure distributions including uniform model and non-uniform experimental pressure models on the maximum tensile stress at the bottom of a concrete slab. Both models yielded similar results, which indicated that contact pressure distribution has little effect on rigid pavement performance.

Sebaaly and Tabatabaee (18) used a modified version of the BISAR computer program package to investigate the effects of tire inflation pressure and tire type on pavement responses based on tire characteristics, including imprint length and width, contact area, spring rate, and contact pressure. The types of tires tested were dual 11-22.5 bias, dual 11R22.5 radial, and wide-base radial single. The tire deflections showed a linear relationship with the net contact area. Contact distributions were neither uniform nor circular in shape and the maximum contact pressure was 1.75 times the tire inflation pressure at the center rib of the tire, while the minimum contact pressure was shown at the tire shoulders. Because the original BISAR computer program can only detect circular uniform contact pressure distribution, the BISAR program was modified to detect non-uniform distribution by dividing the contact area into a number of concentric circles with different pressures. A factorial experiment was conducted with three levels of tire inflation pressure (75, 100, and 125 psi) and three levels of axle load (10, 17, and 22 [20 for wide-base single tire] kilo-pounds) to investigate the responses of four flexible pavement sections with AC surface layers in different thicknesses (2, 4, 6, and 8 inches, respectively). The estimated pavement responses included surface deflection, critical tensile strain at the bottom of the surface layer, and compressive stress at the interface between the base and the surface. Of the three tire types, the wide-base single tire produced the maximum tensile strains and compressive stresses in all cases with different load and surface thickness. The effect of tire pressure on tensile strain and compressive stress decreased as the surface thickness increased. The change in tire pressure affected tensile strain and compressive stress on the 2-inch-thick pavement and had a less-than-5-percent effect on pavements thicker than 4 inches. Surface deflection did not appear to be affected by tire inflation pressure. Axle load was the dominant factor for all pavement response parameters.

Roberts and Tielking (17, 22) employed the analysis program ILLIPAVE for flexible pavements based on finite element methods including linear and nonlinear material properties. The program also estimates pavement rutting, fatigue cracking, slope variance, and present serviceability index (PSI) with time. Analytical results showed tire-pavement contact pressure to be almost twice that of tire inflation pressure, which causes much higher strains in thin pavement surface layers than that predicted in traditional pavement design. As a result, premature fatigue cracking may occur under truck wheel loading when the thickness of the surface course is between 1–3 inches, and contact pressure between truck tires and pavements is estimated to play a dominant role in the increase of rutting on Texas highways. Passenger wheel loading may also produce large enough strains at the bottom of the surface layer to be considered in the design process.

Kestler et al. (10) employed a mechanistic pavement design procedure comprised of four computer programs including FROST, TRANSFORM, NELAPAV, and CUMDAM and developed by the U.S. Army Corps of Engineers for use in areas that experience seasonal freezing to analyze the effect of tire inflation pressure on low-volume roads (i.e. timber access roads and county roads) with thin bituminous surfaces. Computer simulations were conducted with different tire pressures from low to high and constant load on selected pavement cross sections with AC surface thicknesses of 0.5, 2.5, and 4.0 inches, respectively. The simulation results indicated that a truck operating with conventional tire inflation pressure caused significant pavement fatigue cracking on low-volume roads with a thin AC surface layer, and reducing truck tire inflation pressure can effectively decrease pavement damage. Since this mechanistic model approximates the wheel loading uniformly distributed over a circular area, a finite-element program, ABAQUS, was used to check the agreement between a circular uniform distribution and an actual rectangular non-uniform distribution. Preliminary results showed that for pavements with a 0.5-inch AC surface layer, the rectangular non-uniform distribution exhibited higher strains at the bottom of the surface layer by about 17 percent, which implied that the mechanistic procedure used in the previous analysis may somewhat underestimate the pavement damage caused by non-uniform pressure distribution.

Weissman (27) used Symplectic Engineering's StrataGemTM layered linear-elastic software package to compare stresses developed in pavements under two different tire-pavement contact

pressure distributions, one being the uniformly distributed pressure over a circular area and the other being the actual contact distribution of a Goodyear G159A 11R22.5 tire reported by de Beer (5). A dual tire configuration (366mm center to center) was employed in the simulations with an inflation pressure of 690 kPa to bear a load level of 26 kN per tire. The tested pavement section had an AC surface layer of 21.2 cm. The observed pavement distresses were similar for both contact pressure distributions but were vastly different in magnitude. The maximum vertical stress of non-uniform distribution was higher than that of uniform distribution by 50 percent. Different rutting may develop due when contact pressure distributions vary. Maximum tensile stress was observed in transverse direction (causing longitudinal cracking) under low loads, while under large loads maximum tensile stress appeared in the longitudinal direction (producing transverse cracking). As a result, transverse cracks often developed in accelerated tests under higher loads, producing a different contact pressure distribution, while cracks in field were initially in a longitudinal direction.

Yue and Svec (29) developed a computer program, VIEM, to analyze the response of multi-layered elastic pavements under a given uniform or non-uniform contact pressure over any shape of contact area. Using VIEM, the contact area was broken into a finite number of triangular or quadrilateral elements with input value of contact pressure at that point, and load solutions were integrated over the contact area to calculate the elastic response of multilayered asphalt pavements. Both uniform and non-uniform contact pressure distributions were used in the simulations to compare the pavement response under different contact conditions. The uniform contact pressure was assumed to be equal to the tire inflation pressure of 0.75MPa over a circular area with a diameter of 225.68 mm. The in situ non-uniform distribution used in the simulation was given by the Road and Traffic Laboratory, the Technical Research Center of Finland (VTT) and measured under a bald front tire with inflation pressure of 0.75 MPa on a moving vehicle at a speed of 50 km/h. The loads for both cases were 30 kN. The analytical results show that stress and strain in the pavement surface were affected by contact pressure distribution while pavement responses in lower layers were mainly determined by loads. Contact pressure distribution played a significant role in the development of tensile stress at the bottom of thin AC surface layers, which determined the fatigue cracking in flexible pavements. The use of uniform circular contact distribution may underestimate this tensile stress.

Siddharthan et al. (21) used a recently developed finite-layer mechanistic analytical model to generate a database of pavement response parameters under various tire-pavement contact pressure distributions. Two pavement sections of differing thicknesses — to represent thin and thick pavements — were modeled under tandem axles with dual or wide-base tires bearing a maximum total axle load of 180 kN. Section I had an AC layer of 15 mm and base layer of 20 mm, while Section II had an AC surface and base of 25 mm. The thickness of the subgrade for both sections was 6.0 m. The total axle load was supposed to be evenly distributed on each tire. Three contact pressure distributions were studied:

1. uniform contact pressure of 862 kPa over a circular area,
2. uniform contact pressure of 862 kPa over an elliptical area, and
3. non-uniform contact pressure distribution reported by Sebaaly (20).

The non-uniform contact pressure distribution produced the highest longitudinal strain at the bottom of the AC surface, while the circular uniform distribution produced the lowest. However, the maximum compressive strain at the top of the subgrade under non-uniform distribution was about 19 percent lower than that under the other two distributions on both thin and thick pavement sections, and the circular uniform distribution also gave the highest shear strain at a depth of 0.05 m from the pavement surface under the tire shoulder. As a result, the assumption of circular uniform distribution may underestimate fatigue cracking, but it may be conservative for rutting. The thickness of layers also largely affected the strains in pavement layers. The maximum longitudinal tensile strain in the thick pavement was only 53 percent of that in the thin pavement section in all tested cases, and there was a difference of 42 percent in the maximum compressive strain at the top of the subgrade between the thin section and the thick section under all pressure distributions. Vehicle speed significantly impacted the strain magnitude. An increase in vehicle speed from 5–110 km/h led to a reduction in strain of up to 28 percent in both pavement sections.

2.3.3 Comments

Laboratory test and computer simulation are two major approaches adopted by researchers to investigate the effect of tire-related parameters on pavement responses and performances. The

employed computer programs are composed of multi-layered linear-elastic software and finite element analysis program packages. Factorial experiments were widely conducted in both approaches with a number of combinations of load, tire types, tire inflation pressure, pavement surface thickness, vehicle speed, and other parameters. The pavement responses of most concern are the tensile strain at the bottom of the AC surface layer and the compressive strain at the top of the base or subgrade.

Wheel load appeared to be the dominant factor in all the pavement response parameters in all combinations of tire type, tire inflation pressure, and pavement thickness. Pavement with thin AC surface layer (1–3 inches) was more sensitive to tire pressure, while pavement with a thinner surface was slightly affected by the change of tire inflation pressure. Higher vehicle speeds can efficiently reduce pavement strains. The tire-pavement contact distributions used in computer simulation, circular uniform distribution, or actual measured distribution produced different pavement response estimations.

2.4 Current Truck Characteristics in Texas

From late 1999 to early 2000, Wang et al. (23, 24, 25, 26) conducted a survey on truck configurations in Texas with the aid of the License and Weight Division of the Texas DPS. Eighteen locations for data collection were selected based on the factorial design with six geographical regions (Lubbock-Midland, Dallas, Houston, San Antonio, Corpus Christi and El Paso), two highway classes (Interstate and State), and two highway directions (eastbound and westbound), and at each location thirty-five trucks were investigated on truck class, tire type, tire inflation pressure, tire size, tire manufacturer, suspension type, axle type, axle spacing, and transport commodity.

The average tire inflation pressure of 9,600 tires tested in the survey was 96.75 psi with a standard deviation of 15.03 psi. Comparing the results to a similar survey by Texas Transportation Institute (TTI) in 1986 (17), the tire inflation pressure was an average of 4 psi higher than the value investigated in 1986; however, the critical mean tire pressure during summer at 140°F was 108.94 psi, which was 16 psi higher than that of the TTI survey. The bias-ply tire showed a sharp decrease from 32.2 percent in 1986 to 2.2 percent in 2000. The 3-S2

truck accounted for the major part of 80.3 percent in the sampled 623 trucks, and the other two common truck types were SU-3 and SU-2 at 7.5 percent and 6.3 percent, respectively. Tandem axles were widely used, accounting for 70.5 percent, while tri-tandem axles only accounted for 0.9 percent of the sample. Tire sizes of 295-75R22.5, 11R24.5, 11R22.5, and 285-75R24.5 were the major sizes found in the sample trucks, accounting for 25.7 percent, 21.8 percent, 17.3 percent, and 15.4 percent, respectively. Wide-base single tires were rarely found in the survey.

2.5 Conclusions of Literature Review

Based on the literature survey, the following conclusions may be made to summarize the progress of research on tire-pavement contact characteristics and their effects on pavement responses:

1. Traditional pavement design approaches assume the tire-pavement contact pressure is uniformly distributed over a circular area. This assumption cannot appropriately exhibit the actual contact distribution between tires and pavement.
2. The magnitude, shape and area of actual tire-pavement contact distribution vary with the axle load, tire inflation pressure, tire type, vehicle speed, and other parameters. Generally, the contact pressure is not uniform, and the contact area is not in a circular shape.
3. Laboratory test and computer simulation are two methods for investigating the effect of tire-pavement contact pressure on pavement performance. Factorial experiment is an efficient approach to analyzing the effect of related parameters, including wheel load, inflation pressure, tire type, vehicle speed, pavement layer thickness, and other factors on pavement response. The most important pavement responses to consider are the strain at the bottom of the surface layer and the strain at the top of the base or subgrade. As a result, pavement performance such as fatigue cracking and rutting can be estimated.
4. Estimations on pavement response and performance are different with the various tire-pavement contact distributions used. The traditional assumption of uniform circular contact distribution may overestimate or underestimate specific pavement responses.
5. Axle load plays a dominant role in pavement response and fatigue life. Higher vehicle speed can efficiently reduce strains in pavement. Pavements with thinner surface layers (1–3 inches) are more sensitive to tire inflation pressure.

6. Radial tires have gradually replaced bias-ply tires and account for 97.8 percent of all truck tires used in Texas. The tire pressure of trucks operating on Texas highways is increasing. Tandem axle is the major axle type used in Texas, accounting for 70.5 percent.

2.6 Inspiration from Literature Review

The results of the experiments conducted by researchers previously discussed have shown that tire-pavement contact stress is non-uniform and not in a circular shape. As a result, prediction and evaluation of pavement response and performance with most of the pavement design approaches may not be accurate due to their assumption of circular uniform contact stress, which is not accurate. To evaluate the effects of actual stress distributions compared to uniform constant stresses, the available data on wheel loads and contact stress distributions measured by de Beer (4, 5) will be gathered and compiled into a database which will be used for modeling purposes.

A limited number of researchers have addressed this problem using finite element analysis methods, which are usually complex, time-consuming, and require more powerful computers. In this research, a different approach will be followed by adopting a relatively simple and rapid model. Pavement modeling and estimation of pavement response will be carried out using multi-layer linear elastic theory. The computer program CIRCLY will be used, which is capable of simulating multiple load configurations. CIRCLY enables the modeling of traffic loading by superimposing multiple load effects that account for vertical and horizontal load components. A number of pavement structures representative of Texas practice will be modeled and their responses in terms of critical stresses, strains and displacements will be calculated.

Chapter 3. Experimental Design on Pavement Modeling and Estimation of Pavement Response

3.1 A Brief Description of CIRCLY

CIRCLY is a DOS/Windows-based computer package used for the structural analysis of multi-layer linear-elastic systems. This specific feature meets the basic assumption of flexible pavements as layered elastic systems. CIRCLY was first released in Australia in 1977, and later used world wide for more than two decades (14). The most recent version of CIRCLY is CIRCLY 5.0.

Databases in CIRCLY can be used for material properties and loading types. The program can be conveniently used for mechanistic analysis and design of pavement. Isotropic properties, interfaces between layers, and soil and rock layers can be taken into consideration. The most remarkable feature of CIRCLY for pavement structural analysis is the capability to model diverse load types, including vertical force, horizontal force, moment about horizontal axis, moment about vertical axis, radial shear stress, and uniform vertical stress, as illustrated in Figure 7.

However, CIRCLY can model load only in a circular shape. To simulate actual measured contact conditions, in which the stress distribution is non-uniform and the shape is not a circle, careful consideration and proper modeling are required.

CIRCLY requires three key points in the analysis of pavements:

1. traffic loads, which are characterized as circular loads defined by radius, stress, and location,
2. a layered pavement structure system consisting of a number of layers characterized by their mechanical properties, thicknesses and interface type, and
3. an analysis objective such as pavement responses at specific points within the pavement structure.

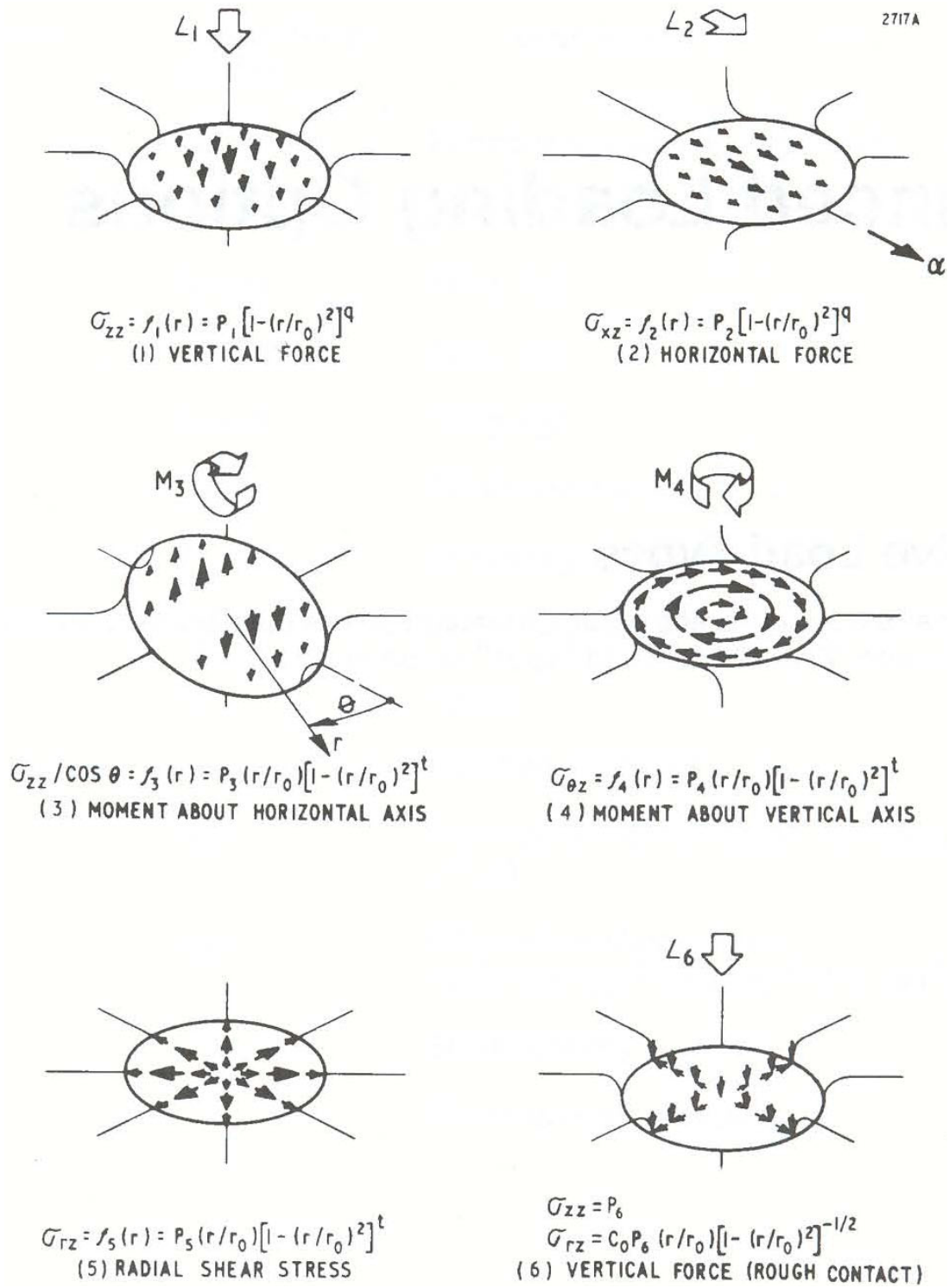


Figure 7. Alternative Load Types Provided by CIRCLY (14)

3.2 Tire-Pavement Contact Stress Modeling

3.2.1 Model for Actual Measured Tire-Pavement Contact Stress Distribution

The Texas Department of Transportation (TxDOT) provided the data of actual measured tire-pavement contact stress used in this research (6). The test tire was a Goodyear 11R24.5 G G159A (Figure 8) which is one of the most common tire sizes in Texas. The target wheel loading in the experiment varied from 20.4–34.6 kN and the tire inflation pressure from 483–896 kPa. To study the effect of loading and tire inflation pressure on pavement responses, nine sets of data were selected for analysis considering different combinations of loading levels and tire inflation pressure (see Table 1). Of the 3-dimensional contact stresses measured under the nine combinations, only vertical stresses are evaluated in this research because of their dominant effect on critical pavement responses.



Figure 8. Test Tire: Goodyear 11R24.5 G G159A

http://www.goodyear.ca/tires/tirecatalog/G159A-Metro11R24_5___GData.html

Table 1. Filename of the Nine Combinations Studied

Filename		Target Wheel loading (kN)		
		24	27.5	31.1
Tire Inflation Pressure (kPa)	793	LTEX009	LTEX014	LTEX019
	690	LTEX008	LTEX013	LTEX018
	586	LTEX007	LTEX012	LTEX017

To model the measured contact characteristics in CIRCLY, a number of loads in a circular shape with a very small radius were combined to simulate the measured wheel loading, which is slightly different from the target loading (Table 1). Each circular load component was assigned to a specific value of stress based on the measured contact stress data provided by TxDOT. Figure 9 illustrates the model of actual measured contact vertical stresses in the case of LTEX013. The contact area consisted of 204 tangent circles (12 columns \times 17 rows) with a diameter of 17 mm. These dimensions are adopted based on the characteristics of the measuring equipment (4, 5, 6). Each circle load had a specific contact stress, the value of which is shown inside the circle. The traffic loading in CIRCLY includes all the circular loads with their radii (8.5 mm), stresses and center location.

Four typical pavement structures used in Texas were analyzed in this research, as shown in Table 2. Each layer of the pavement was assumed to be homogenous, isotropic, and linearly elastic with a Poisson ratio of 0.35 and an elastic modulus as given in the table. The only difference between these four pavement structures is the thickness of asphalt layer, which varies from 40–130mm.

Table 2. Pavement Structures Analyzed in CIRCLY

Pavement (No.)	Materials for Different Layers	Thickness (mm)	Modulus (MPa)
1	Dense asphalt pavement	40	3500
	A-1-b base course	250	500
	A-2-4 subbase	200	250
	A-6 subgrade	--	75
2	Dense asphalt pavement	70	3500
	A-1-b base course	250	500
	A-2-4 subbase	200	250
	A-6 subgrade	--	75
3	Dense asphalt pavement	100	3500
	A-1-b base course	250	500
	A-2-4 subbase	200	250
	A-6 subgrade	--	75
4	Dense asphalt pavement	130	3500
	A-1-b base course	250	500
	A-2-4 subbase	200	250
	A-6 subgrade	--	75

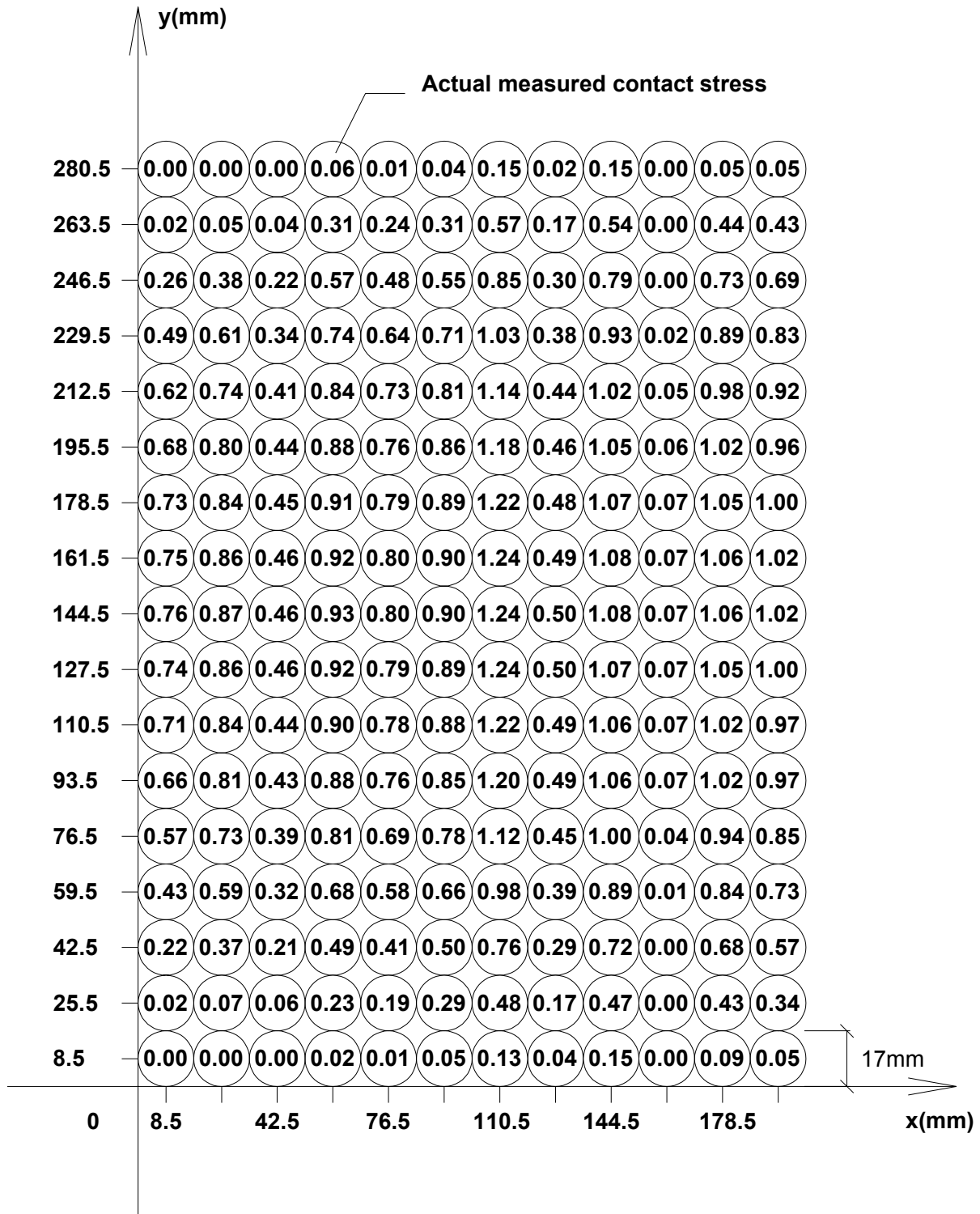


Figure 9. Model of Actual Measured Contact Stresses (LTEX013) in CIRCLY

For the design of flexible pavements, two types of strains were considered as the most critical:

1. the horizontal tensile strain at the bottom of the asphalt layer, which is the criterion of fatigue cracking, and
2. the vertical compressive strain on the top of the subgrade, which is the main reason for rutting (8).

The particular responses of interest for this research were:

1. horizontal tensile strains at the bottom of surface layer in the travel direction (ϵ_{yy}),
2. horizontal tensile strains at the bottom of surface layer perpendicular to the travel direction (ϵ_{xx}), and
3. vertical compressive strains at the top of subgrade (ϵ_{zz}).

The results of CIRCLY can be laid out using the following aerial coordinates:

1. an array of equally spaced points along a line parallel to the x -axis (Figure 10(a)), or
2. a uniform spacing grid of points in both x -direction and y -direction (Figure 10(b)).

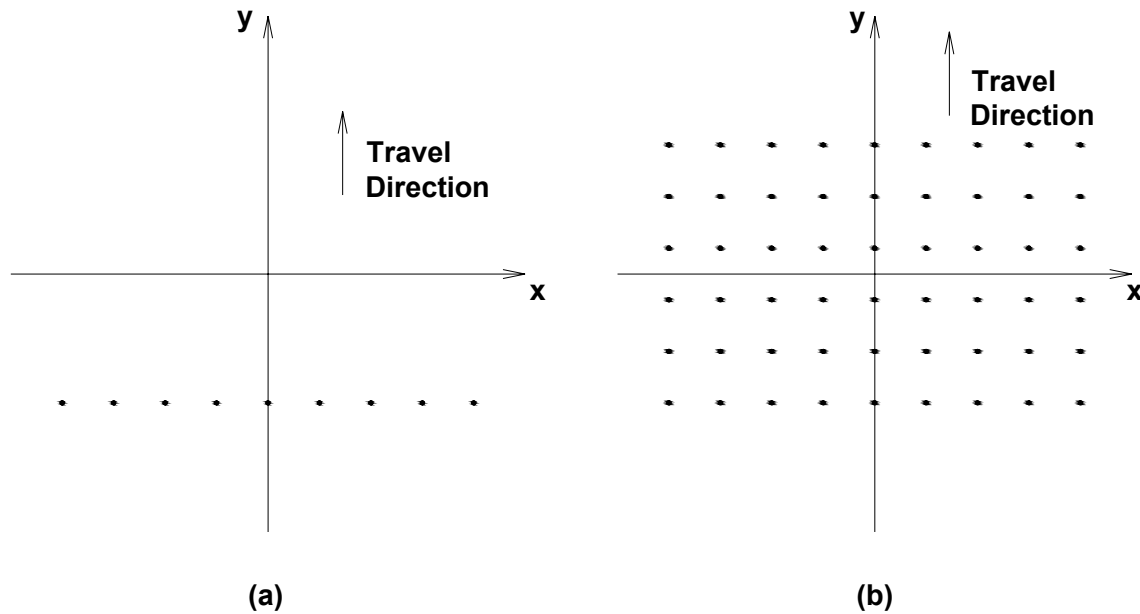


Figure 10. Layout of a Line of Spaced Points in CIRCLY

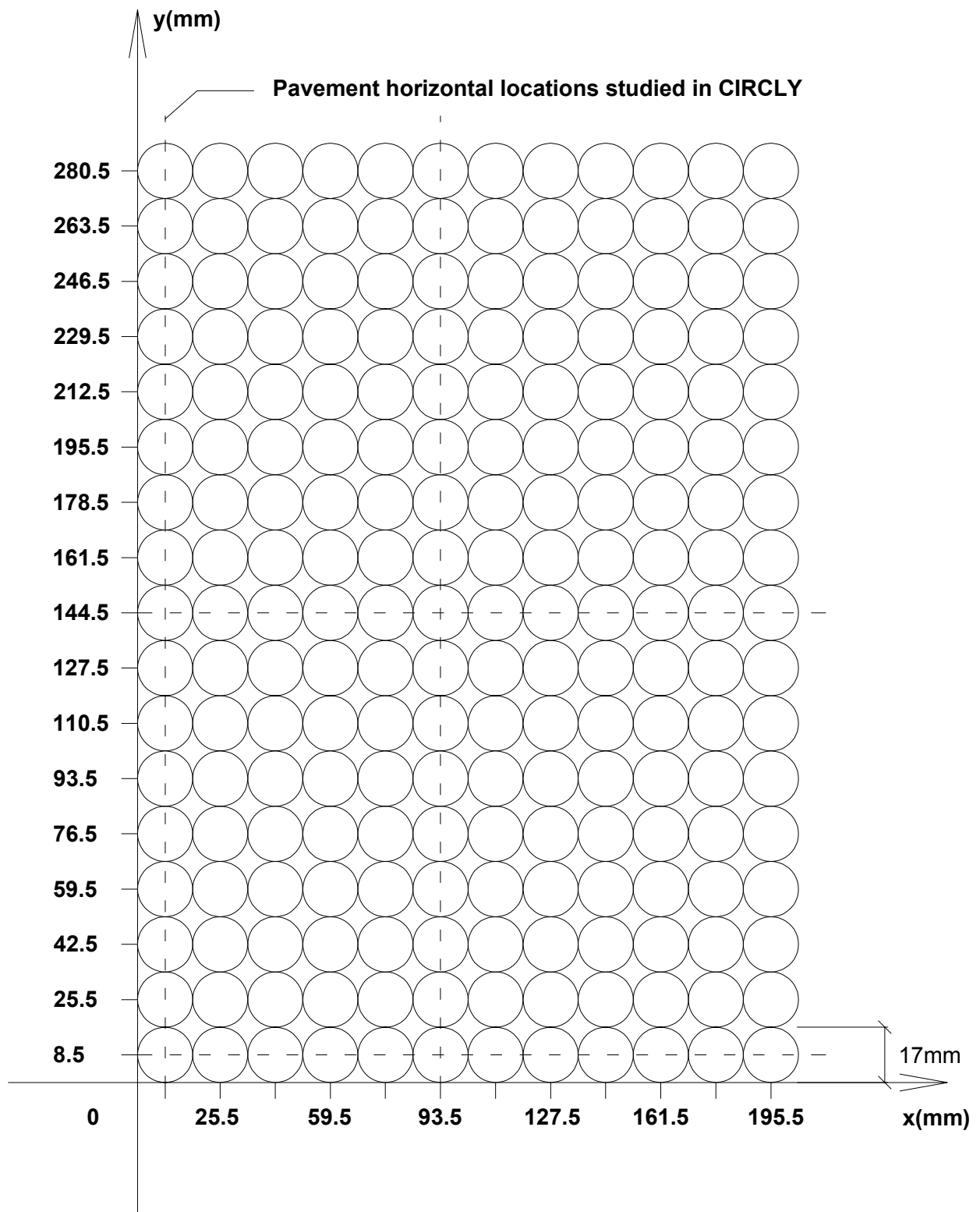


Figure 11. Pavement Horizontal Locations Studied in CIRCLY

The pavement responses under the tire edge and tire center were considered since they are the critical in all cases. In the case of LTEX013, for example, pavement strains along four lines were studied, as shown in Figure 11. Lines $x=8.5$ and $x=144.5$ mm were studied using the array layout shown in Figure 10(a) with a minimum of -8.5 to the maximum 212.5 with a step of 17mm. To analyze lines $y=8.5$ and $y=93.5$, the grid layout (Figure 10(b)) was used with the coordinates from 8.5–93.5 in the x -direction with a step of 85mm and from -8.5–297.5 in the y -direction with a step of 17mm. The step is an increment along the studied line, whose value was determined to obtain the pavement responses beneath the center of each load, where they were critical. The output data of CIRCLY was processed in Microsoft Excel. Recall there were 204 circular loads in this model, and each load caused pavement responses, including displacement, stress and strain. Therefore, there were 204 sets of pavement response data due to each load at the locations studied. All values of pavement responses at the same location were superimposed to obtain the summary response value of displacements, stresses and strains at the point under evaluation.

3.2.2 Model for Traditional Tire-Pavement Contact Conditions

As mentioned previously, tire-pavement contact pressure is assumed to be uniformly distributed over a circular contact area in most pavement design approaches, and the contact stress is assumed to be equal to the tire inflation pressure. To compare the pavement responses evaluated by the different models, the same pavement structures were used to study the nine cases given in Table 2. The radius of the circular contact area was calculated as follows:

$$\text{Contact Area} = \frac{\text{Load}}{\text{Tire Inflation Pressure}}$$

Equation 13

and

$$r = \sqrt{\frac{S}{\pi}} = \sqrt{\frac{L/p}{\pi}} = \sqrt{\frac{L}{p\pi}}$$

Equation 14

in which r = radius of contact area;

S = contact area;

L = applied load; and

p = tire inflation pressure, which is assumed to be equal to the contact stress.

Figure 12 illustrates the horizontal coordinate of the traditional design model of a single circle in the case of LTEX013. The radius of the load circle was 110.15 mm, and the contact stress was assumed to 690 kPa. Critical pavement responses were located under the centerline of a circular load and are symmetrically distributed. Therefore, the maximum pavement responses under the centerline of the circle were selected for analysis and compared with those of the model introduced in the previous section, in which actual measured stresses were used.

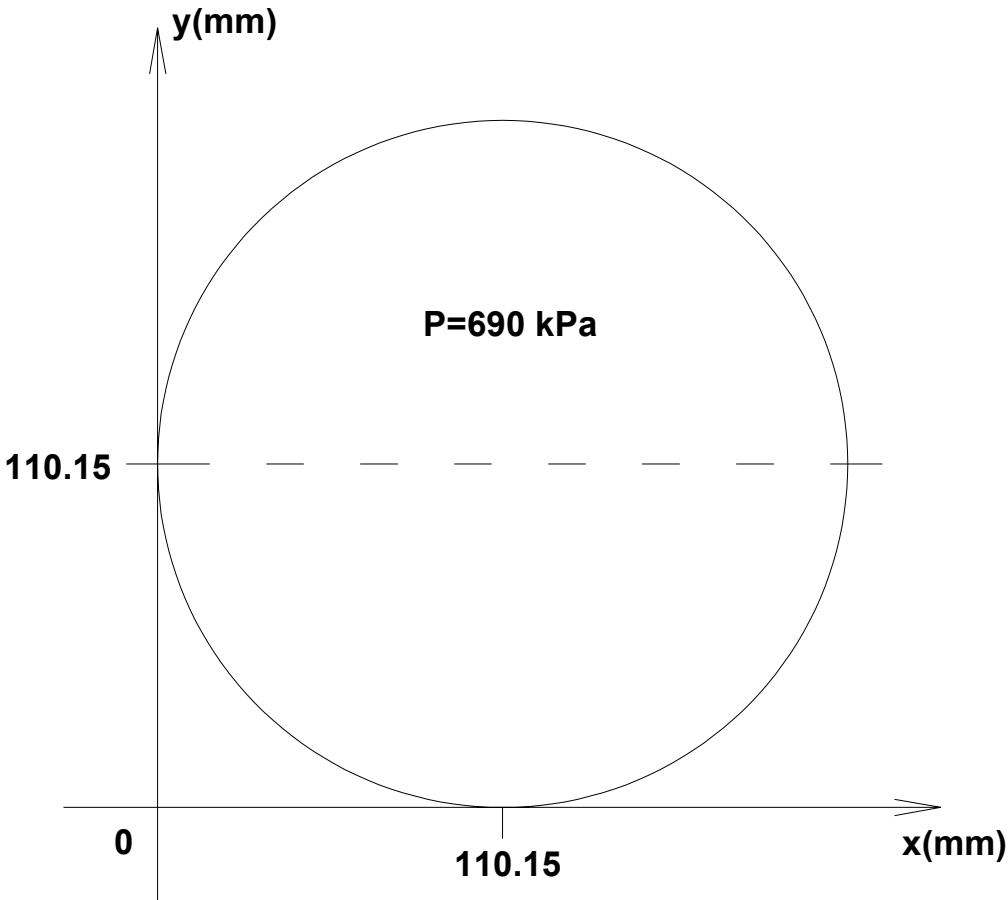


Figure 12. Traditional Model for LTEX013 in CIRCLY

3.3 Pavement Responses Evaluated in the Two Models

In both models, the maximum (critical) vertical and horizontal strains were found under the tire center, both for the surface layer and the subgrade. Surface horizontal strains (responsible for initiating top-down cracking) were not analyzed due to the uncertainty on the estimated values by means of linear elasticity. The strains through the centerline of the contact area in the two models are plotted and compared in Appendices 1–9. Tables 3, 4, and 5 give the maximum strains calculated by both models for each combination of pavement structure, tire inflation pressure and wheel loading. The pavement strains in these three tables are expressed in microstrain (10^{-6}). The values before the “/” represent pavement strains calculated using actual stress distribution (“new model”), while the values after the “/” represent the strains computed using uniform stress distribution (“traditional model”).

3.3.1 Pavement Strains Estimated in the Traditional Model

As can be seen in Tables 3, 4 and 5, wheel loading had a significant effect on the three types of strains studied. For the thin pavement (Pavement 1), the tensile strains at the bottom of the asphalt layer in both x -direction and y -direction decreased with the increase of wheel loading. When the pavement became thicker (Pavements 2, 3 and 4), the tensile strains in both directions increased with the increase in wheel loading. The compressive strains on the top of the subgrade followed an identical trend for the loading of all four pavement structures, i.e. the compressive strains increased with the increase of loading.

Tire inflation pressure is positively correlated to the tensile strains in both directions at the bottom of the asphalt layer for the four pavement structures studied. As the tire inflation pressure decreased from 793–586 kPa, the tensile strains at the bottom of the asphalt layer decreased significantly in both the x -direction and y -direction. However, tire pressure does not have a significant effect on the strains at the top of subgrade, which varies irregularly and slightly with the change of tire pressure.

The thickness of the asphalt layer plays an important role in the pavement strains. When the thickness increased, the tensile strains increased first to reach a critical value and then decreased

gradually. The compressive strains at the top of the subgrade decreased as the thickness of asphalt layer increased.

3.3.2 Pavement Strains Calculated in the New Model

Wheel loading affects the three types of strains. For the thin pavement structure (Pavements 1 and 2), as wheel load increases, most tensile strains in both x -direction and y -direction at the bottom of the asphalt layer increased initially and then decreased. This phenomenon may be explained by the thickness of the asphalt layer; when the asphalt layer thickness is relatively thin as compared to the load radius, tensile strains do not fully develop and a thin layer transfers more load through the layers beneath. For thicker pavement (Pavements 3 and 4), the increase in wheel loading was associated with increased tensile strains at the bottom of the asphalt layer. Compressive strains on the top of the subgrade were in direct proportion to wheel loading for the three pavement structures.

The higher tire pressure was associated with greater tensile strains at the bottom of the asphalt layer for all four pavement structures. The compressive strains on the top of the subgrade vary unsystematically with the increase in tire pressure for all three pavement structures.

The thickness of the asphalt layer affected the strains considerably. As the asphalt layer became thicker, the tensile strains at the bottom of the asphalt layer increased first to reach critical values and then decreased gradually.

Table 3. Comparison of Tensile Strains in the x -Direction at the Bottom of the Asphalt Layer (ϵ_{txx}) in the Two Models

(a) Pavement 1 (AC=40mm)

ϵ_{txx} ($\times 10^{-6}$, New/Traditional)		Target Load (kN)		
		24	27.5	31.1
Tire Inflation Pressure (kPa)	793	164 / 213	224 / 203	191 / 198
	690	150 / 177	190 / 173	189 / 163
	586	111 / 145	156 / 136	156 / 133

(b) Pavement 2 (AC=70mm)

ϵ_{txx} ($\times 10^{-6}$, New/Traditional)		Target Load (kN)		
		24	27.5	31.1
Tire Inflation Pressure (kPa)	793	173 / 214	215 / 221	205 / 224
	690	168 / 192	190 / 194	207 / 198
	586	142 / 166	176 / 169	180 / 169

(c) Pavement 3 (AC=100mm)

ϵ_{txx} ($\times 10^{-6}$, New/Traditional)		Target Load (kN)		
		24	27.5	31.1
Tire Inflation Pressure (kPa)	793	145 / 175	176 / 191	176 / 198
	690	144 / 165	158 / 170	178 / 181
	586	128 / 147	154 / 155	159 / 158

(d) Pavement 4 (AC=130mm)

ϵ_{txx} ($\times 10^{-6}$, New/Traditional)		Target Load (kN)		
		24	27.5	31.1
Tire Inflation Pressure (kPa)	793	117 / 133	141 / 151	144 / 159
	690	118 / 130	127 / 136	147 / 151
	586	107 / 119	128 / 132	133 / 136

Table 4. Comparison of Tensile Strains in the y -Direction at the Bottom of the Asphalt Layer (ϵ_{yy}) in the Two Models

(a) Pavement 1 (AC=40mm)

ϵ_{yy} ($\times 10^{-6}$, New/Traditional)		Target Load (kN)		
		24	27.5	31.1
Tire Inflation Pressure (kPa)	793	175 / 212	175 / 201	147 / 194
	690	149 / 175	149 / 171	146 / 158
	586	115 / 142	123 / 131	109 / 126

(b) Pavement 2 (AC=70mm)

ϵ_{yy} ($\times 10^{-6}$, New/Traditional)		Target Load (kN)		
		24	27.5	31.1
Tire Inflation Pressure (kPa)	793	180 / 214	192 / 221	181 / 224
	690	166 / 192	170 / 194	182 / 198
	586	141 / 166	157 / 169	150 / 169

(c) Pavement 3 (AC=100mm)

ϵ_{yy} ($\times 10^{-6}$, New/Traditional)		Target Load (kN)		
		24	27.5	31.1
Tire Inflation Pressure (kPa)	793	148 / 176	164 / 191	161 / 198
	690	142 / 165	147 / 170	162 / 181
	586	124 / 147	142 / 156	140 / 158

(d) Pavement 4 (AC=130mm)

ϵ_{yy} ($\times 10^{-6}$, New/Traditional)		Target Load (kN)		
		24	27.5	31.1
Tire Inflation Pressure (kPa)	793	118 / 133	134 / 151	135 / 159
	690	116 / 130	121 / 136	136 / 151
	586	104 / 119	120 / 132	120 / 136

Table 5. Comparison of Compressive Strains at the Top of the Subgrade (ϵ_{czz}) in the Two Models

(a) Pavement 1 (AC=40mm)

ϵ_{czz} ($\times 10^{-6}$, New/Traditional)		Target Load (kN)		
		24	27.5	31.1
Tire Inflation Pressure (kPa)	793	160 / 163	194 / 197	212 / 215
	690	167 / 169	180 / 182	216 / 218
	586	160 / 163	193 / 194	205 / 207

(b) Pavement 2 (AC=70mm)

ϵ_{czz} ($\times 10^{-6}$, New/Traditional)		Target Load (kN)		
		24	27.5	31.1
Tire Inflation Pressure (kPa)	793	136 / 138	165 / 167	180 / 182
	690	142 / 143	153 / 155	184 / 185
	586	136 / 138	164 / 165	174 / 176

(c) Pavement 3 (AC=100mm)

ϵ_{czz} ($\times 10^{-6}$, New/Traditional)		Target Load (kN)		
		24	27.5	31.1
Tire Inflation Pressure (kPa)	793	115 / 116	140 / 141	153 / 154
	690	120 / 121	130 / 131	156 / 157
	586	115 / 117	139 / 140	148 / 149

(d) Pavement 4 (AC=130mm)

ϵ_{czz} ($\times 10^{-6}$, New/Traditional)		Target Load (kN)		
		24	27.5	31.1
Tire Inflation Pressure (kPa)	793	98 / 99	119 / 120	130 / 131
	690	102 / 103	110 / 111	133 / 134
	586	98 / 99	118 / 119	126 / 127

Chapter 4. Comparison of Pavement Strains Estimated by Different Models

4.1 Absolute Strain Difference between Two Models

4.1.1 Absolute Difference of Tensile Strains between the Two Models at the Bottom of the Asphalt Layer

Tables 6 and 7 give the absolute differences of tensile strains at the bottom of the asphalt layer in the x -direction and y -direction. Equation 15 shows the calculation of the absolute strain difference. The negative sign indicates that the tensile strains calculated by the traditional model are less than that computed by the new model. As a result, a positive strain difference implies the traditional model overestimates the actual strains, while a negative strain difference shows the traditional model underestimates the actual strains. Tables 6 and 7 exhibit that the traditional model may overestimate the tensile strains in the y -direction for all the experimental combinations and the tensile strains in the x -direction for thick pavements; however, for a combination of thin pavement, low tire pressure and large wheel loading, the traditional model may underestimate the actual strains.

$$\text{Absolute Strain Difference} = \varepsilon_T - \varepsilon_N$$

Equation 15

To study the relationship between the strain difference and the asphalt layer thickness, the wheel loading inflation pressure, linear regression analysis is used for the two types of tensile strains.

Equations 16 and 17 and show the regression model on the tensile strain at the bottom of the asphalt layer in the x -direction and y -direction respectively. Table 8 and Table 9 give the regression statistics, which indicate the reliability of the two regression models.

$$D = 49.3445 + 0.1026 \cdot H + (-3.5714) \cdot L + 0.0699 \cdot P$$

Equation 16

$$D = -10.4428 + (-0.0941) \cdot H + (-0.1108) \cdot L + 0.0635 \cdot P$$

Equation 17

in which D = strain difference between the two models;

H = thickness of asphalt layer;

L = wheel loading;

P = tire inflation pressure.

Table 6. Absolute Difference of Tensile Strains in the x -Direction at the Bottom of the Asphalt Layer (ε_{txx}) between the Two Models

(a) Pavement 1

ε_{txx} Difference ($\times 10^{-6}$)		Target Load (kN)		
		24	27.5	31.1
Tire Inflation Pressure (kPa)	793	49	-21	7
	690	27	-17	-26
	586	34	-20	-23

(b) Pavement 2

ε_{txx} Difference ($\times 10^{-6}$)		Target Load (kN)		
		24	27.5	31.1
Tire Inflation Pressure (kPa)	793	41	6	19
	690	24	-17	-9
	586	24	-7	-11

(c) Pavement 3

ε_{txx} Difference ($\times 10^{-6}$)		Target Load (kN)		
		24	27.5	31.1
Tire Inflation Pressure (kPa)	793	30	15	22
	690	21	12	3
	586	19	1	-1

(d) Pavement 4

ε_{txx} Difference ($\times 10^{-6}$)		Target Load (kN)		
		24	27.5	31.1
Tire Inflation Pressure (kPa)	793	16	10	15
	690	12	9	4
	586	12	4	3

Table 7. Absolute Difference of Tensile Strains in the y -Direction at the Bottom of the Asphalt Layer (ε_{yy}) between the Two Models

(a) Pavement 1

ε_{yy} Difference ($\times 10^{-6}$)		Target Load (kN)		
		24	27.5	31.1
Tire Inflation Pressure (kPa)	793	37	26	47
	690	26	22	12
	586	27	8	17

(b) Pavement 2

ε_{yy} Difference ($\times 10^{-6}$)		Target Load (kN)		
		24	27.5	31.1
Tire Inflation Pressure (kPa)	793	34	29	43
	690	26	22	16
	586	25	12	19

(c) Pavement 3

ε_{yy} Difference ($\times 10^{-6}$)		Target Load (kN)		
		24	27.5	31.1
Tire Inflation Pressure (kPa)	793	28	27	37
	690	23	23	19
	586	23	14	18

(d) Pavement 4

ε_{yy} Difference ($\times 10^{-6}$)		Target Load (kN)		
		24	27.5	31.1
Tire Inflation Pressure (kPa)	793	15	17	24
	690	14	15	15
	586	15	12	16

Table 8. Regression Statistics of Model on the Absolute Difference of Tensile Strains in x - Direction at the Bottom of the Asphalt Layer

	Coefficients	Standard Error	t Stat	P-value
Intercept	49.3445	29.6522	1.6641	0.1059
AC Thickness	0.1026	0.0690	1.4873	0.1467
Load	-3.5714	0.7982	-4.4743	0.0001
Pressure	0.0699	0.0274	2.5548	0.0156

Table 9. Regression Statistics of Model on the Absolute Difference of Tensile Strains in y - Direction at the Bottom of the Asphalt Layer

	Coefficients	Standard Error	t Stat	P-value
Intercept	-10.4428	14.2882	-0.7309	0.4702
AC Thickness	-0.0941	0.0332	-2.8302	0.0080
Load	-0.1108	0.3846	-0.2880	0.7752
Pressure	0.0635	0.0132	4.8164	0.0000

As can be seen from Equation 16, wheel loading is the most important parameter affecting the strain difference in the x -direction. A larger load yields a smaller strain difference. Asphalt layer thickness and tire inflation pressure have a slight effect on the strain difference. When either the asphalt thickness or tire pressure is increased, the strain difference will be increased in a small amount. As a result, the traditional model, which is based on a circular load area with uniform contact stress, tends to overestimate the actual tensile strains at the bottom of the asphalt layer when the wheel load is relatively low. When wheel loading increases, the traditional model may properly simulate the actual strains or even underestimate tensile strains.

Based on Equation 17, the tensile strains in the y -direction do not show a strong relationship with wheel loading, tire pressure or asphalt thickness. An increase in asphalt thickness or wheel loading may result in a slight decrease in strain difference. In the meantime, the increase in tire inflation pressure leads to a small increase in strain difference.

4.1.2 *Absolute Difference of Compressive Strains at the Top of the Subgrade between the Two Models*

Table 10 shows the absolute difference of compressive strains at the top of the subgrade between the two models. Apparently, this difference was in the range from 1–3 as changes occurred with asphalt thickness, wheel loading or tire pressure. In other words, this difference was minimally affected by the above three factors. The strain difference remained constant as a value of 1 particularly when the asphalt layer was thick.

Table 10. Absolute Difference of Compressive Strains at the Top of the Subgrade (ϵ_{czz}) between the Two Models

(a) Pavement 1

ϵ_{czz} Difference ($\times 10^{-6}$)		Target Load (kN)		
		24	27.5	31.1
Tire Inflation Pressure (kPa)	793	3	3	3
	690	2	2	2
	586	3	1	2

(b) Pavement 2

ϵ_{czz} Difference ($\times 10^{-6}$)		Target Load (kN)		
		24	27.5	31.1
Tire Inflation Pressure (kPa)	793	2	2	2
	690	1	2	1
	586	2	1	2

(c) Pavement 3

ϵ_{czz} Difference ($\times 10^{-6}$)		Target Load (kN)		
		24	27.5	31.1
Tire Inflation Pressure (kPa)	793	1	1	1
	690	1	1	1
	586	2	1	1

(d) Pavement 4

ϵ_{czz} Difference ($\times 10^{-6}$)		Target Load (kN)		
		24	27.5	31.1
Tire Inflation Pressure (kPa)	793	1	1	1
	690	1	1	1
	586	1	1	1

From a statistical view, the regression model (Equation 18) also proved the weak correlation between strain difference with the asphalt thickness, wheel load and tire inflation pressure. Table 11 shows the regression statistics of this mode. Since the strain difference was very small (in 3×10^{-6}) and it varied slightly, the traditional model may properly estimate the actual compressive strains on the top of the subgrade under any combination of load conditions, tire pressure, and pavement structures.

$$D = 2.5046 + (-0.0141) \cdot H + (-0.0231) \cdot L + 0.0012 \cdot P$$

Equation 18

Table 11. Regression Statistics of Model on the Absolute Difference of Compressive Strains

	Coefficients	Standard Error	t Stat	P-value
Intercept	2.5046	1.0973	2.2826	0.0292
AC Thickness	-0.0141	0.0026	-5.5136	0.0000
Load	-0.0231	0.0295	-0.7835	0.4391
Pressure	0.0012	0.0010	1.1863	0.2442

4.2 Relative Strain Difference between Two Models

4.2.1 Relative Difference of Tensile Strains at the Bottom of the Asphalt Layer between the Two Models

Table 12 and Table 13 show the relative differences (in percentage) of tensile strains at the bottom of the asphalt layer between the two models. The relative difference of strains is calculated as follows:

$$\text{Relative Strain Difference} = \frac{\varepsilon_T - \varepsilon_N}{\varepsilon_T} \times 100\%$$

Equation 19

in which ε_T = strains calculated by the traditional model; and
 ε_N = strains calculated by the new model.

Table 12. Relative Difference of Tensile Strains in the x -Direction at the Bottom of the Asphalt Layer (ε_{txx}) between the Two Models

(a) Pavement 1

ε_{txx} Difference (%)		Target Load (kN)		
		24	27.5	31.1
Tire Inflation Pressure (kPa)	793	22.75	-10.56	3.53
	690	15.03	-9.74	-15.82
	586	23.50	-14.34	-17.17

(b) Pavement 2

ε_{txx} Difference (%)		Target Load (kN)		
		24	27.5	31.1
Tire Inflation Pressure (kPa)	793	19.01	2.57	8.34
	690	12.45	2.18	-4.34
	586	14.44	-4.45	-6.59

(c) Pavement 3

ε_{txx} Difference (%)		Target Load (kN)		
		24	27.5	31.1
Tire Inflation Pressure (kPa)	793	17.28	7.96	11.02
	690	12.78	7.55	1.62
	586	13.33	1.08	-0.74

(d) Pavement 4

ε_{txx} Difference (%)		Target Load (kN)		
		24	27.5	31.1
Tire Inflation Pressure (kPa)	793	11.77	6.63	9.22
	690	9.31	6.76	3.13
	586	10.21	2.96	2.06

Table 13. Relative Difference of Tensile Strains in the y -Direction at the Bottom of the Asphalt Layer (ϵ_{yy}) Between the Two Models

(a) Pavement 1

ϵ_{yy} Difference (%)		Target Load (kN)		
		24	27.5	31.1
Tire Inflation Pressure (kPa)	793	17.76	12.69	24.17
	690	14.84	12.80	7.26
	586	19.06	6.21	13.55

(b) Pavement 2

ϵ_{yy} Difference (%)		Target Load (kN)		
		24	27.5	31.1
Tire Inflation Pressure (kPa)	793	15.99	13.05	19.22
	690	13.30	12.29	8.29
	586	15.38	6.95	11.30

(c) Pavement 3

ϵ_{yy} Difference (%)		Target Load (kN)		
		24	27.5	31.1
Tire Inflation Pressure (kPa)	793	15.57	14.37	18.57
	690	14.16	13.55	10.21
	586	15.49	8.70	11.71

(d) Pavement 4

ϵ_{yy} Difference (%)		Target Load (kN)		
		24	27.5	31.1
Tire Inflation Pressure (kPa)	793	10.82	11.35	15.25
	690	10.91	11.05	9.81
	586	12.83	8.90	11.70

The values in Table 12 suggest that the traditional model overestimates the tensile strains in the x -direction in most cases, while under a combination of thin asphalt layer, low tire pressure and large wheel loading, the traditional model may underestimate the actual strains. The relative difference of the tensile strains in the x -direction at the bottom of the asphalt layer was significant, up to 24 percent.

Next, regression analysis was applied to quantify the relationship between the absolute strain difference and wheel loading, asphalt thickness and tire pressure. As can be seen from the regression model shown in Equation 20, only the wheel loading has significant negative correlation with this strain difference and the other two variables have slight positive effect on it. This formula also indicates the underestimation of traditional model on the type of tensile strains under a combination of thin asphalt layer, low tier pressure and large load. The details of the regression analysis are presented in Table 14.

$$D = 34.5462 + 0.0825 \cdot H + (-2.1919) \cdot L + 0.0343 \cdot P$$

Equation 20

The differences of tensile strains in the y -direction at the bottom of asphalt layer in Table 13 are all positive, which implies that the traditional model overestimate this type of strains in all the experimental combinations. The regression model in Equation 21 shows that all the three parameters do not have strong relationship with this relative strains difference, which stays in a relatively small range with an average of 13 percent and a standard deviation of 3.8.

$$D = 6.9770 + (-0.0261) \cdot H + (-0.1728) \cdot L + 0.0189 \cdot P$$

Equation 21

Table 14. Regression Statistics of Model on the Relative Difference of Tensile Strains in x - Direction at the Bottom of the Asphalt Layer

	Coefficients	Standard Error	t Stat	P-value
Intercept	34.5462	15.5070	2.2278	0.0331
AC Thickness	0.0825	0.0361	2.2883	0.0289
Load	-2.1919	0.4174	-5.2509	0.0000
Pressure	0.0343	0.0143	2.3940	0.0227

Table 15. Regression Statistics of Model on the Relative Difference of Tensile Strains in y -Direction at the Bottom of the Asphalt Layer

	Coefficients	Standard Error	t Stat	P-value
Intercept	6.9770	7.3483	0.9495	0.3495
AC Thickness	-0.0261	0.0171	-1.5296	0.1359
Load	-0.1728	0.1978	-0.8737	0.3888
Pressure	0.0189	0.0068	2.7854	0.0089

4.2.2 *Relative Difference of Compressive Strains at the Top of the Subgrade between the Two Models*

Table 16 shows the relative differences of compressive strains at the top of the subgrade between the two models, which are quite small, i.e. within 2 percent. Relative difference stays within 1 percent particularly for the thick pavement (Pavement 4 for example).

Regression analysis can be used to prove the poor link between relative strain difference and the three parameters (load, tire pressure and asphalt thickness). The regression model, Equation 22, implies the weak relationships. Asphalt layer thickness, wheel loading and inflation pressure do not show definite direct or inverse ratios to the difference of strains calculated by other models. The regression statistics, shown in Table 17, indicate the strong reliability of this regression. Since the strain difference is small and varies slightly, it is indicated that for the cases evaluated, the traditional model is reliable for estimating the compressive strains on the top of the subgrade.

$$D = 1.9288 + (-0.0056) \cdot H + (-0.0435) \cdot L + 0.0010 \cdot P$$

Equation 22

Table 16. Relative Difference of Compressive Strains at the Top of the Subgrade (ϵ_{czz}) between the Two Models

(a) Pavement 1

ϵ_{czz} Difference (%)		Target Load (kN)		
		24	27.5	31.1
Tire Inflation Pressure (kPa)	793	1.53	1.34	1.43
	690	1.34	1.31	0.95
	586	1.53	0.82	1.00

(b) Pavement 2

ϵ_{czz} Difference (%)		Target Load (kN)		
		24	27.5	31.1
Tire Inflation Pressure (kPa)	793	1.29	1.08	1.15
	690	1.14	1.11	0.77
	586	1.30	0.70	0.84

(c) Pavement 3

ϵ_{czz} Difference (%)		Target Load (kN)		
		24	27.5	31.1
Tire Inflation Pressure (kPa)	793	1.12	0.93	0.91
	690	0.91	0.88	0.64
	586	1.12	0.56	0.72

(d) Pavement 4

ϵ_{czz} Difference (%)		Target Load (kN)		
		24	27.5	31.1
Tire Inflation Pressure (kPa)	793	0.94	0.81	0.74
	690	0.82	0.78	0.55
	586	0.97	0.51	0.59

Table 17. Regression Statistics of the Model on the Relative Difference of Compressive Strains

	Coefficients	Standard Error	t Stat	P-value
Intercept	1.9288	0.2962	6.5115	0.0000
AC Thickness	-0.0056	0.0007	-8.1750	0.0000
Load	-0.0435	0.0080	-5.4572	0.0000
Pressure	0.0010	0.0003	3.8381	0.0006

Chapter 5. Conclusions and Recommendations

Most of the traditional pavement design methods assume that tire-pavement contact stresses are uniformly distributed on a circular area. Actual measurements, however, showed that the contact stresses are not uniform and the contact area is not a circular shape. To study the actual pavement response and evaluate the adequacy of a traditional pavement design model, the experiment-measured actual tire-pavement contact stresses are employed to calculate the pavement responses by the computer program CIRCLY. The traditional model with uniform contact stress over a circular shape was also used to compute the pavement responses at pavement interfaces. Pavement strains calculated by these two models were compared and the differences between them were analyzed.

Four pavement structures, three tire inflation pressure levels and three wheel loads comprised a factorial experiment to quantify the effect of the three parameters on the strain difference between the two modes. The four pavement structures selected had the same base, subbase, subgrade, and asphalt material. The only difference among them was the thickness of the asphalt layer, which varied from 40–130 mm, respectively, for each pavement structure. Tire inflation pressure levels were 586 kPa, 690 kPa, and 793 kPa, and the target wheel loading levels were 24 kN, 27.5 kN, and 31.1 kN.

The new model, which used the actual measured contact stresses, divided the contact area into a number of small circles, each with a radius of 8.5mm, and was regarded as a load component with an assigned value of contact stress. Each circular load produced pavement responses. Pavement strains produced by each load were superimposed to obtain the total strains at specific locations studied. The pavement responses considered are the tensile strains at the bottom of the asphalt layer, which is related to pavement fatigue cracking, and the compressive strains on the top of the subgrade, which controls pavement rutting. Three types of pavement strains were studied in this research, including compressive strains on the top of the subgrade, and tensile strains at the bottom of the asphalt layer in the x -direction and in the y -direction.

Both absolute difference and relative difference were studied between the two models by statistical regression analysis. Most of the strains calculated by the traditional model were greater than those computed by the new model, which indicated an over-estimation of pavement strains. The difference was significant — up to 23 percent. Wheel loading exhibited the most important effect on both absolute and relative difference of tensile strains in the x -direction. When the effect of wheel load was relatively low, the traditional model overestimated the tensile strains in the x -direction. As the wheel load increased, the difference between the two models decreased gradually to zero, and the strains calculated by the traditional model became less than those computed by the new model. Results indicated the traditional model's underestimation of the tensile strains in the x -direction at the bottom of the asphalt layer. A combination of high load, low tire pressure and thin asphalt layer may lead to the underestimation by the traditional model on the tensile strains in the x -direction. Asphalt thickness and tire inflation pressure do not significantly affect both strain differences.

The traditional model overestimated the tensile strain difference in the y -direction in all the combinations studied. Variations of the relative differences were within a small range with a mean of 13.03 percent and a standard deviation of 3.8. The three parameters did not show a strong relationship with both absolute and relative strain differences.

For the compressive strains on the top of the subgrade, both absolute difference and relative difference were small and varied slightly with the change of asphalt thickness, wheel load and tire pressure. As a result, the traditional model could be considered adequate and reliable in calculating the compressive strains on the top of the subgrade, and therefore properly predicted pavement rutting.

Since pavement fatigue cracking is regarded to be determined by the tensile strains at the bottom of the asphalt layer, and pavement rutting is controlled by the compressive strains on the top of the subgrade, estimating pavement performance in terms of critical responses is an interesting area for further research. Based on the strain difference of the two models stated in this paper, the traditional pavement transfer functions may be adjusted for more accurate prediction on pavement performance. The effect of the variables on pavement behavior may be quantified to

assist with the process of pavement design and analysis. Guidelines and recommendations can be advanced to specifically address the differences between expected performance under uniform stress assumption and performance under actual tire-pavement contact stress distribution.

In summary, the findings of this research suggest that there are significant differences in critical pavement response when the uniform and actual contact stress distributions are compared. However, if wheel load and tire inflation pressure are known, this difference can be accounted for by means of relatively simple models as those developed in this research.

References

1. Blab, R. "Introducing Improved Loading Assumptions into Analytical Pavement Models Based on Measured Contact Stresses of Tires." *Proceedings of the International Conference on Accelerated Pavement Testing, No. CS5-3*. Reno, NV, 1999. This paper is available online at: <http://www.ksu.edu/pavements/trb/A2B09/CS05-03.PDF>
2. Bonaquist, R., R. Surdahl, and W. Mogawer. Effect of Tire Pressure on Flexible Pavement Response and Performance. *Transportation Research Record No. 1227*, Transportation Research Board, Washington D.C., 1989, pp97-106.
3. Chatti, K., H.B. Kim, K.K. Yun, J.P. Mahoney, and C.L. Monismith. "Field Investigation into Effects of Vehicle Speed and Tire Pressure on Asphalt Concrete Pavement Strains." *Transportation Research Record No. 1539*, Transportation Research Board, Washington D.C., 1996, pp66-71.
4. De Beer, M., and C. Fisher. *Contact Stresses of Pneumatic Tires Measured with the Vehicle-Road Surface Pressure Transducer Array (VRSPTA) System for the University of California at Berkeley (UCB) and the Nevada Automotive Test Center (NATC)*. Division of Roads and Transport Technology, CSIR, South Africa, Research Report No. CR-97/053, June 1997.
5. De Beer, M., C. Fisher and F. J. Jooste. "Determination of Pneumatic Tyre/Pavement Interface Contact Stresses under Moving Loads and Some Effects on Pavements with Thin Asphalt Surfacing Layers." *Proceedings of the 8th International Conference on Asphalt Pavements, Volume I*. Seattle, Washington. August 10-14, 1997, pp179-227.
6. De Beer, M., and C. Fisher. Tire Contact Stress Measurements with the Stress-In-Motion (SIM) Mk IV System for the Texas Transportation Institute (TTI). Under Research Project 0-4361 funded by the Texas Transportation Department, November 2002.
7. Himeno, K., and T. Ikeda. "Distribution of Tire Contact Pressure of Vehicles and Its Influence on Pavement Distress." *Proceedings of the 8th International Conference on Asphalt Pavements, Volume I*. Seattle, Washington. August 10-14, 1997, pp127-139.
8. Huang, Y. H. *Pavement Analysis and Design*. Prentice-Hall, Inc., Englewood Cliffs, New Jersey, 1993.

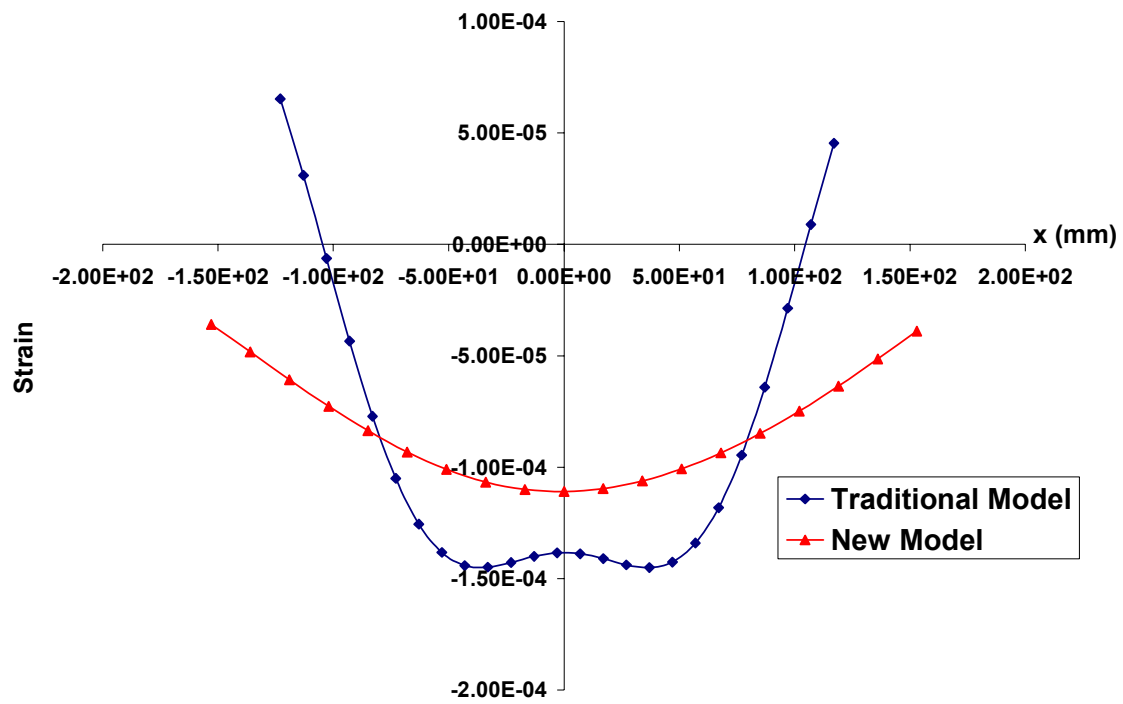
9. Huhtala, M., J. Pihlajamaki, and M. Pienimaki. "Effects of Tires and Tire Pressures on Road Pavements." *Transportation Research Record No. 1227*, Transportation Research Board, Washington D.C., 1989, pp107-114.
10. Kestler, M.A., R.L. Berg, and T.L. Moore. "Reducing Damage to Low-Volume Roads by Using Trucks with Reduced Tire Pressures." *Transportation Research Record No. 1589*, Transportation Research Board, Washington D.C., 1997, pp9-18.
11. Marshek, K.M., W. R. Hudson, R. B. Connell, H. H. Chen, and C. L. Saraf. *Experimental Investigation of Truck Tire Inflation Pressure on Pavement-Tire Contact Area and Pressure Distribution*. The University of Texas at Austin, Center for Transportation Research, Research Report 386-1, August 1985.
12. Marshek, K.M., W. R. Hudson, H. H. Chen, and C. L. Saraf, and R. B. Connell. *Effect of Truck Tire Inflation Pressure and Axle Load on Pavement Performance*. The University of Texas at Austin, Center for Transportation Research, Research Report 386-2F, August 1985.
13. Marshek, K.M., W. R. Hudson, R. B. Connell, H. H. Chen, and C. L. Saraf. "Effect of Truck Tire Inflation Pressure and Axle Load on Pavement Performance." *Transportation Research Record No. 1070*, Transportation Research Board, Washington D.C., 1986, pp14-21.
14. MINCAD Systems Pty. Ltd. *CIRCLY 4 User Manual*. February 1999.
15. Owende, P.M.O., A.M. Hartman, S.M. Ward, M.D. Gilchrist, and M.J. O'Mahony. "Minimizing Distress on Flexible Pavements Using Variable Tire Pressure." *ASCE Journal of Transportation Engineering*, Vol.127, No. 3, 2001, pp254-262.
16. Pezo, R.F., K. M. Marshek, and W. R. Hudson. *Truck Tire Pavement Contact Pressure Distribution Characteristics for the Bias Goodyear 18-22.5, the Radial Michelin 275/80R/24.5, the Radial Michelin 255/70R/22.5, and the Radial Goodyear 11R24.5 Tires*. The University of Texas at Austin, Center for Transportation Research, Research Report 1190-2F, September 1989.
17. Roberts, F.L., J. T. Tielking, D. Middleton, R. L. Lytton, and K. Tseng. *The Effect of Tire Pressures on Flexible Pavements*. Texas Transportation Institute, Texas A&M University System, College Station, Research Report 372-1F, Texas, August 1986.

18. Sebaaly, P.E., and N. Tabatabaee. "Effect of Tire Pressure and Type on Response of Flexible Pavement." *Transportation Research Record No. 1227*, Transportation Research Board, Washington D.C., 1989, pp115-127.
19. Sebaaly, P.E., and N. Tabatabaee. "Effect of Tire Parameters on Pavement Damage and Load-Equivalency Factors." *ASCE Journal of Transportation Engineering*, Vol. 118, No. 6, 1992, pp805-819.
20. Sebaaly, P.E. *Dynamic Forces on Pavements: Summary of Tire Testing Data*. Report on FHWA Project DTFH 61-90-C-00084, 1992.
21. Siddharthan, R.V., N. Krishnamenon, M. El-Mously, and P.E. Sebaaly. "Investigation of Tire Contact Stress Distributions on Pavement Response." *ASCE Journal of Transportation Engineering*, Vol. 128, No. 2, 2002, pp136-144.
22. Tielking, J.T., and F.L. Roberts. "Tire Contact Pressure and Its Effect on Pavement Strain." *ASCE Journal of Transportation Engineering*, Vol. 113, No.1, 1987, pp56-71.
23. Wang, F., R. F. Inman, R. B. Machemehl, Z. Zhang, and C. M. Walton. *Study of Current Truck Configurations*. The University of Texas at Austin, Center for Transportation Research, Research Report 0-1862-1, December 2000.
24. Wang, F., and R. B. Machemehl. "Study of Truck Tire Pressure in Texas." *Proceedings of the 7th International Conference on Applications of Advanced Technology in Transportation*. Cambridge, Massachusetts, 2002, pp489-496.
25. Wang, F., R. B. Machemehl, R. F. Inman, Z. Zhang, and C. M. Walton. "A Survey Study of Current Pavement-Related Truck Characteristics in Texas." *Proceedings of the 30th Annual Canadian Society of Civil Engineering (CSCE) Conference*. Montreal, Quebec, Canada, June 2002.
26. Wang, F., and R. B. Machemehl. "The Current Status and Variability of In-Service Truck Tire Pressures in Texas." *Transportation Research Record No. 1853*, Transportation Research Board, Washington D.C., 2003, pp157-164.
27. Weissman, S.L. "Influence of Tire-Pavement Contact Stress Distribution on Development of Distress Mechanisms in Pavements." *Transportation Research Record No. 1655*, Transportation Research Board, Washington D.C., 1999, pp161-167.
28. Woods, K.B. (Editor). *Highway Engineering Handbook*. McGraw-Hill, Inc., New York, 1960.

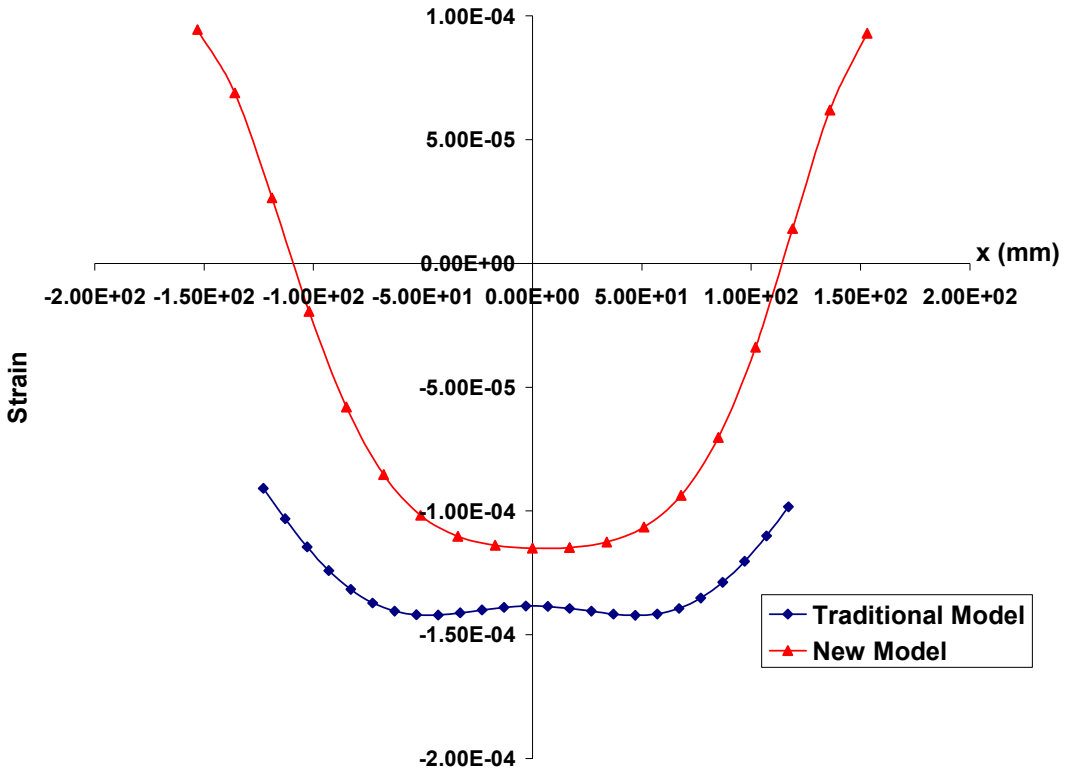
29. Yue, Z.Q., and O.J. Svec. "Effects of Tire-pavement Contact Pressure Distributions on the Response of Asphalt Concrete Pavement." *Canadian Journal of Civil Engineering*, Vol. 22, 1995, pp849-860.

Appendix 1: Strain Comparison in LTEX007 (L=23.5 kN, P=586 kPa)

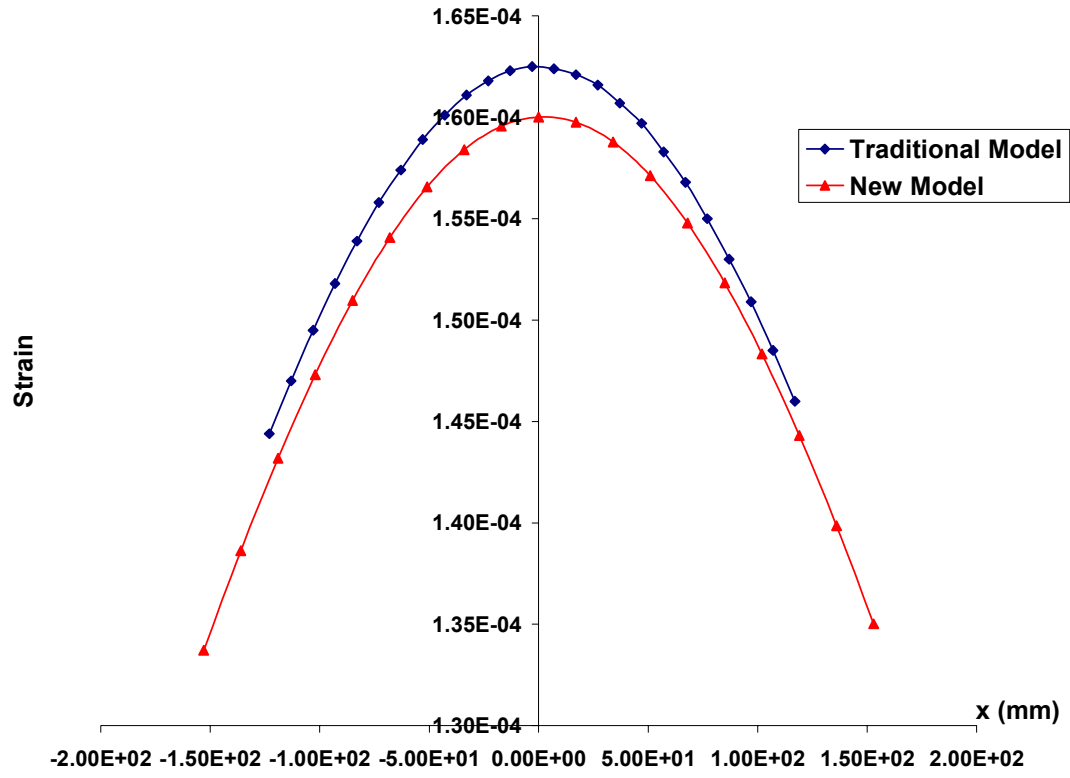
A. Pavement 1



(a) ϵ_{txx}

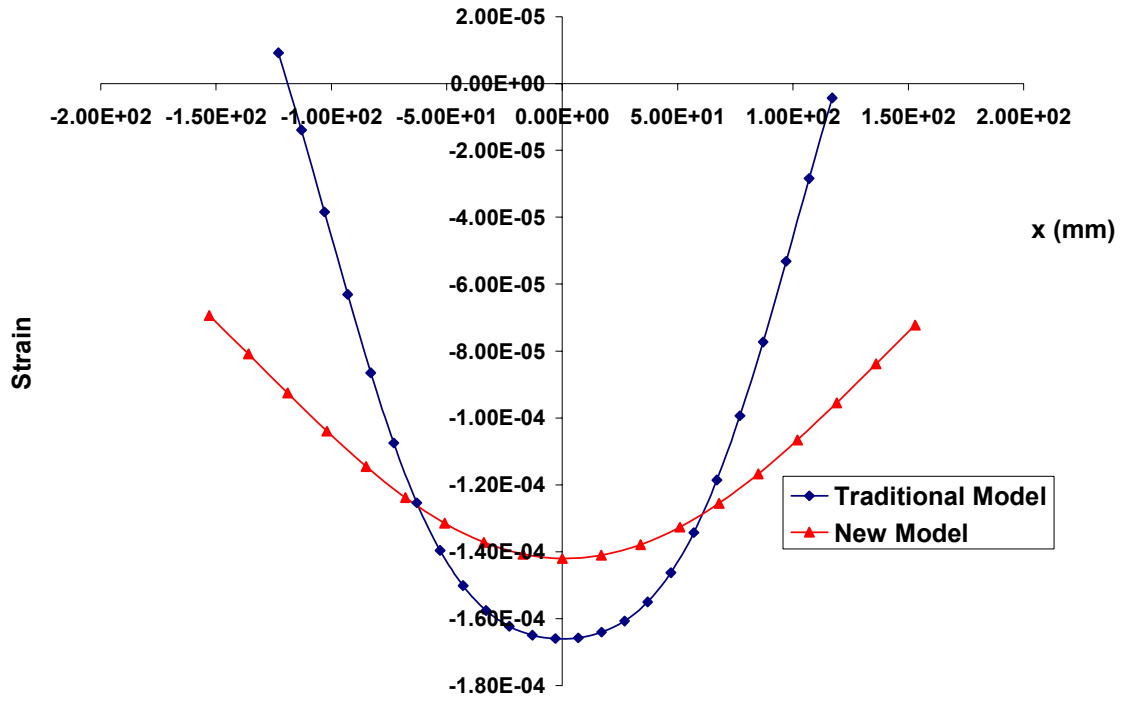


(b) ϵ_{yy}

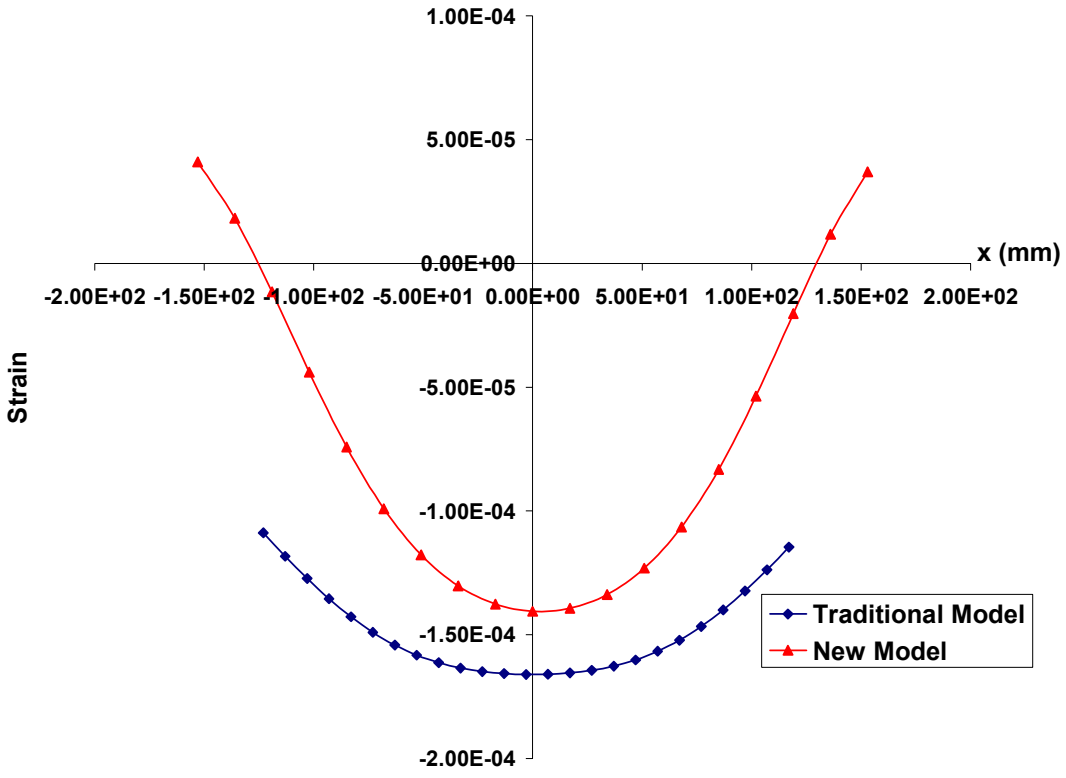


(c) ϵ_{czz}

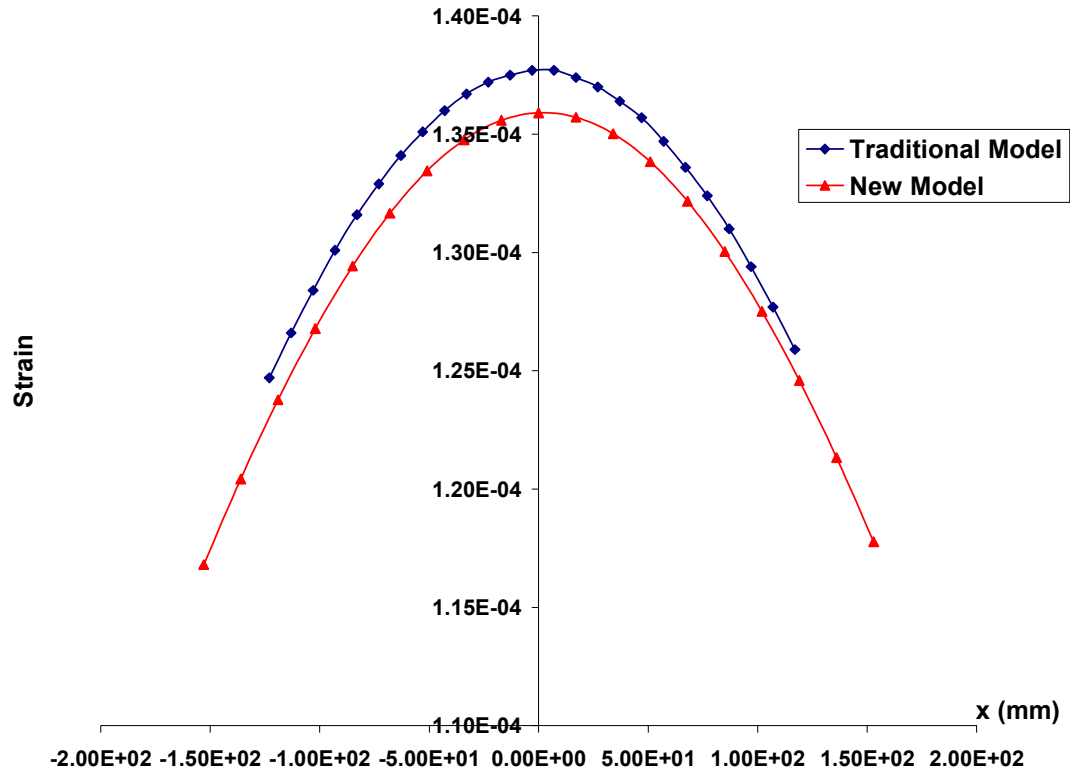
B. Pavement 2



(a) ϵ_{txx}

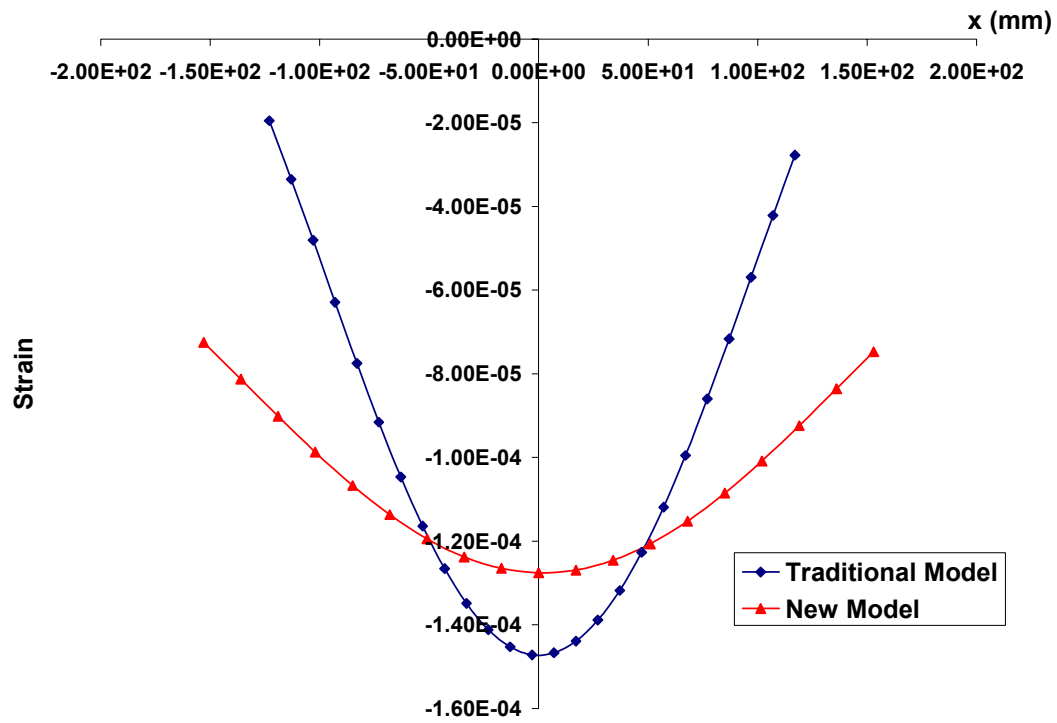


(b) ϵ_{yy}

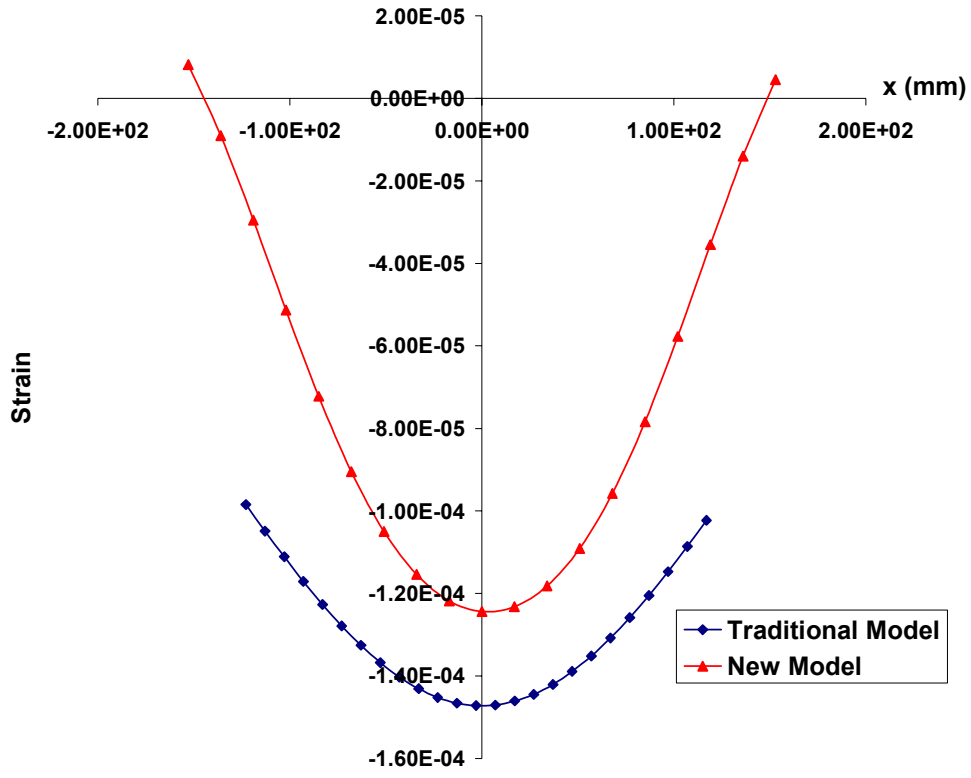


(c) ϵ_{czz}

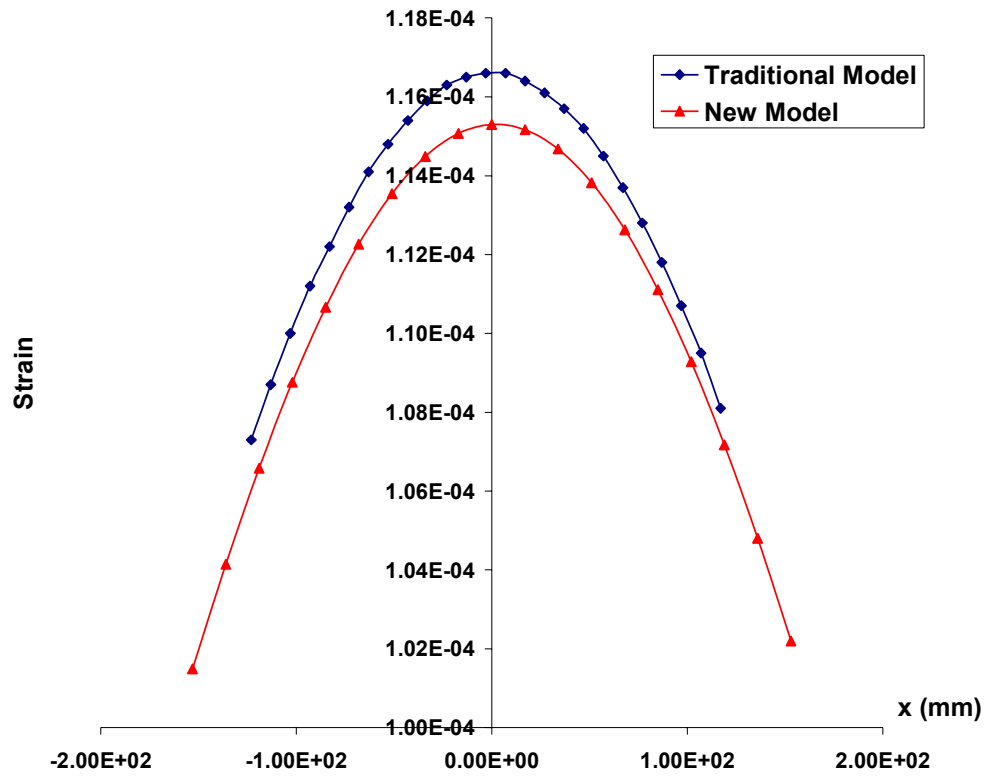
C. Pavement 3



(a) ϵ_{txx}

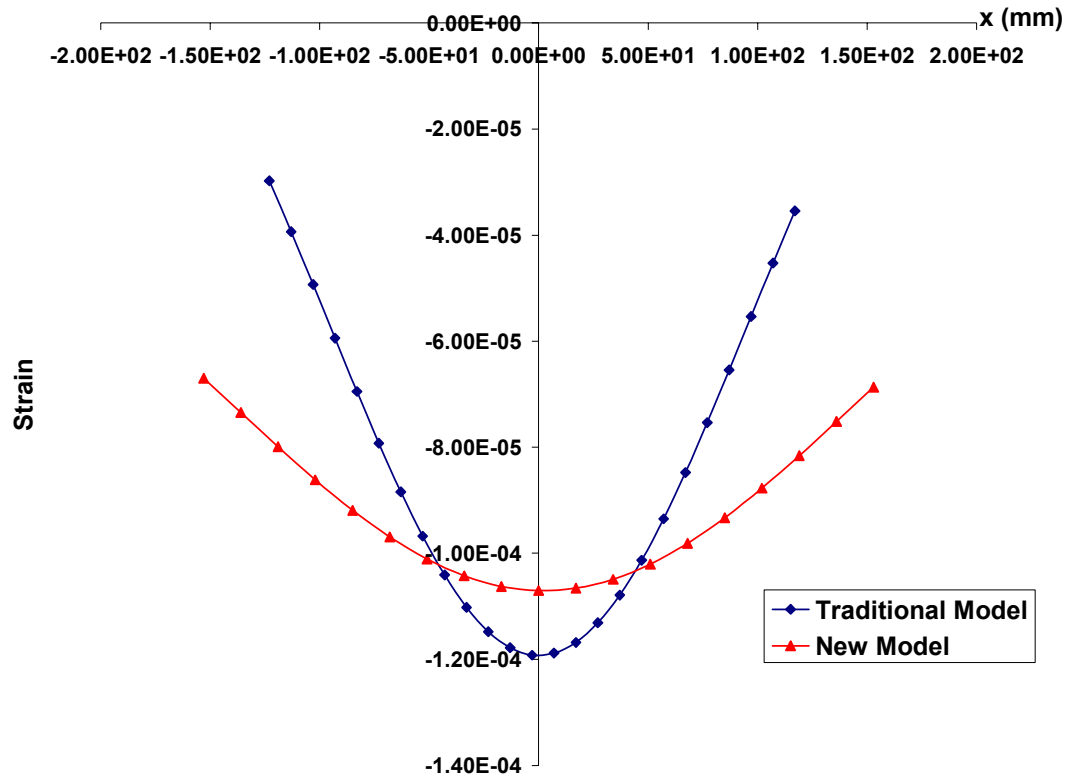


(b) ϵ_{yy}

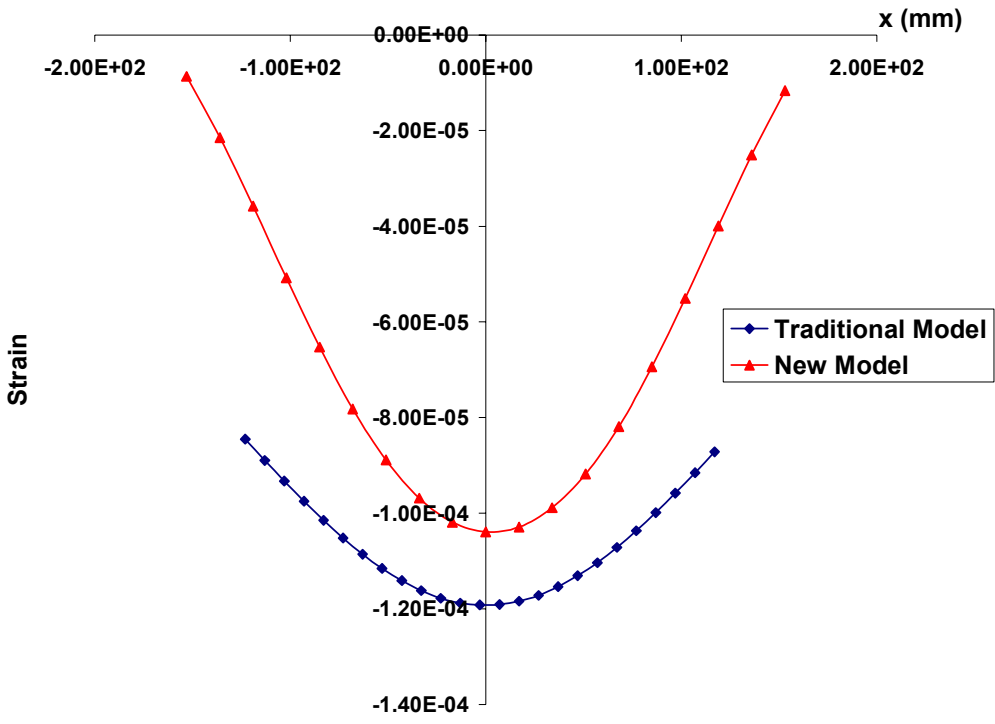


(c) ϵ_{czz}

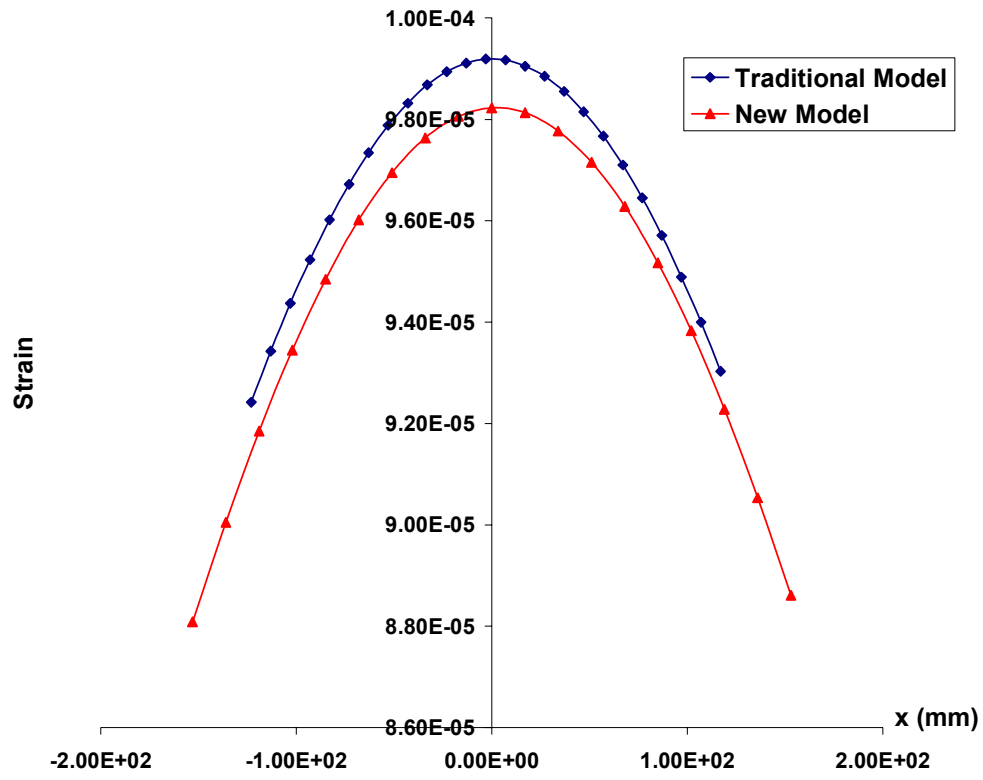
D. Pavement 4



(a) ϵ_{txx}



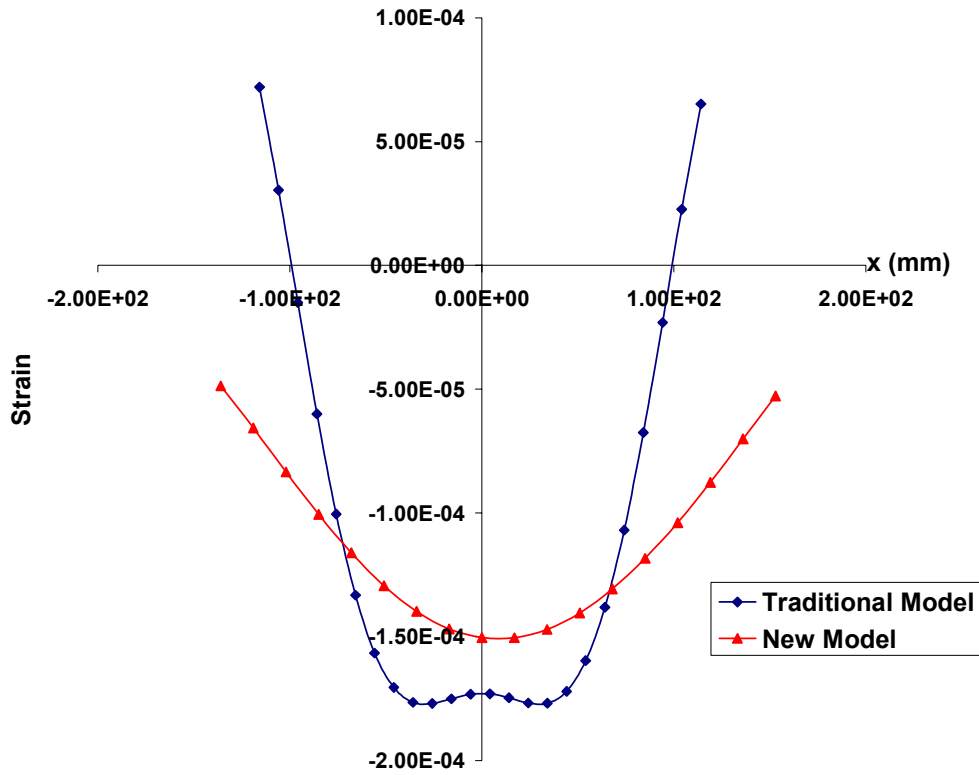
(b) ϵ_{yy}



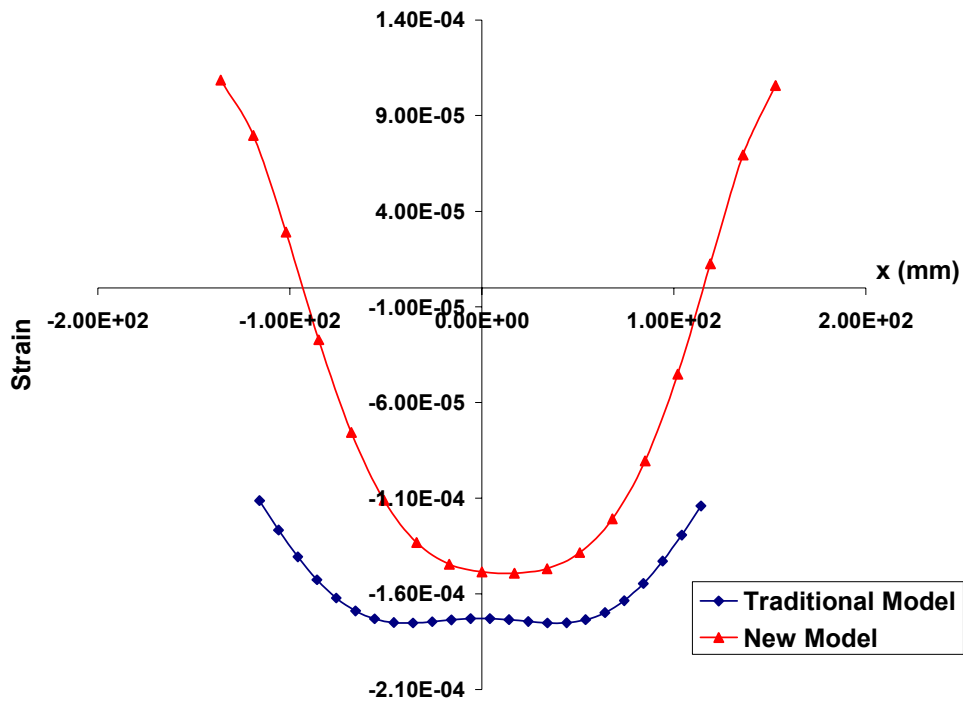
(c) ϵ_{czz}

Appendix 2: Strain Comparison in LTEX008 (L=24.3 kN, P=690 kPa)

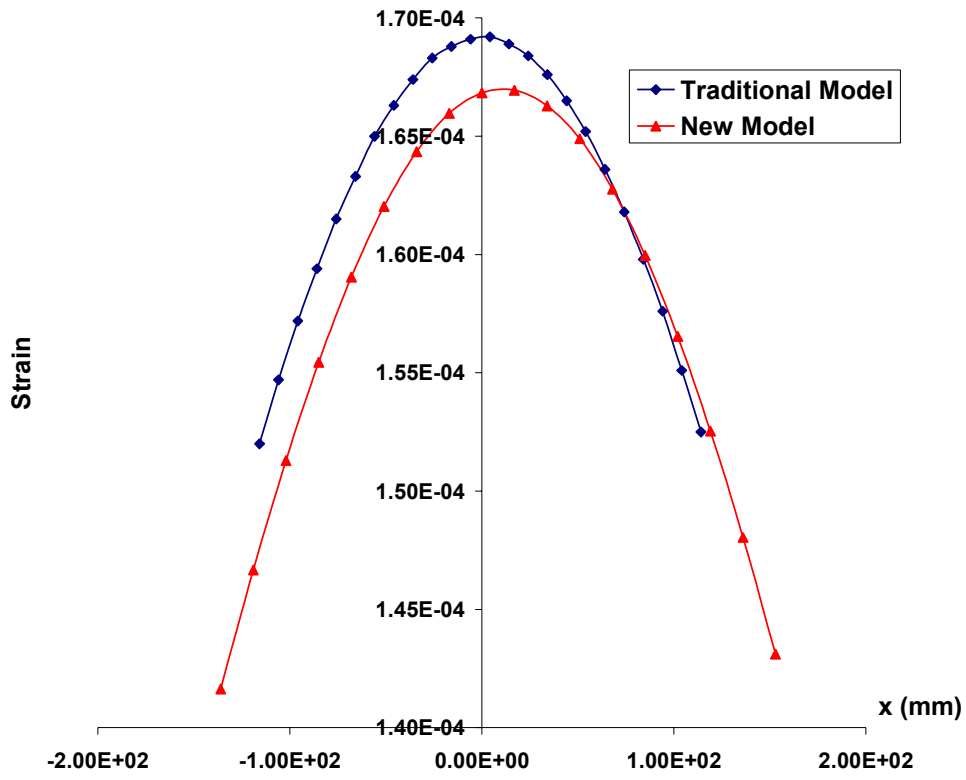
A. Pavement 1



(a) ϵ_{txx}

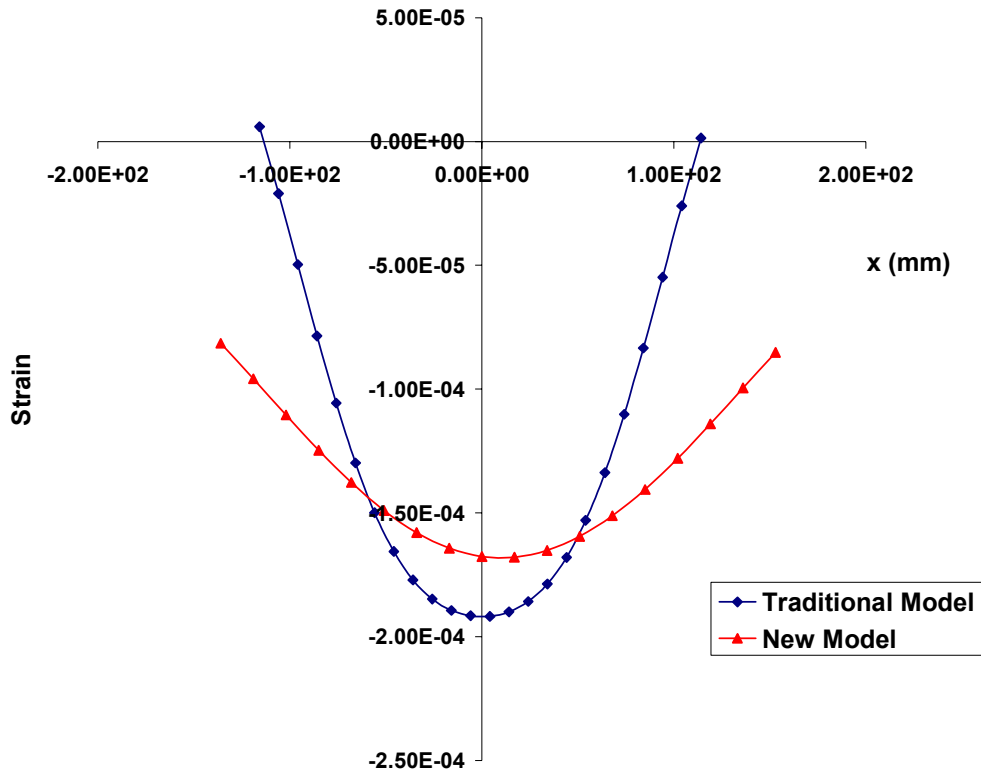


(b) ϵ_{yy}

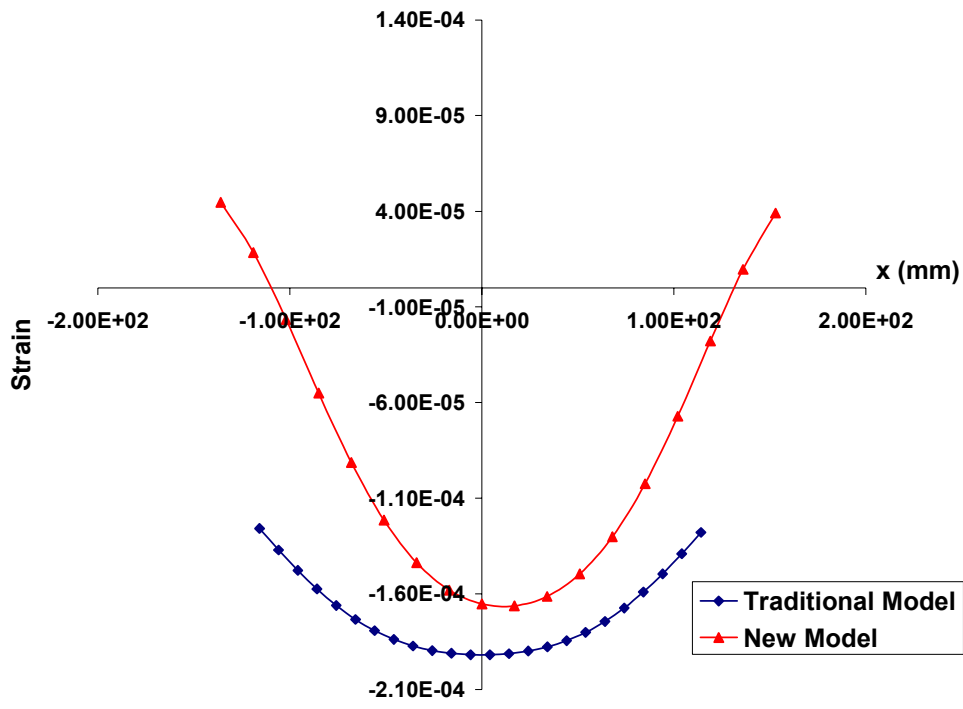


(c) ϵ_{czz}

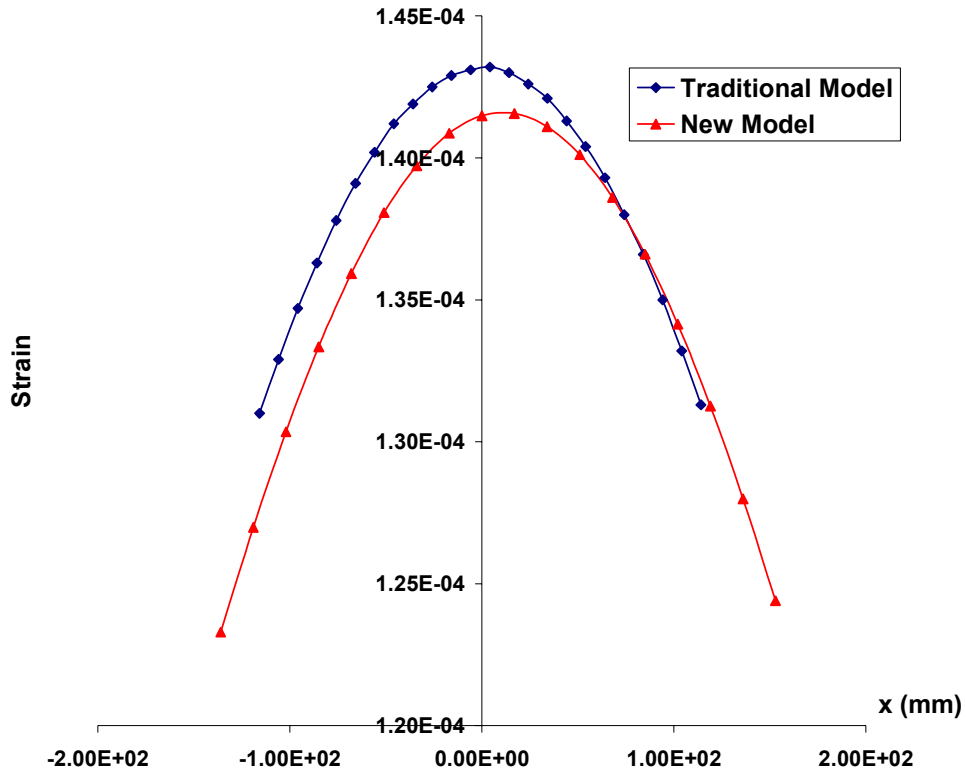
B. Pavement 2



(a) ϵ_{txx}

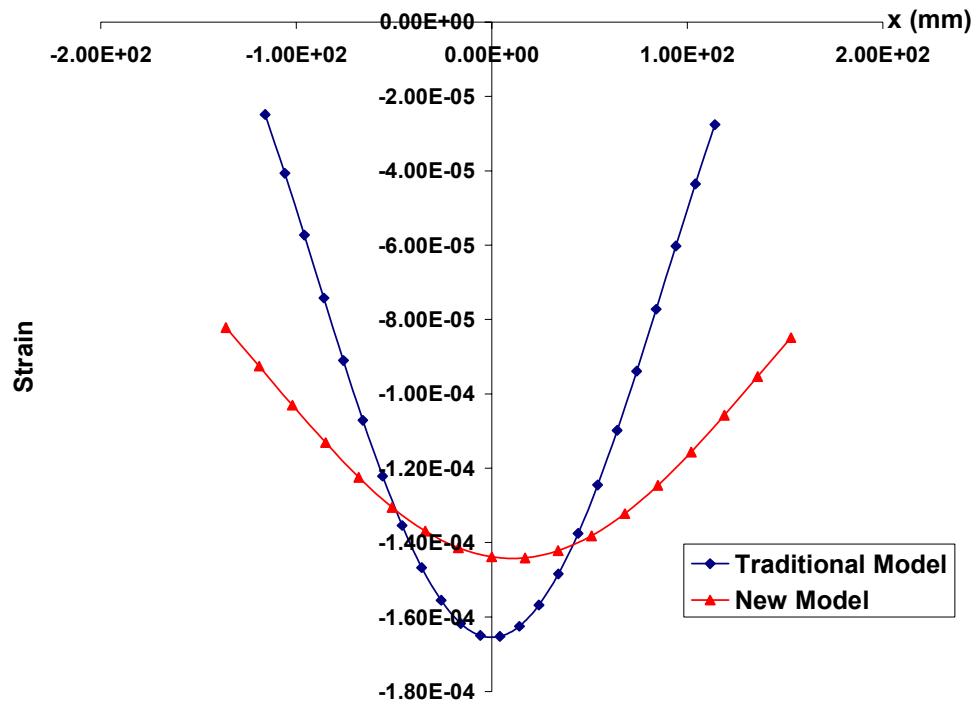


(b) ϵ_{yy}

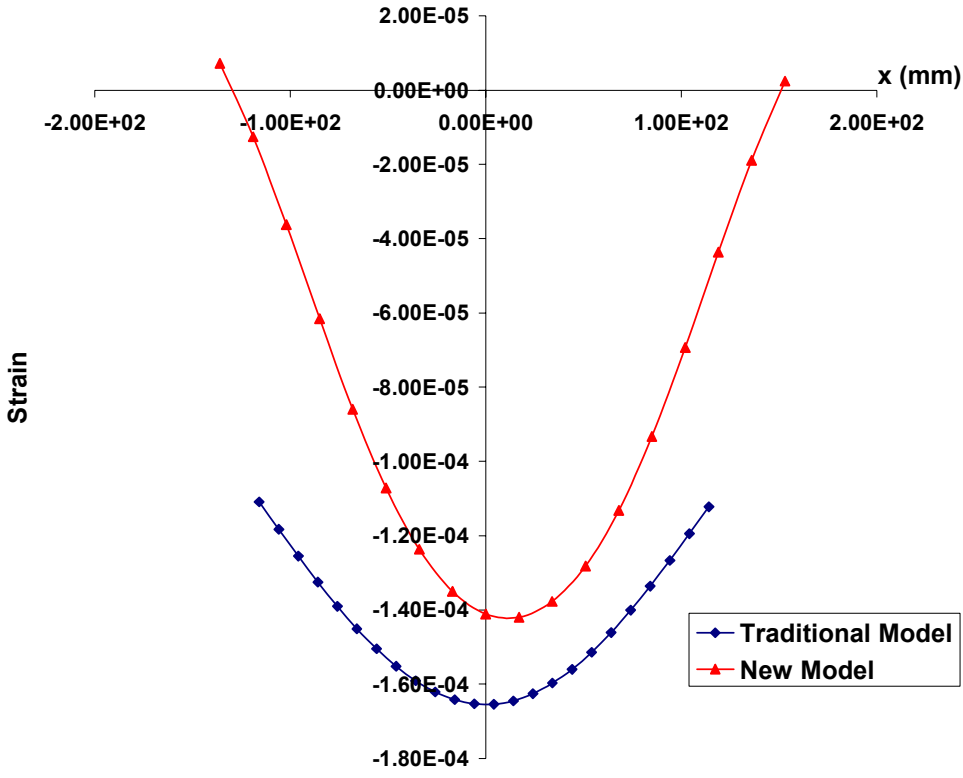


(c) ϵ_{czz}

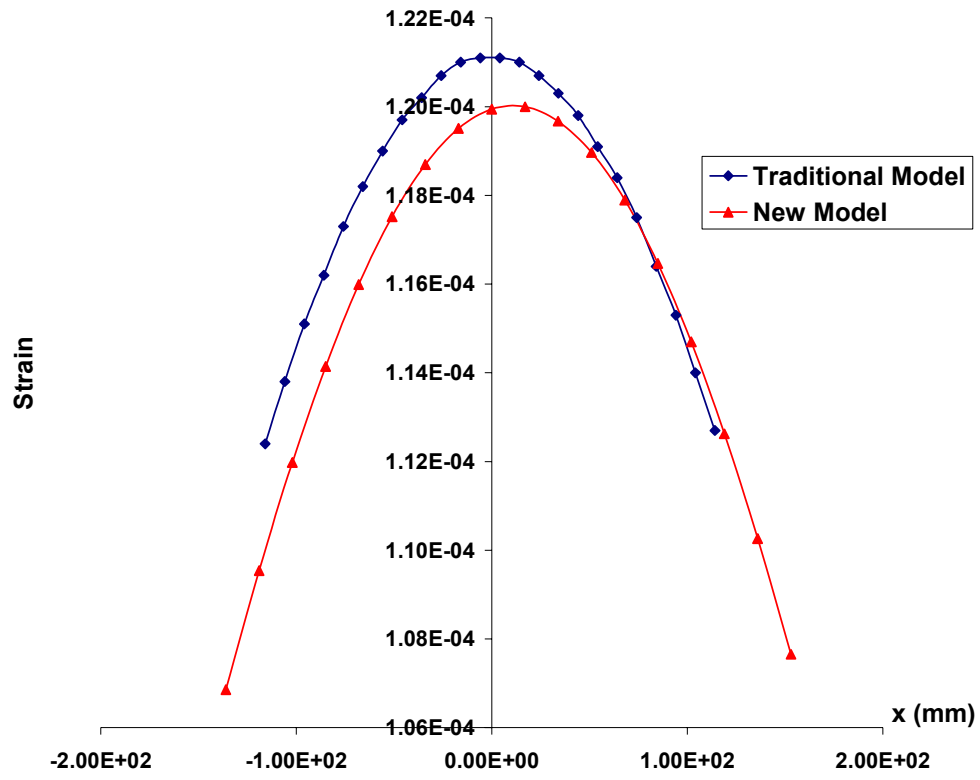
C. Pavement 3



(a) ϵ_{txx}

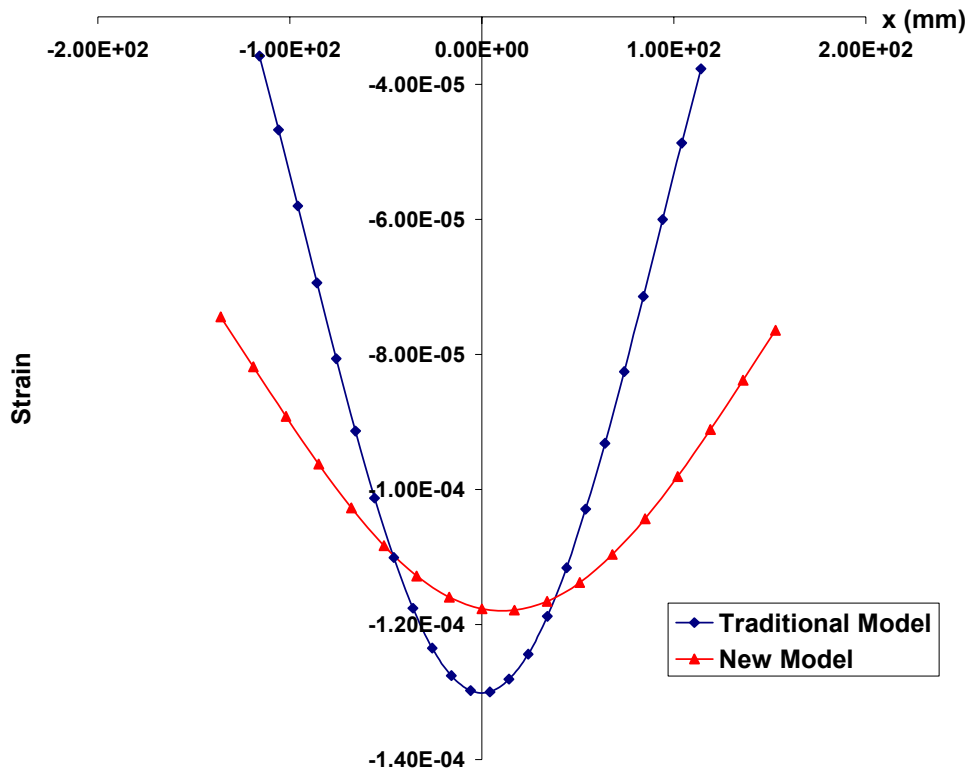


(b) ϵ_{yy}

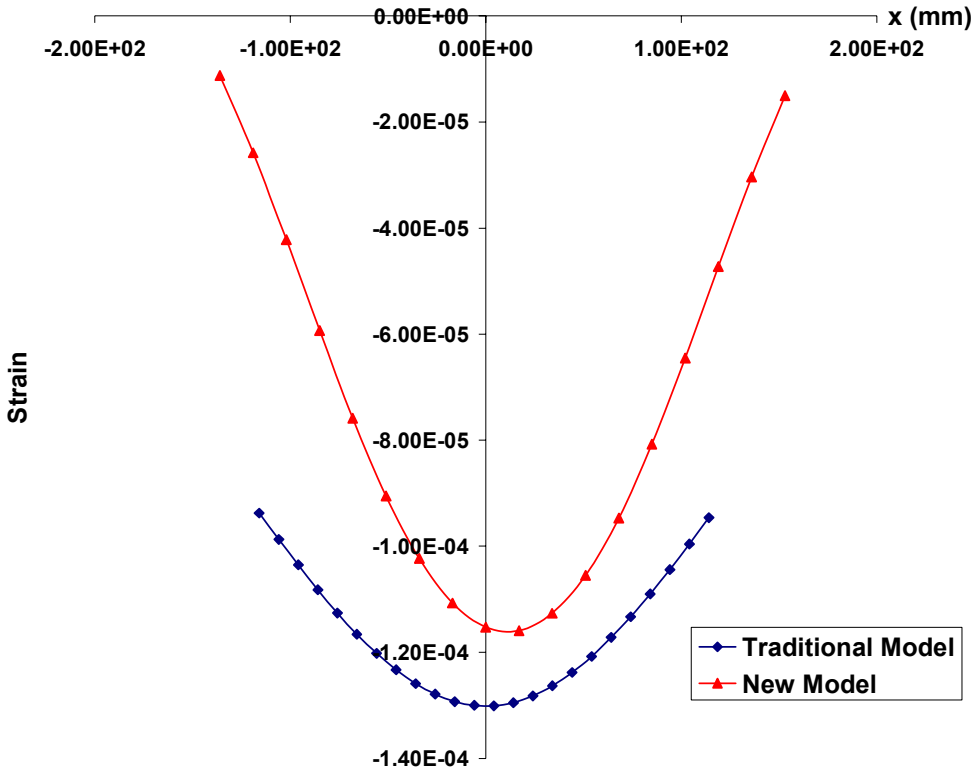


(c) ϵ_{czz}

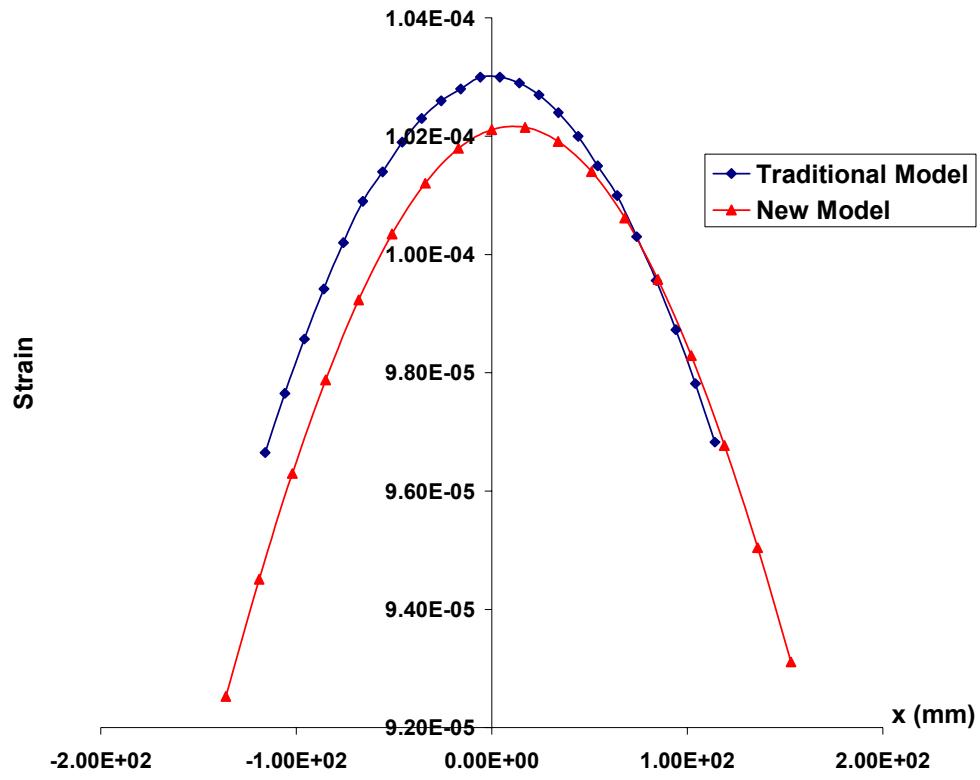
D. Pavement 4



(a) ϵ_{txx}



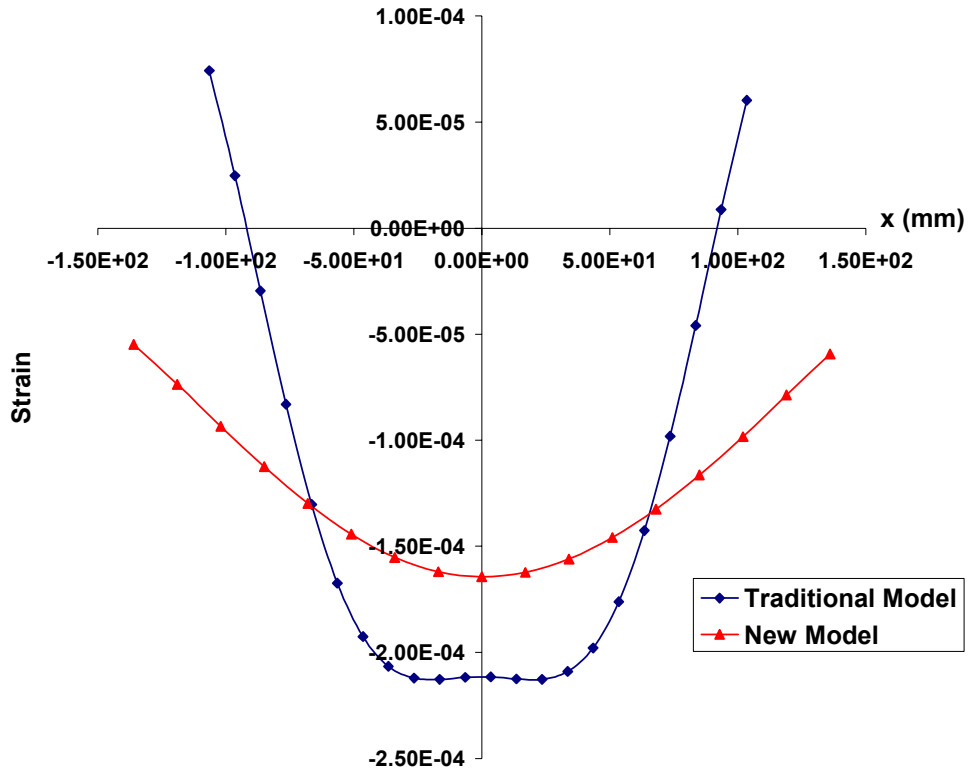
(b) ϵ_{yy}



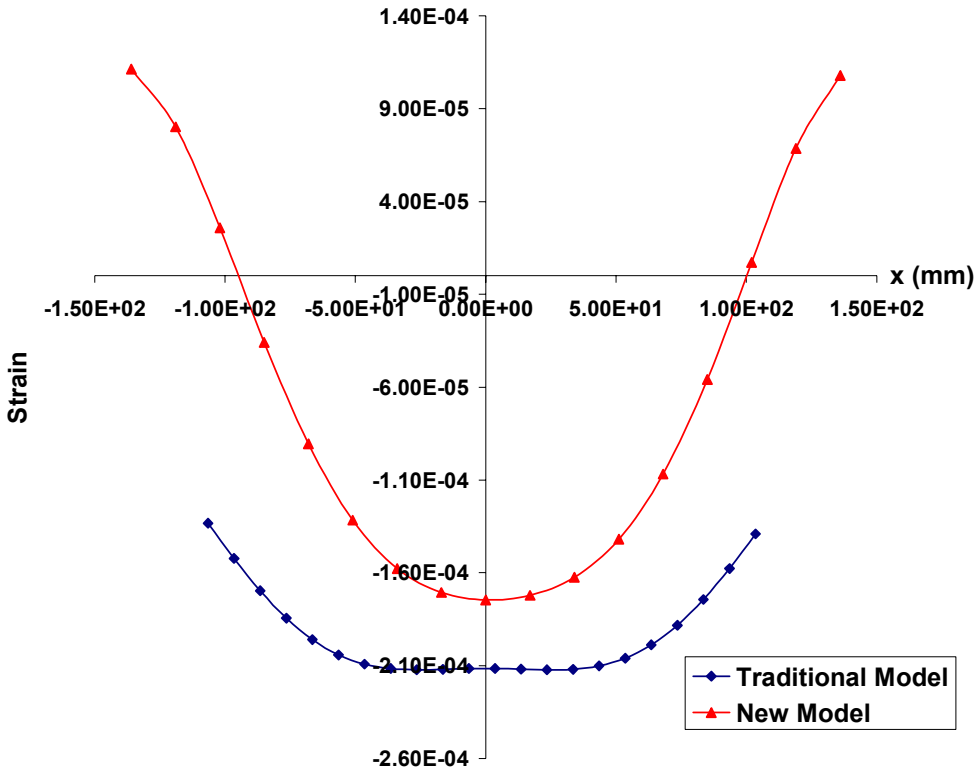
(c) ϵ_{czz}

Appendix 3: Strain Comparison in LTEX009 (L=23.2 kN, P=793 kPa)

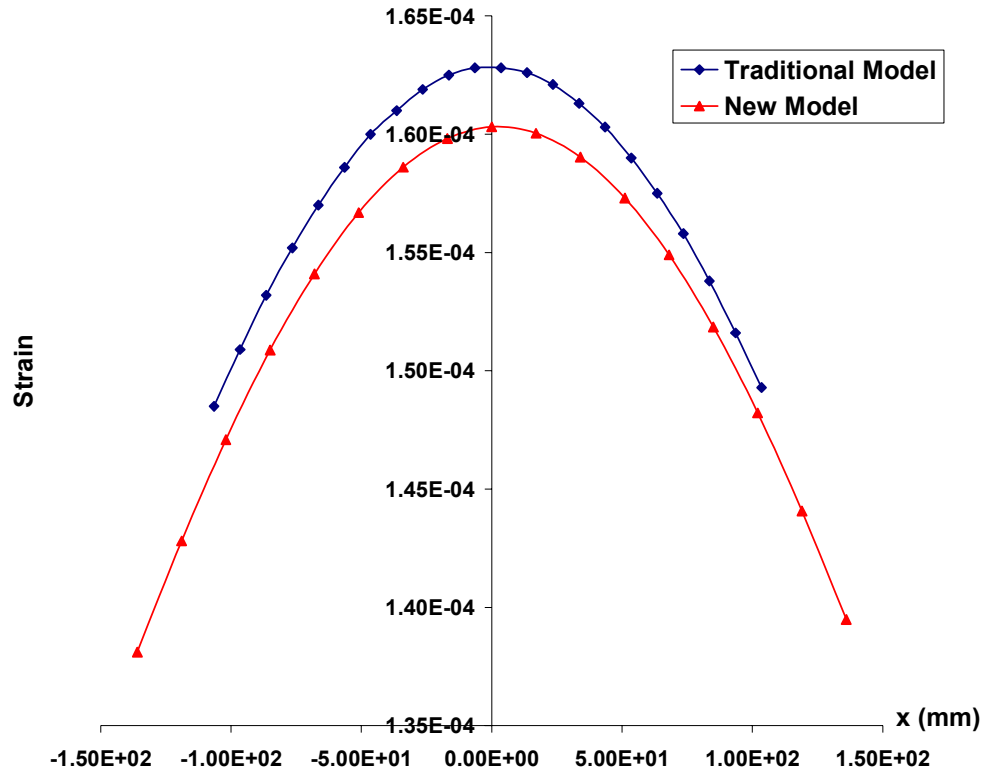
A. Pavement 1



(a) ϵ_{txx}

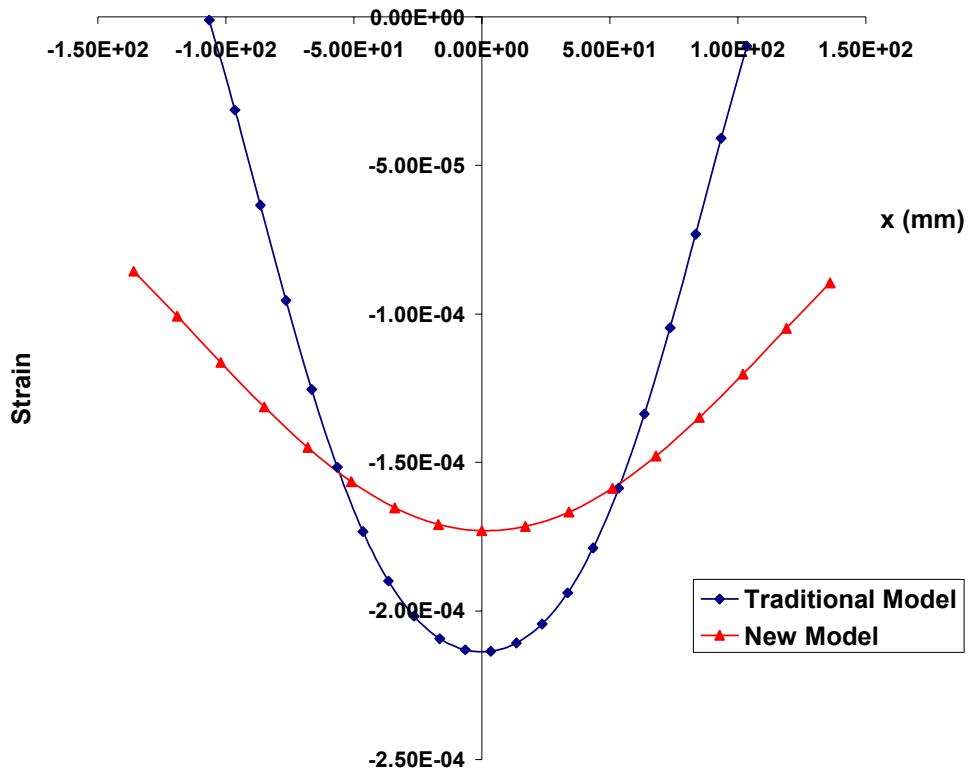


(b) ϵ_{yy}

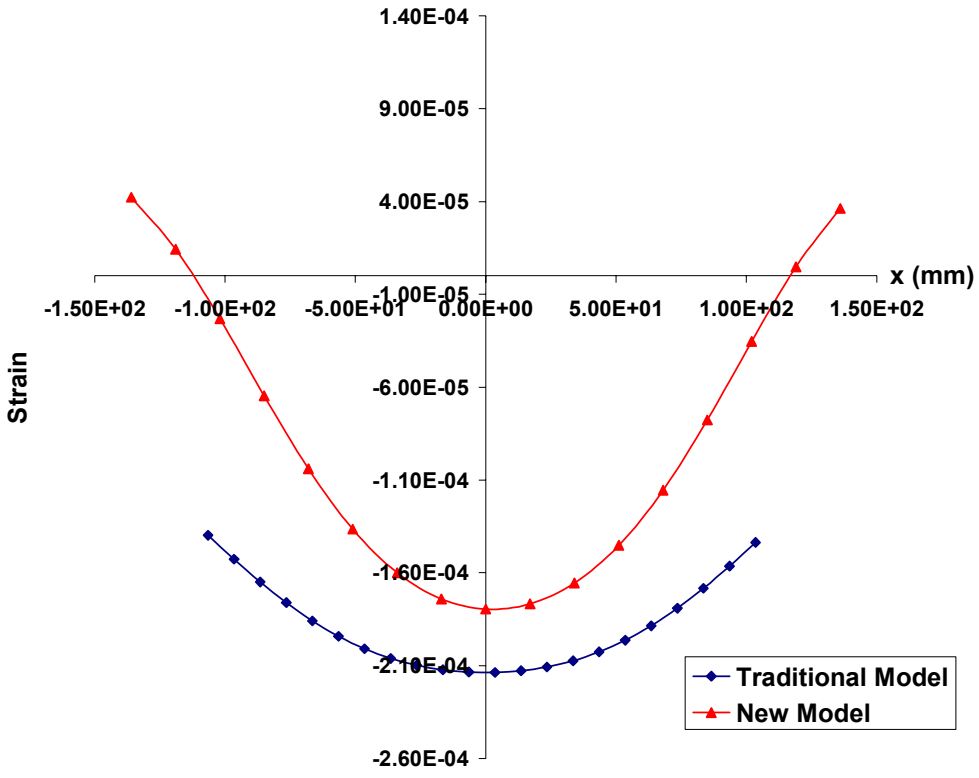


(c) ϵ_{czz}

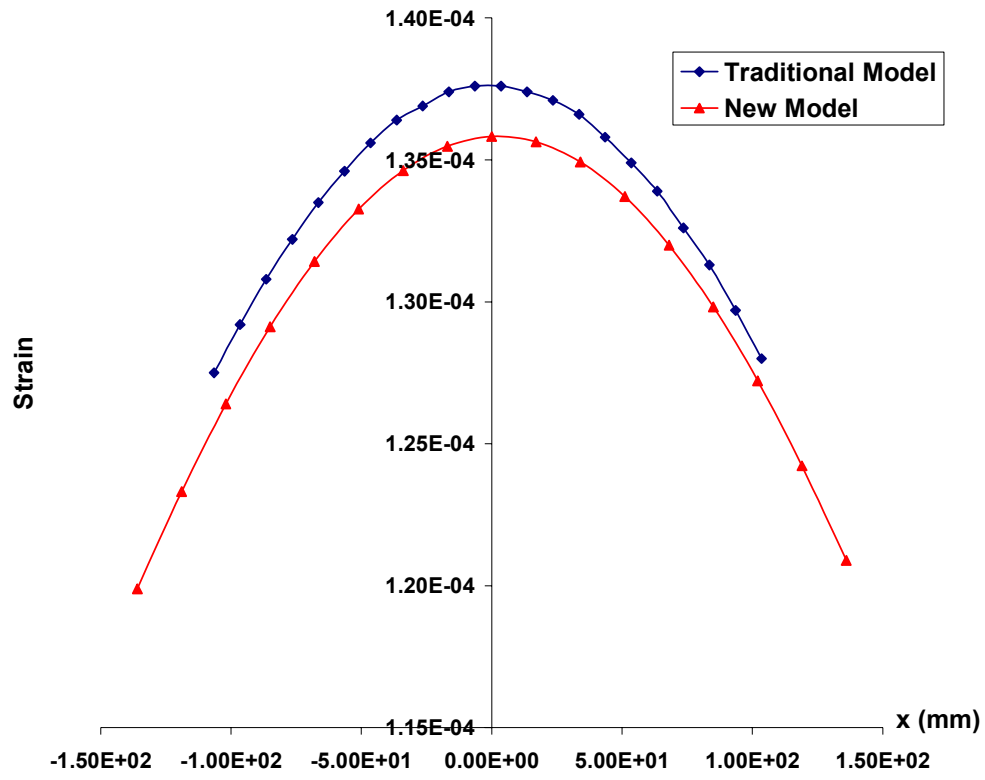
B. Pavement 2



(a) ϵ_{txx}

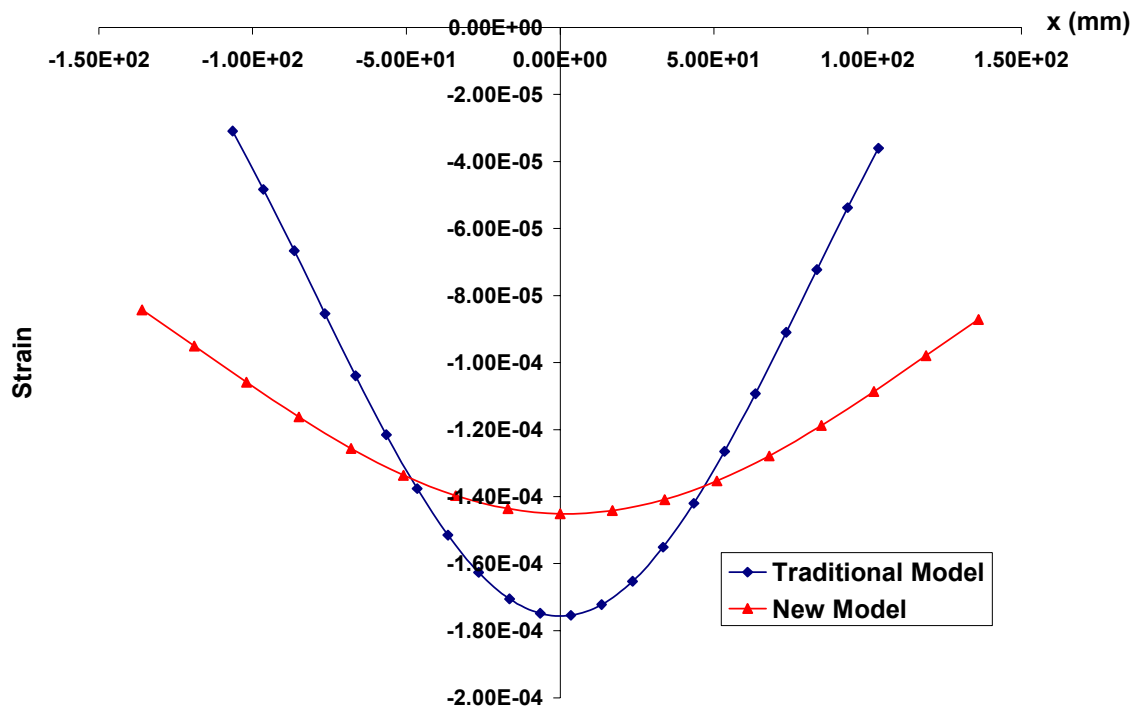


(b) ϵ_{yy}

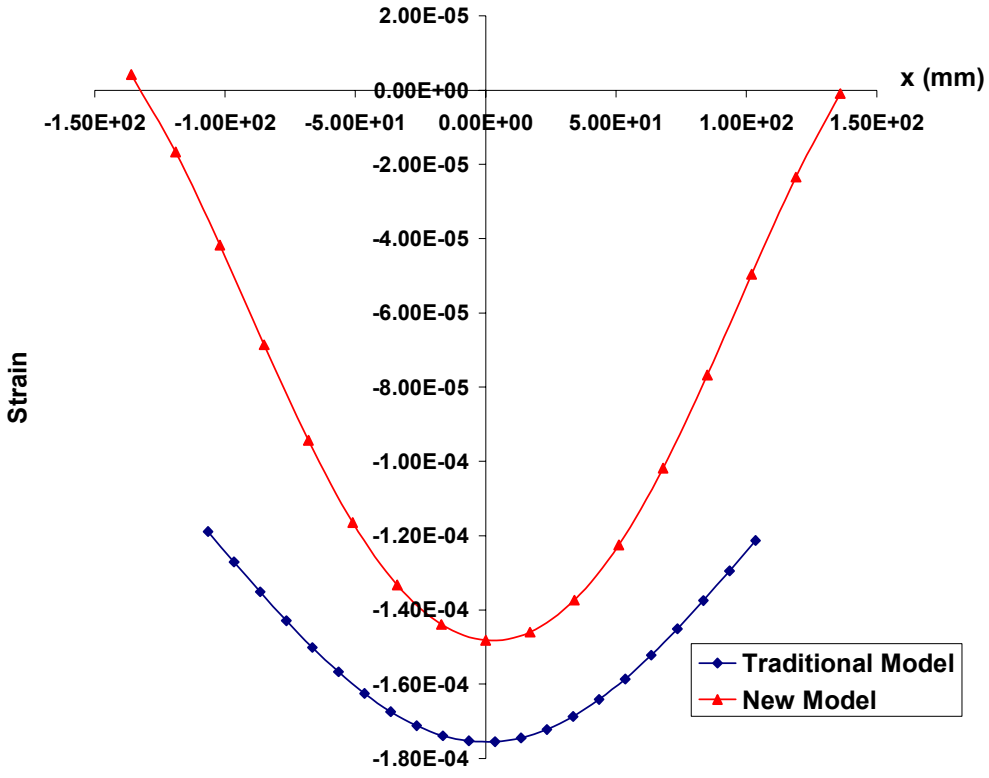


(c) ϵ_{czz}

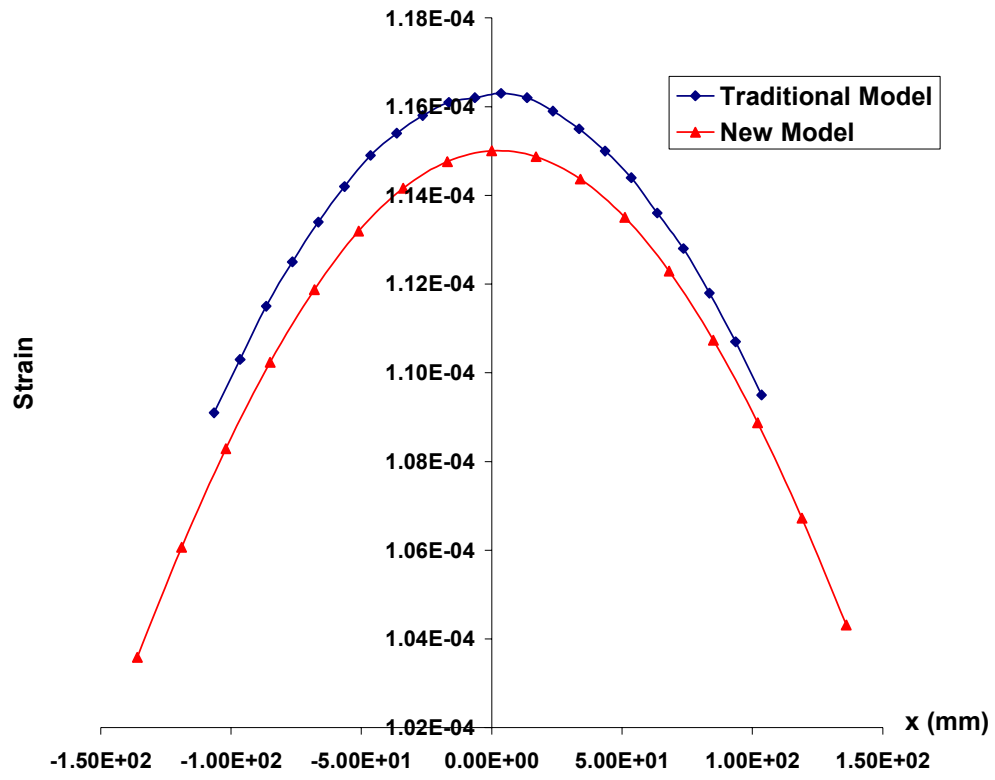
C. Pavement 3



(a) ϵ_{txx}

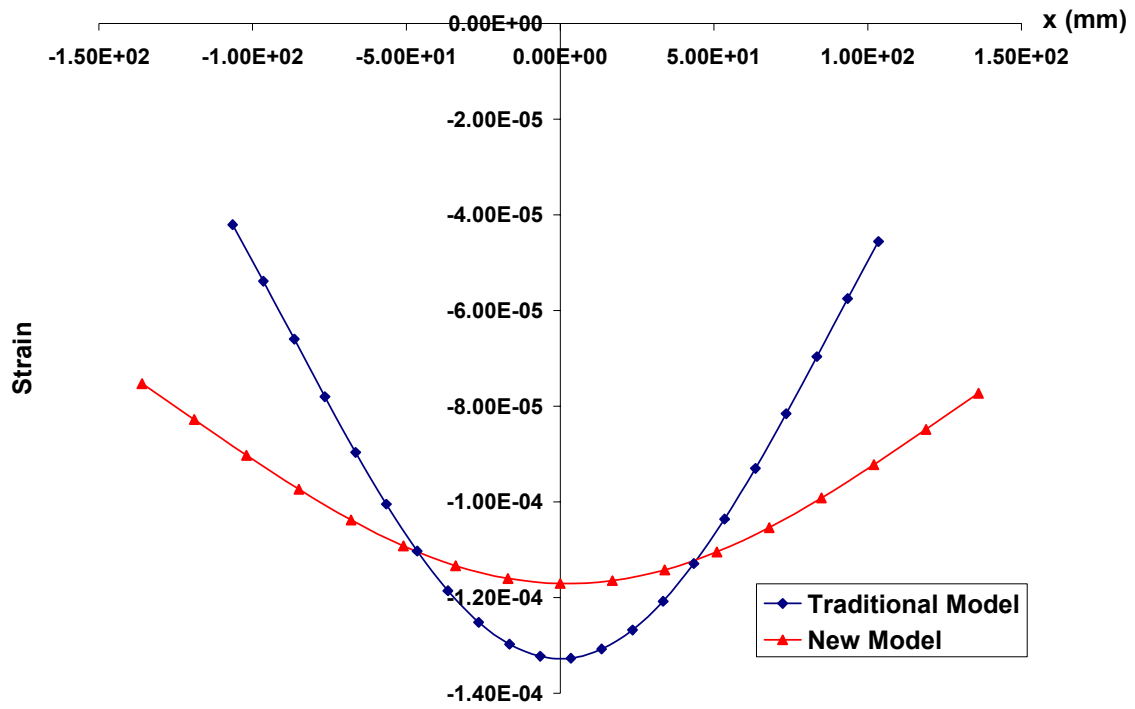


(b) ϵ_{yy}

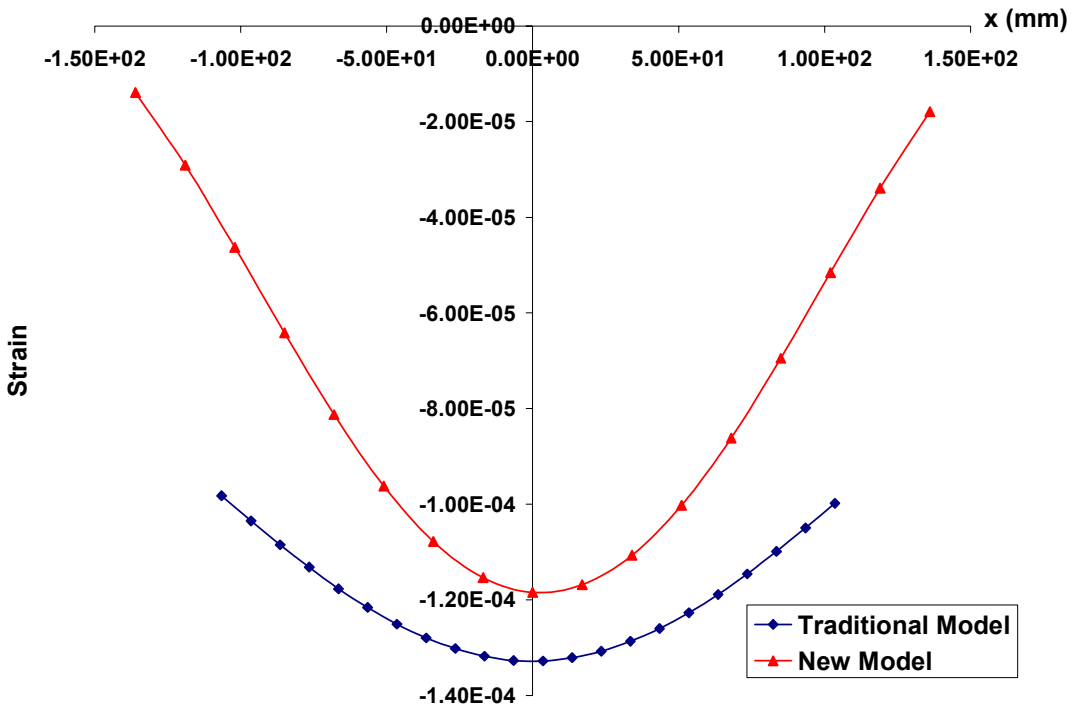


(c) ϵ_{czz}

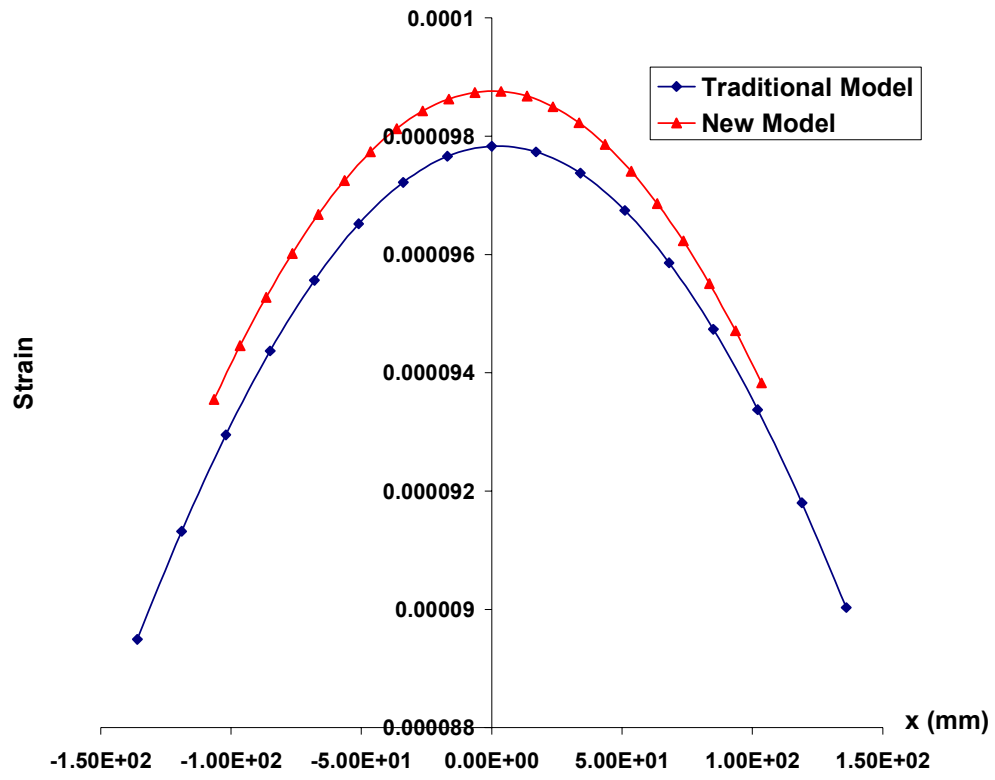
D. Pavement 4



(a) ϵ_{txx}



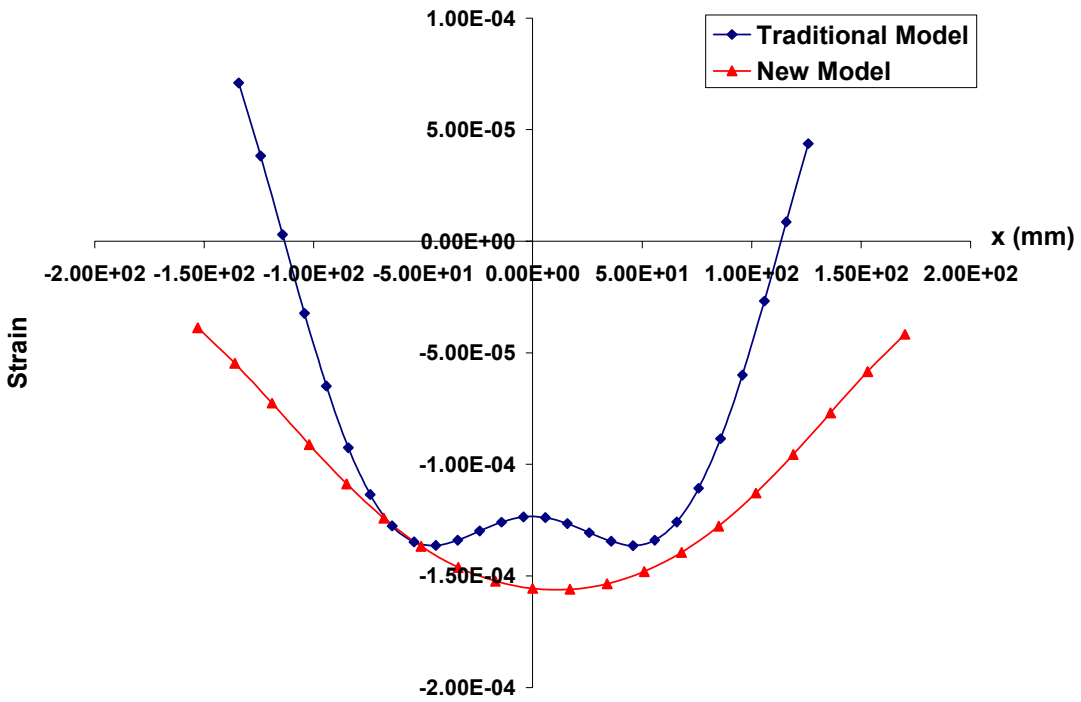
(b) ϵ_{yy}



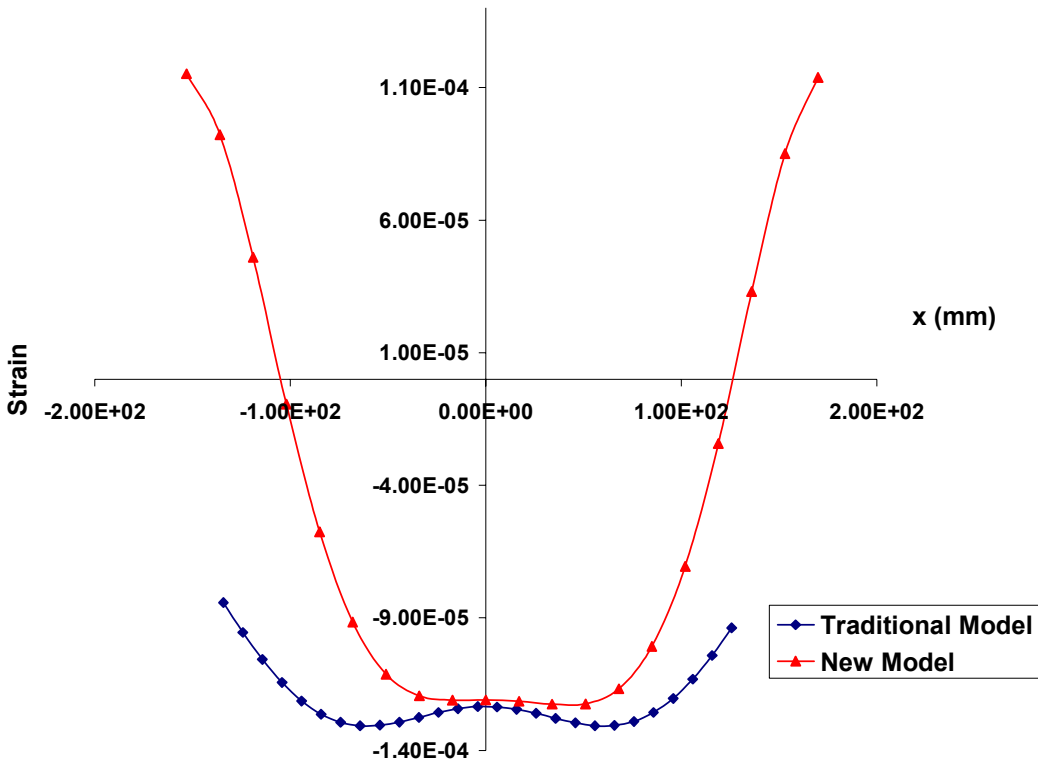
(c) ϵ_{czz}

Appendix 4: Strain Comparison in LTEX012 (L=28.4 kN, P=586 kPa)

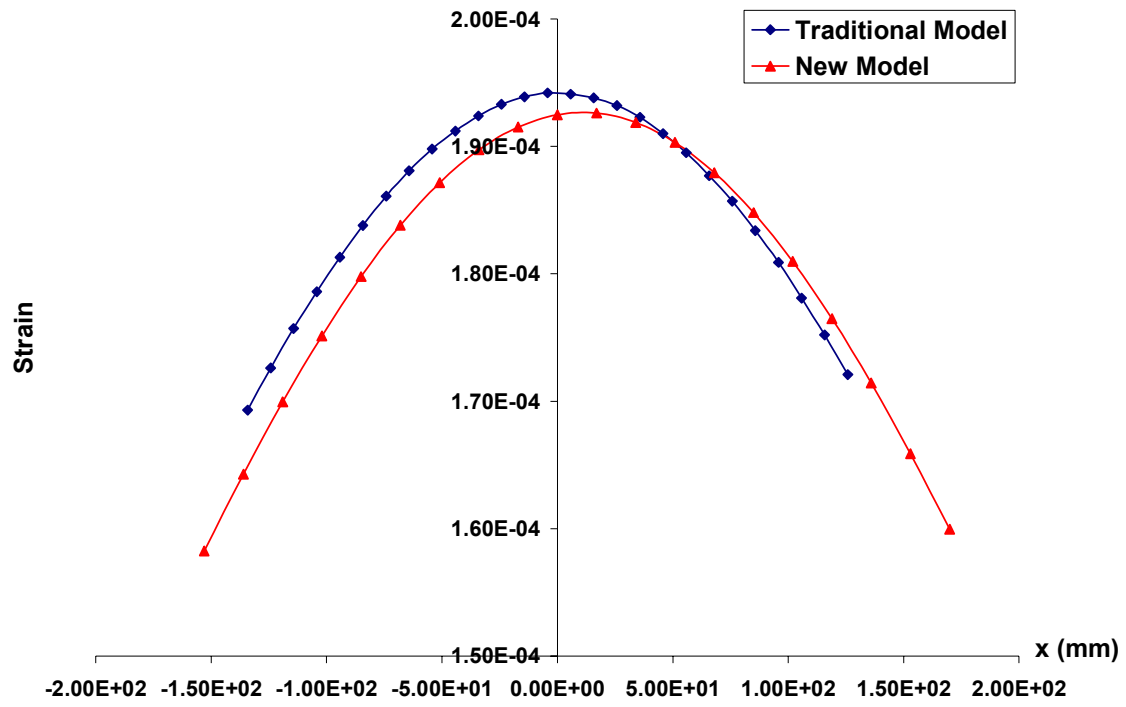
A. Pavement 1



(a) ϵ_{txx}

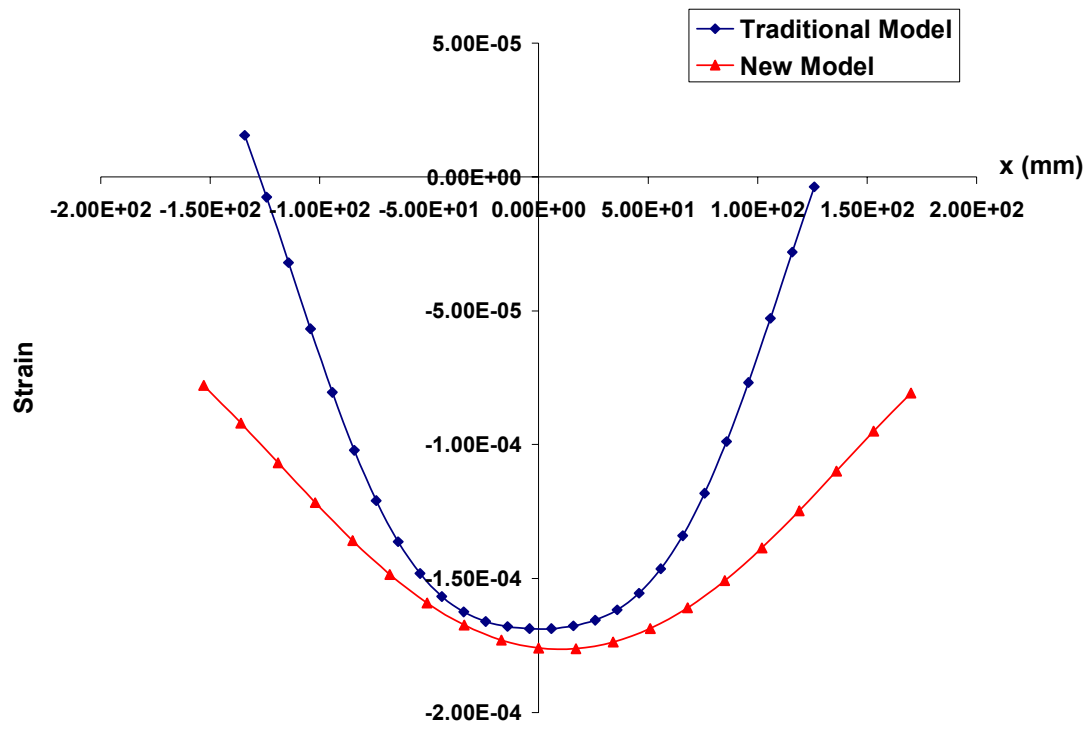


(b) ϵ_{yy}

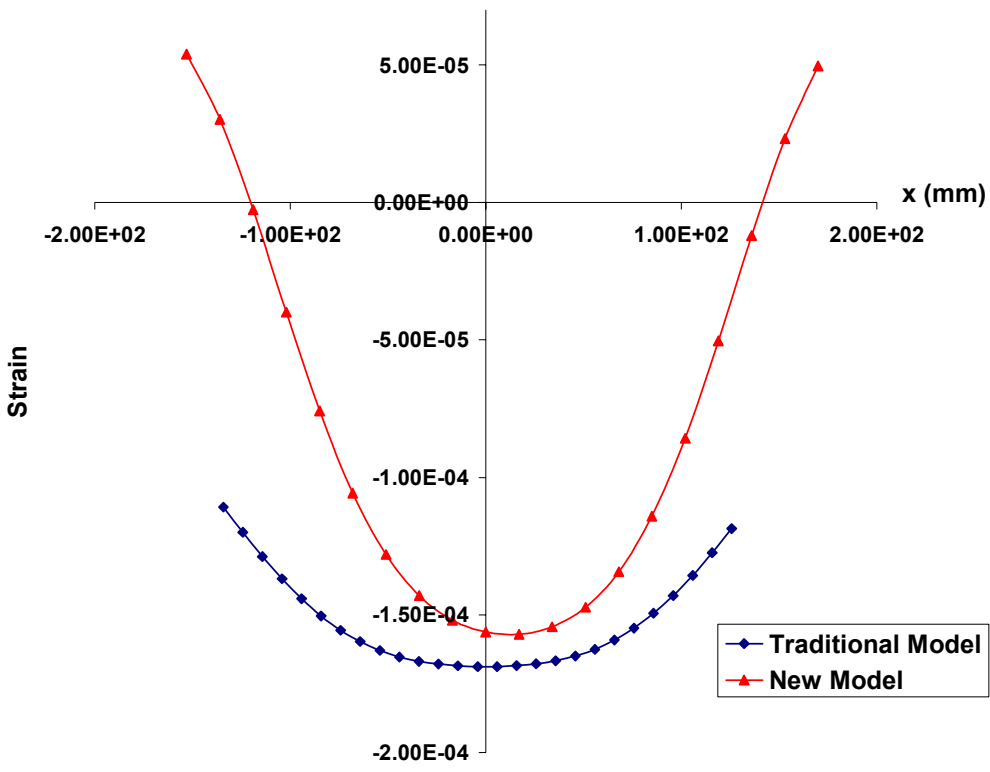


(c) ϵ_{czz}

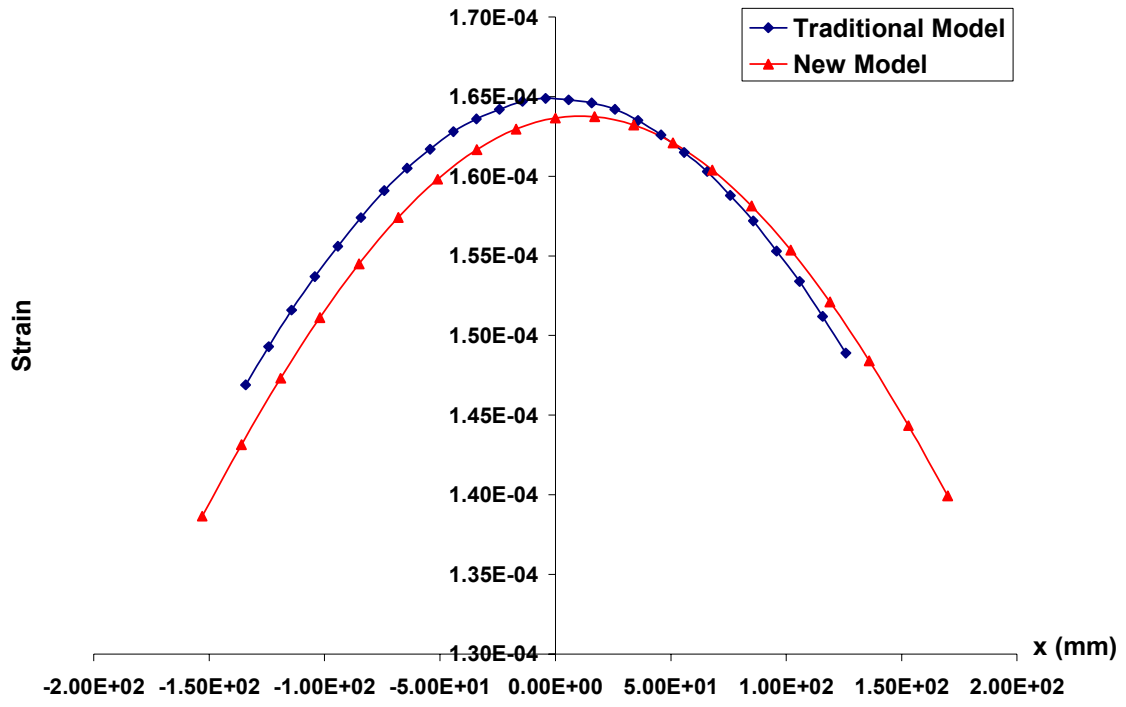
B. Pavement 2



(a) ϵ_{txx}

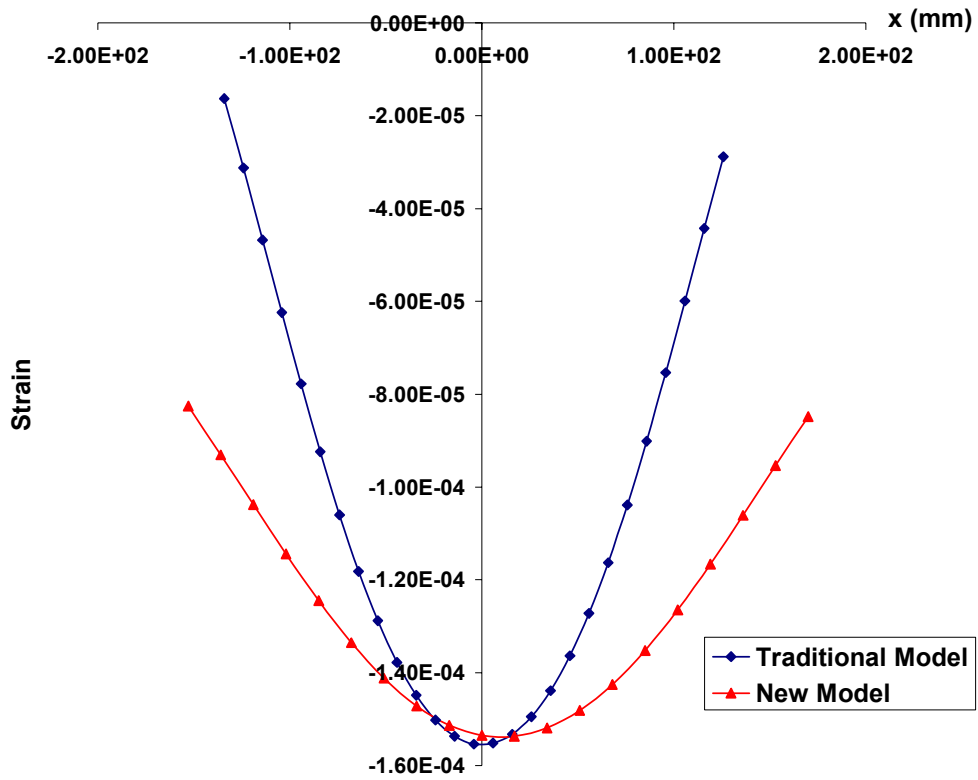


(b) ϵ_{yy}

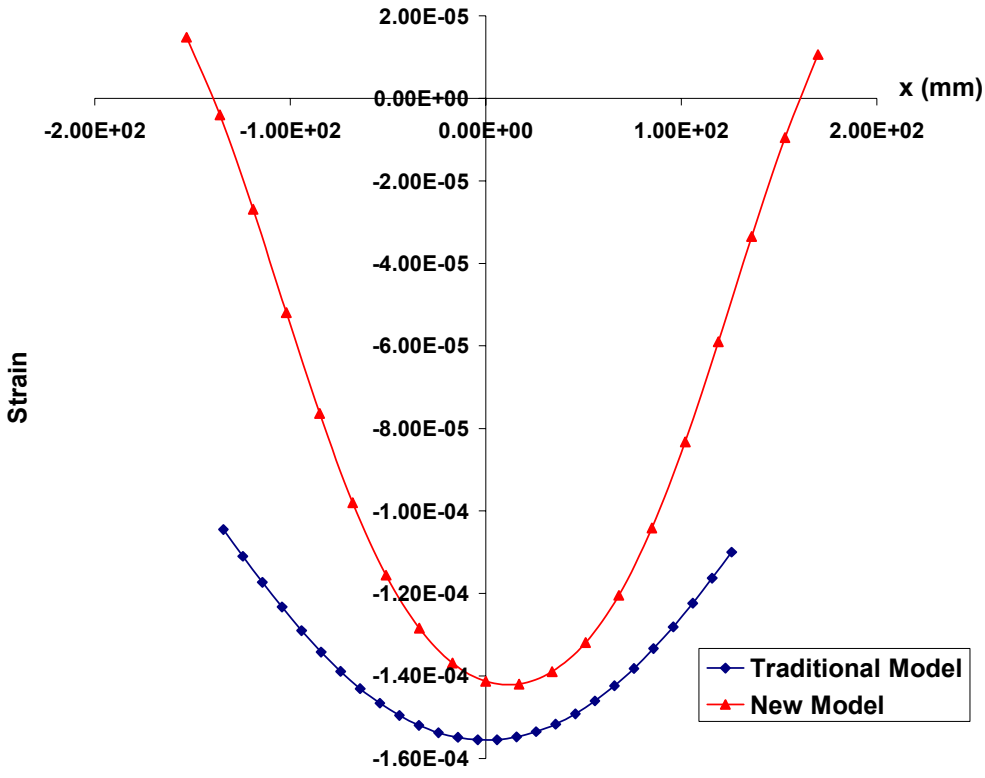


(c) ϵ_{czz}

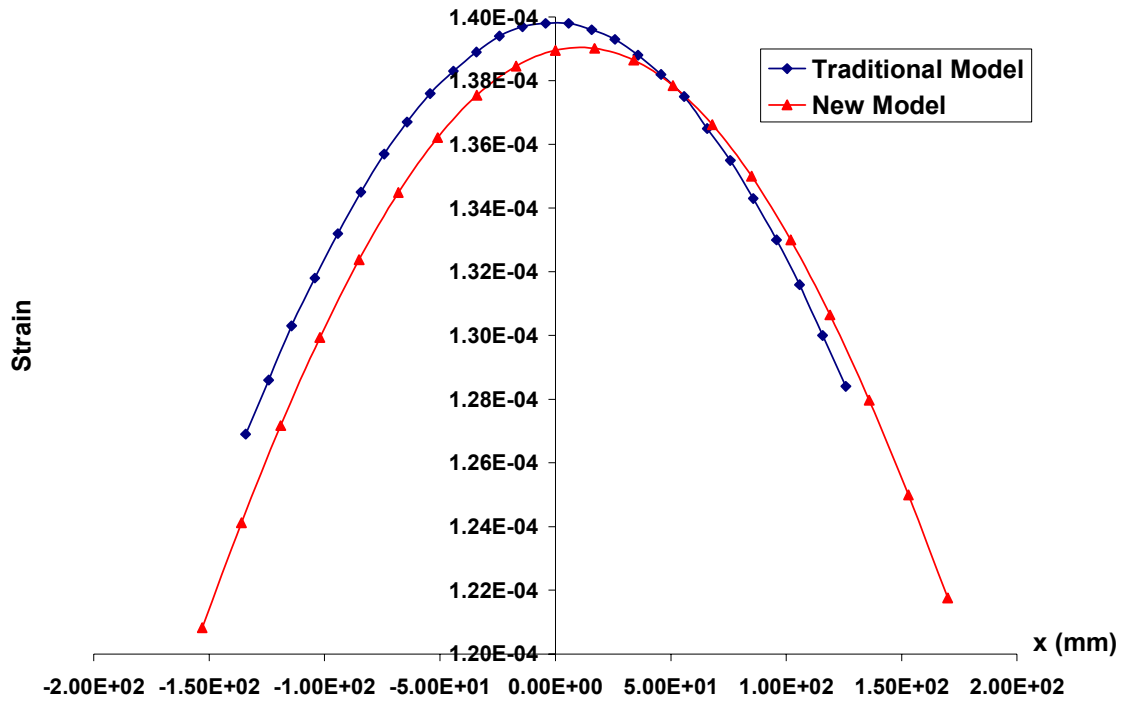
C. Pavement 3



(a) ϵ_{txx}

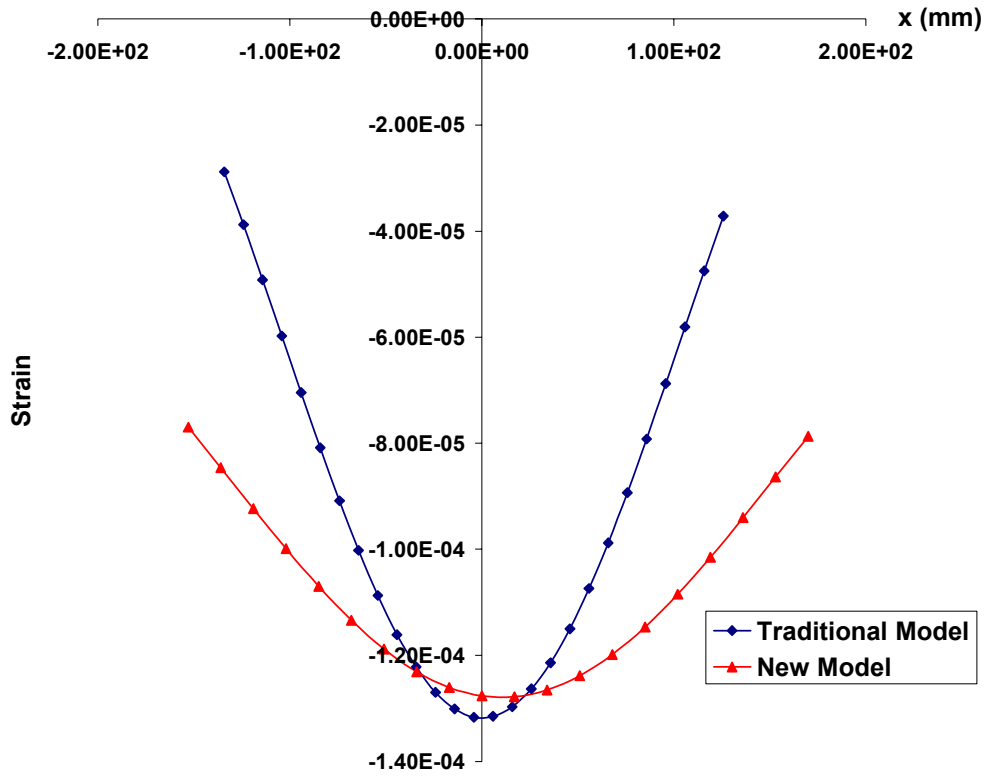


(b) ϵ_{yy}

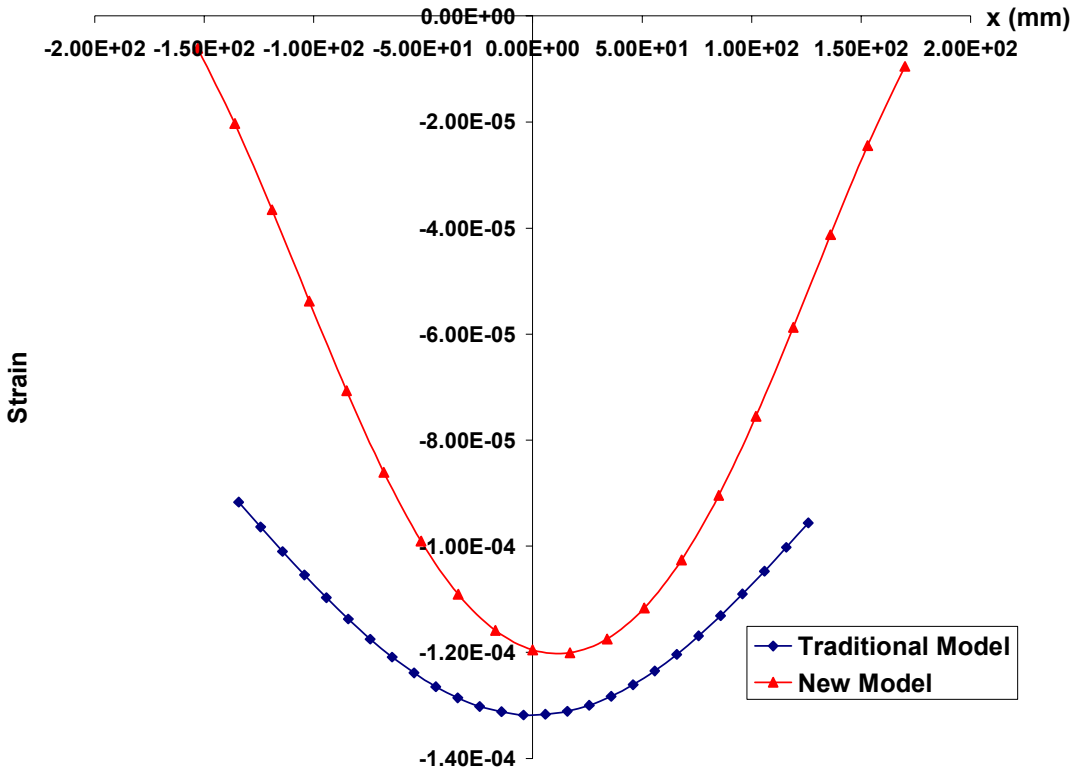


(c) ϵ_{czz}

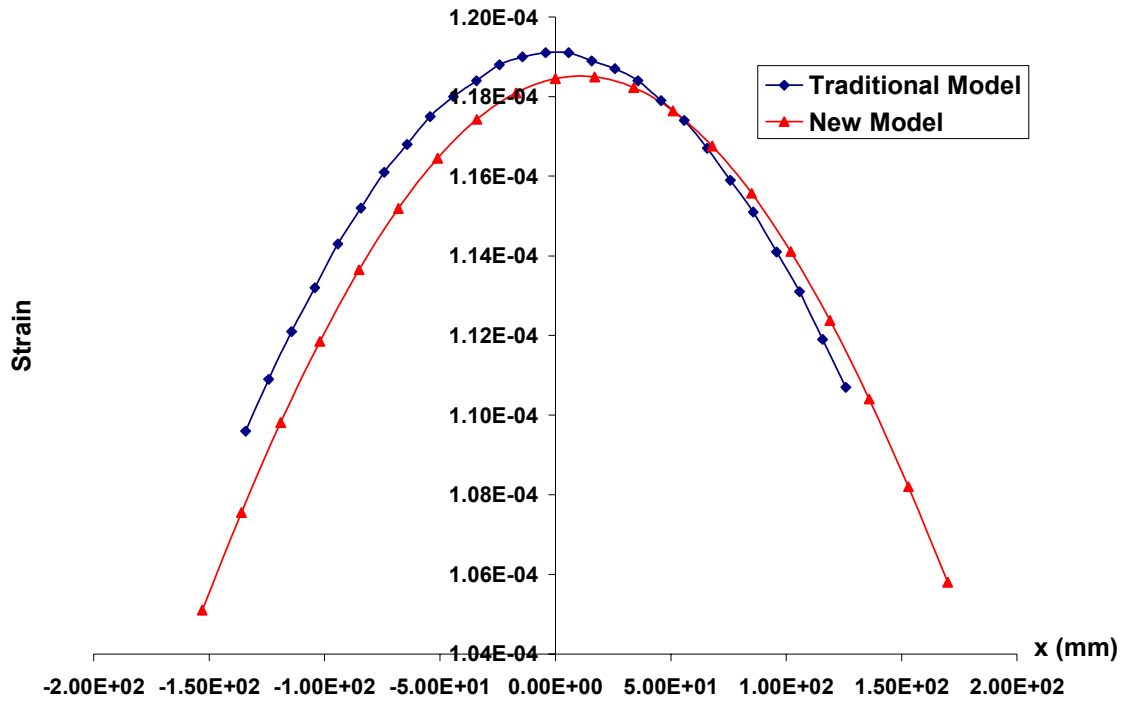
D. Pavement 4



(a) ϵ_{txx}



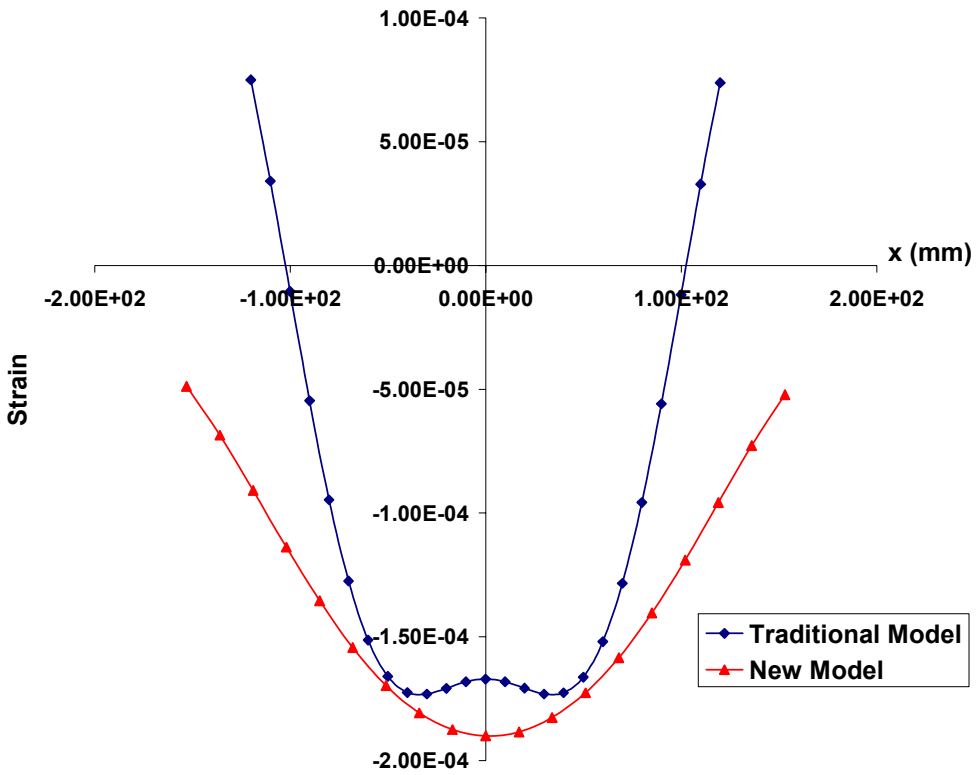
(b) ϵ_{yy}



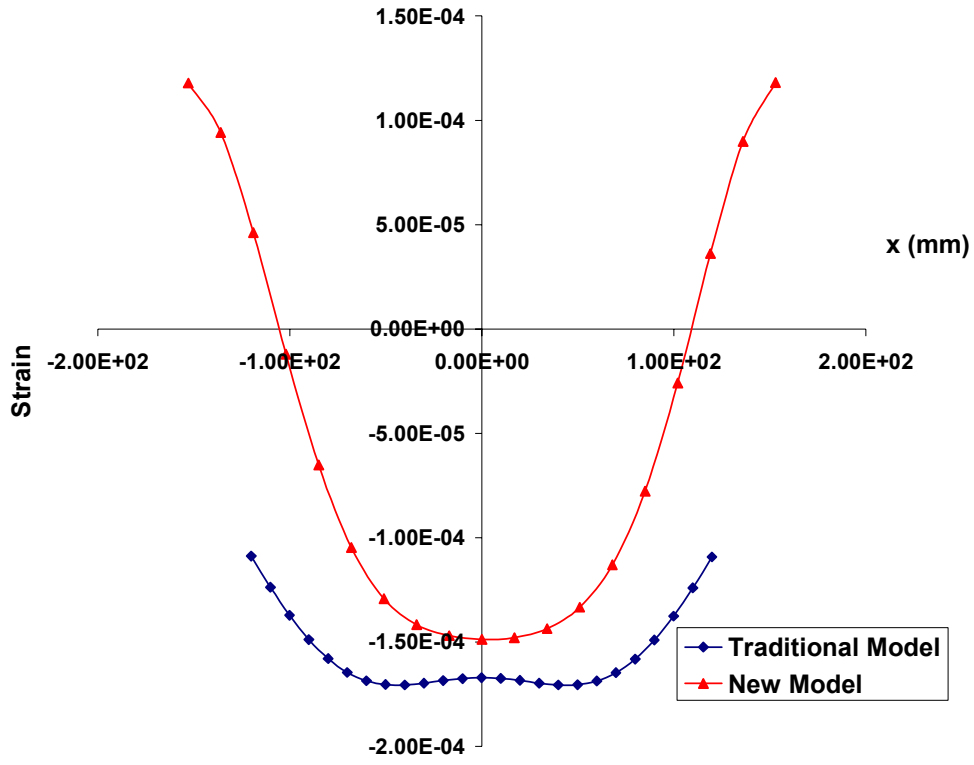
(c) ϵ_{czz}

Appendix 5: Strain Comparison in LTEX013 (L=26.3 kN, P=690 kPa)

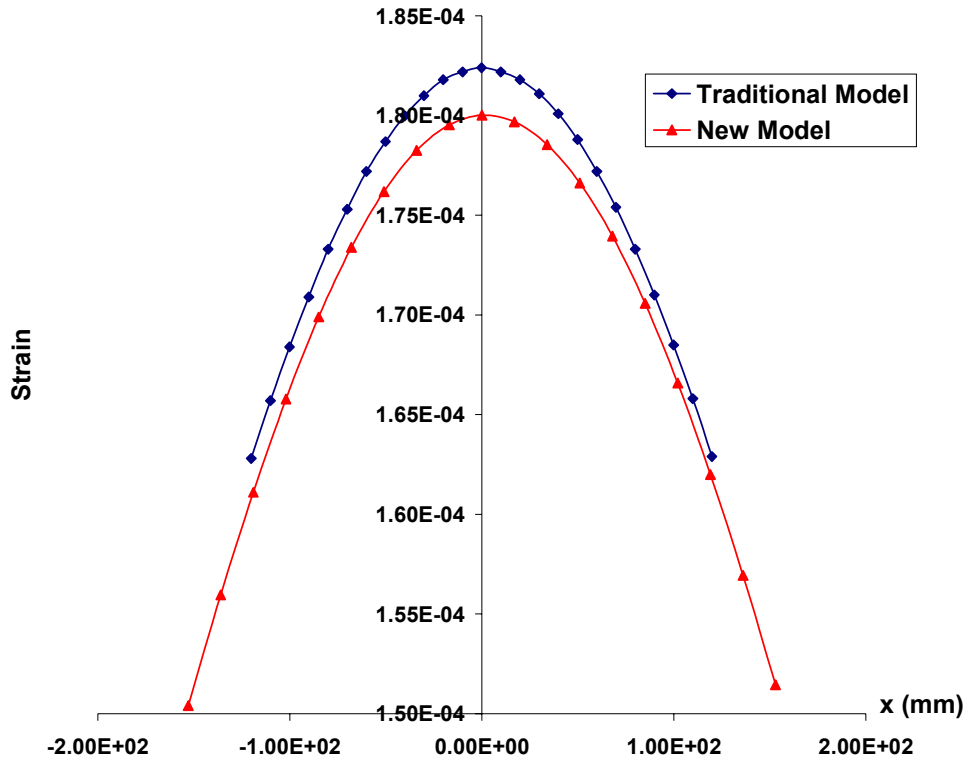
A. Pavement 1



(a) ϵ_{txx}

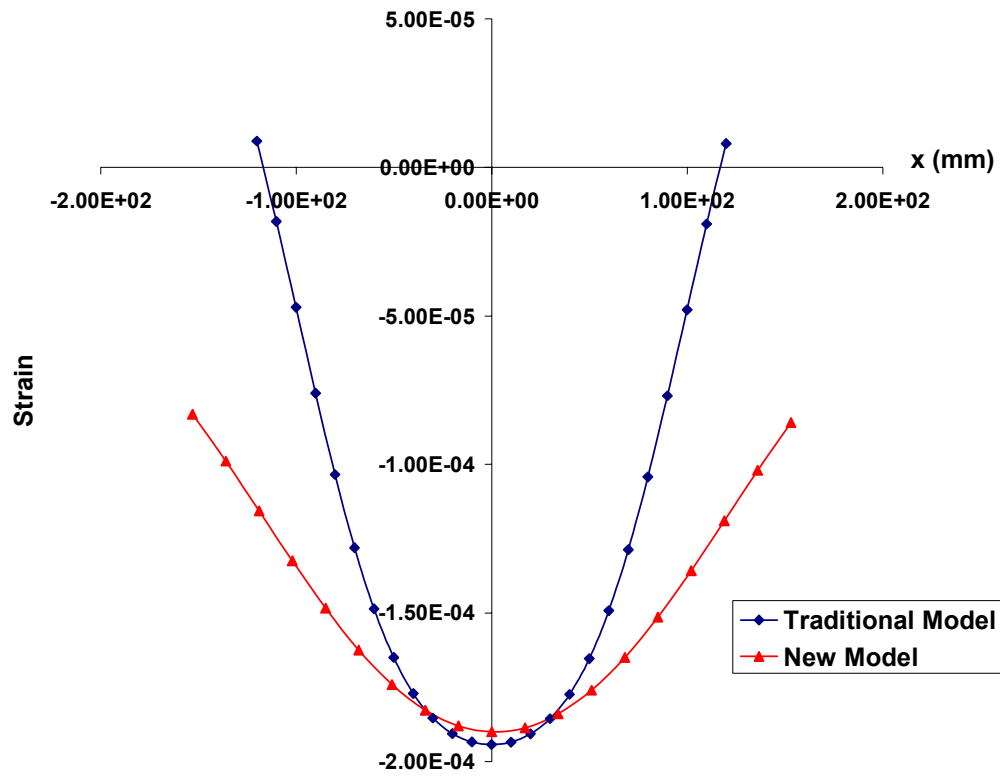


(b) ϵ_{yy}

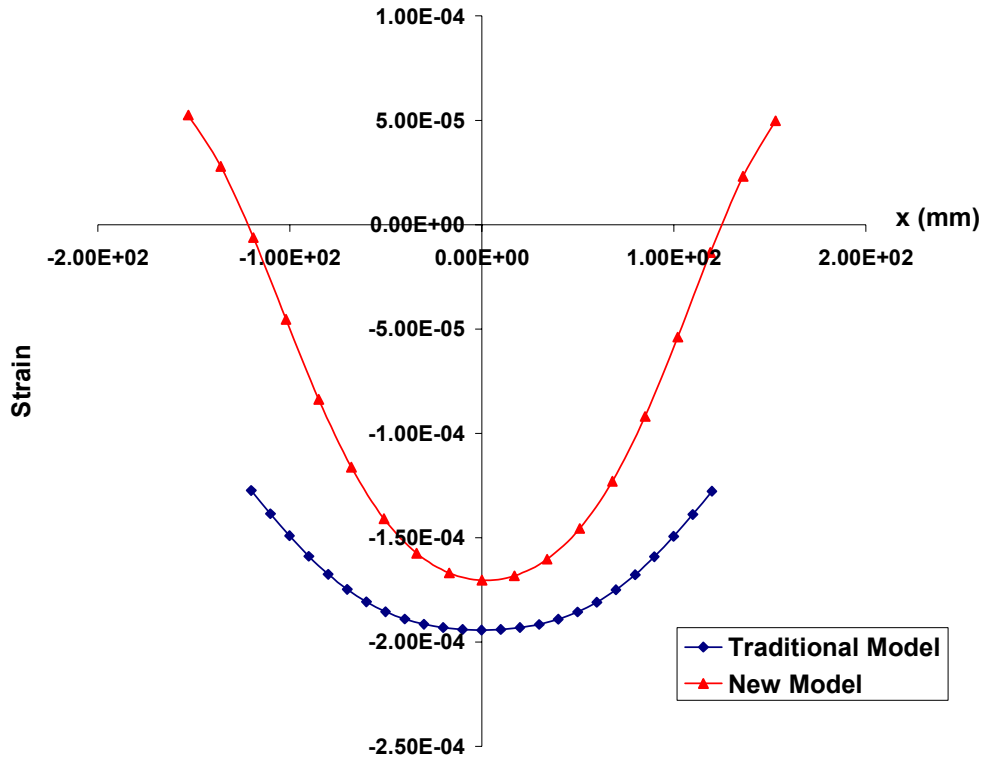


(c) ϵ_{czz}

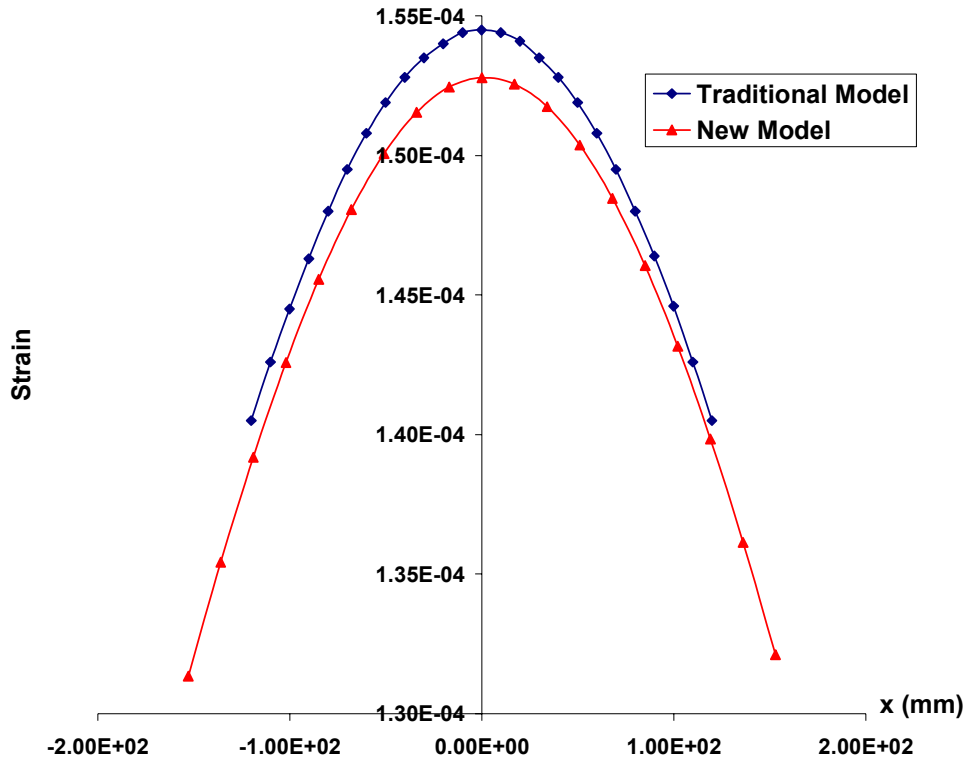
B. Pavement 2



(a) ϵ_{txx}

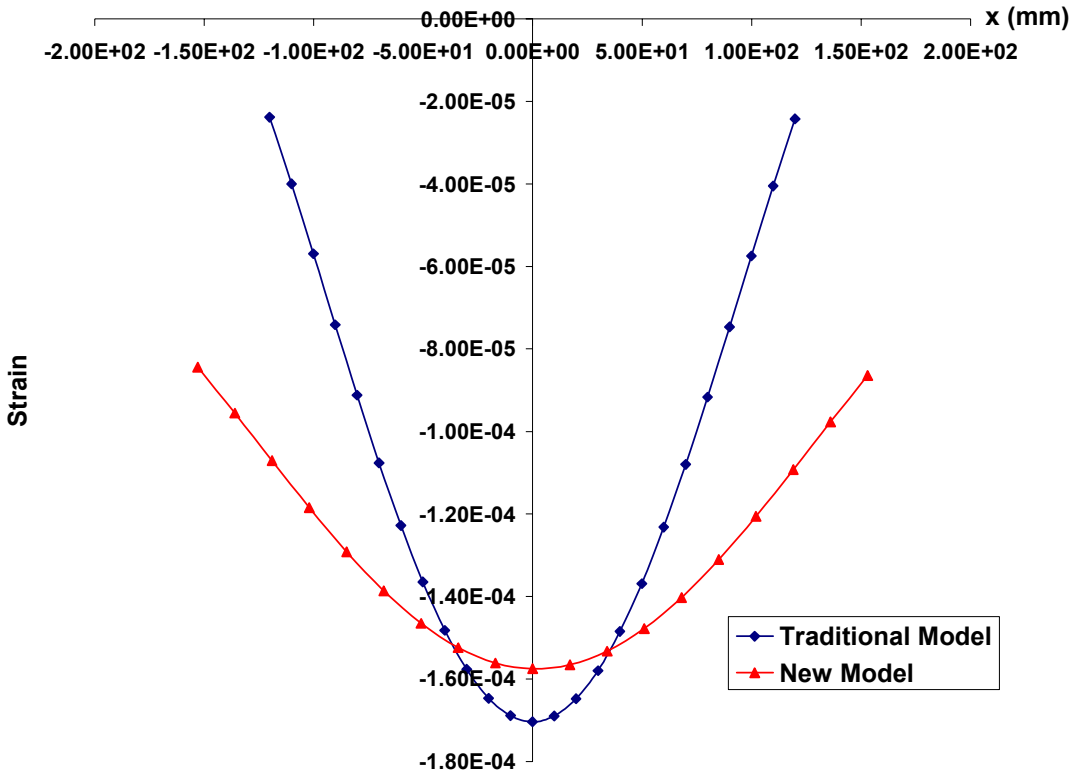


(b) ϵ_{yy}

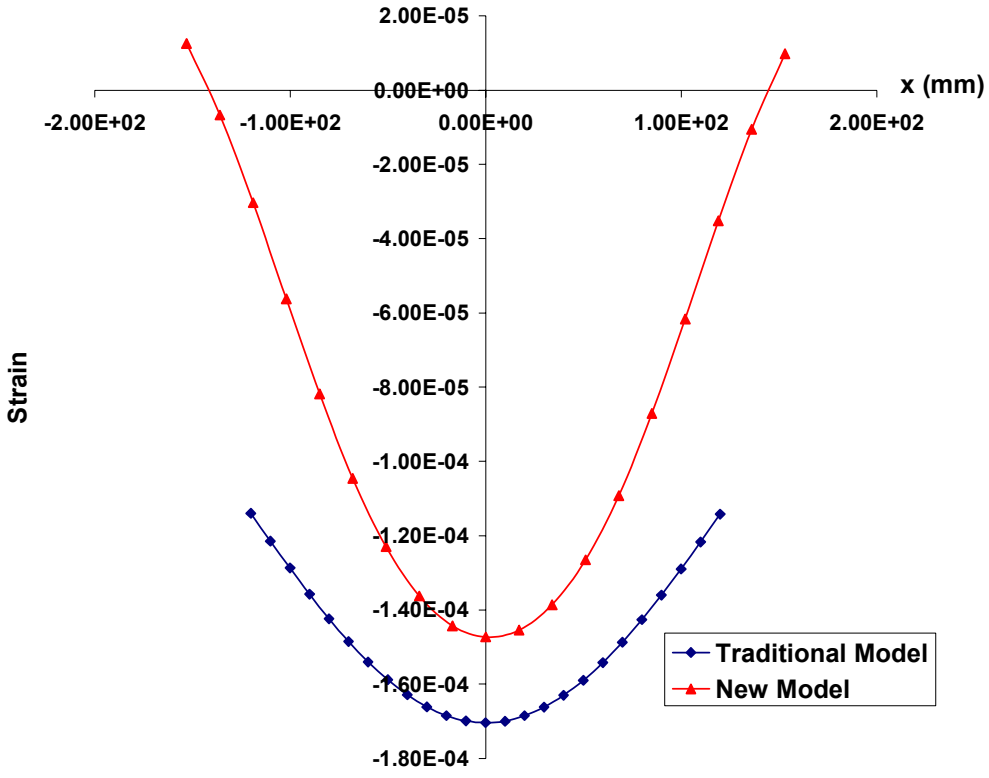


(c) ϵ_{czz}

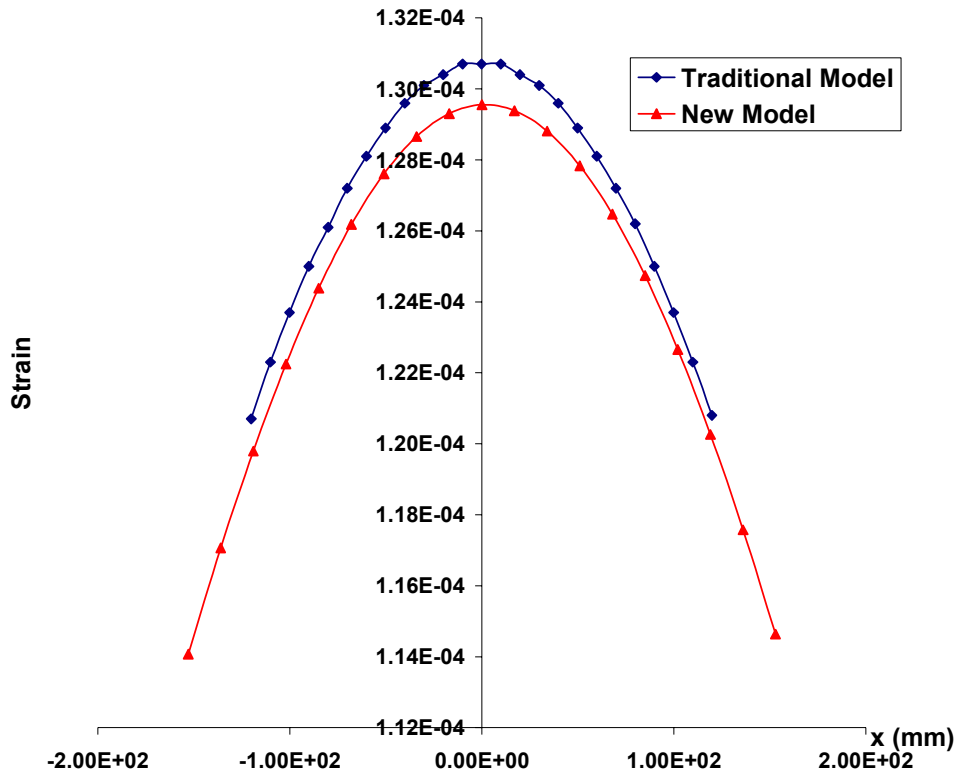
C. Pavement 3



(a) ϵ_{txx}

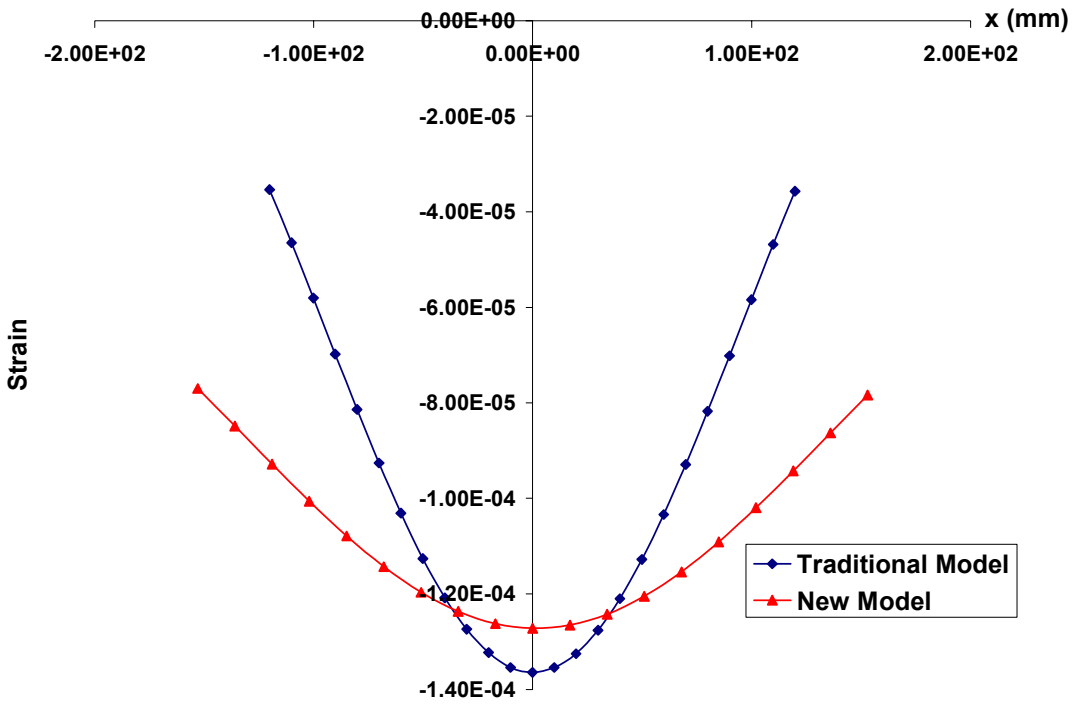


(b) ϵ_{yy}

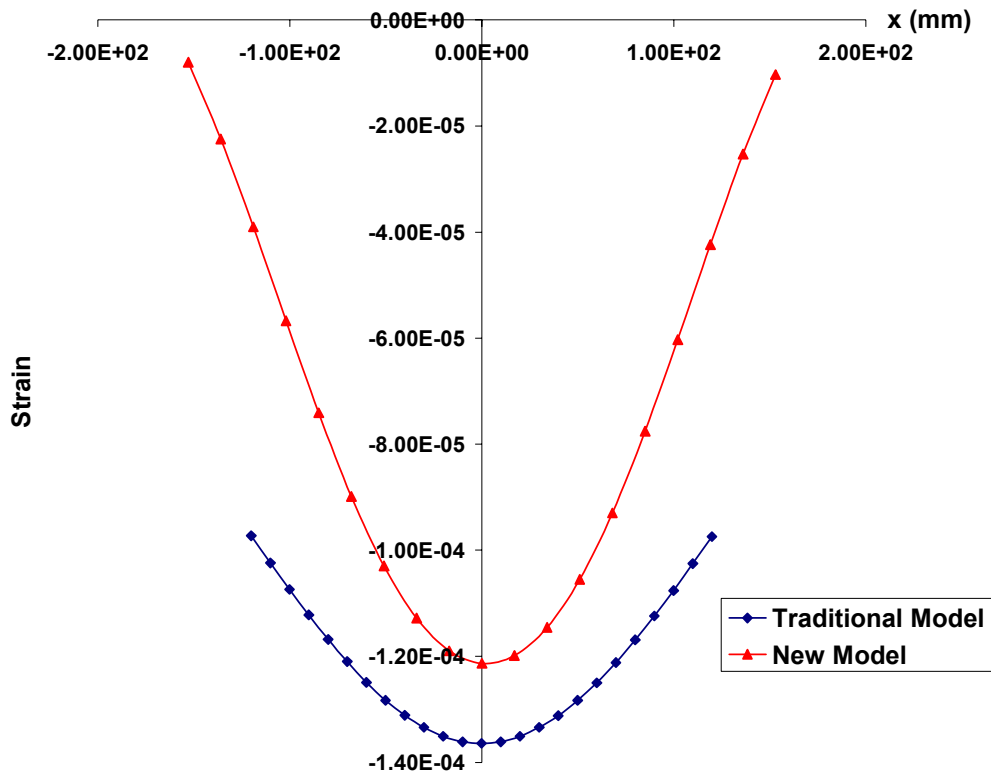


(c) ϵ_{czz}

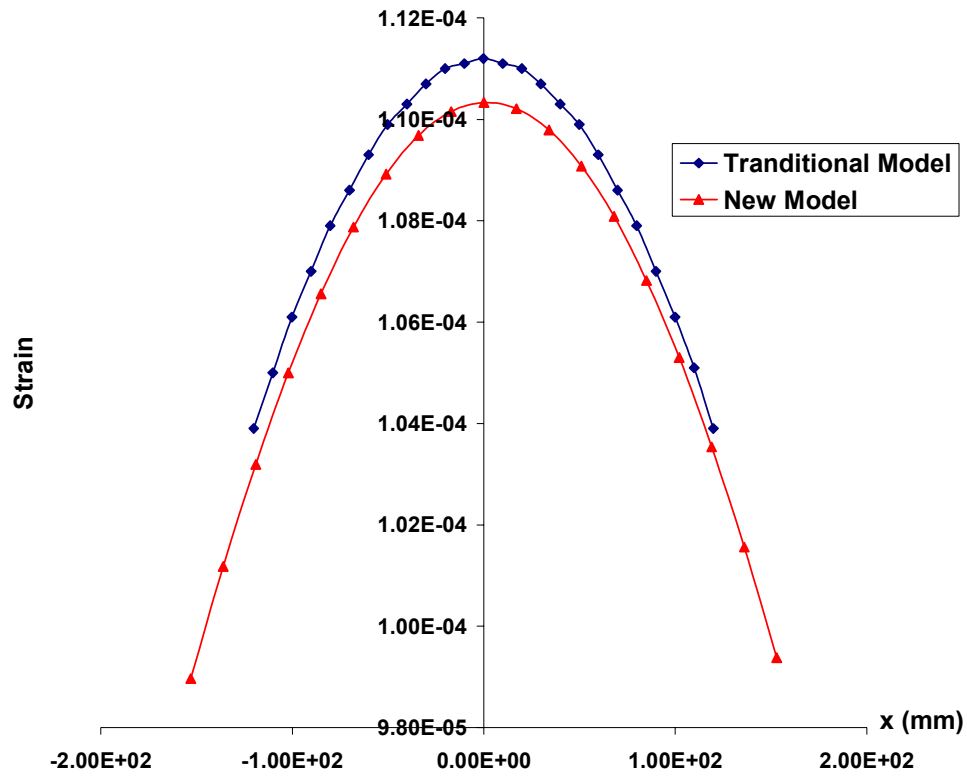
D. Pavement 4



(a) ϵ_{txx}



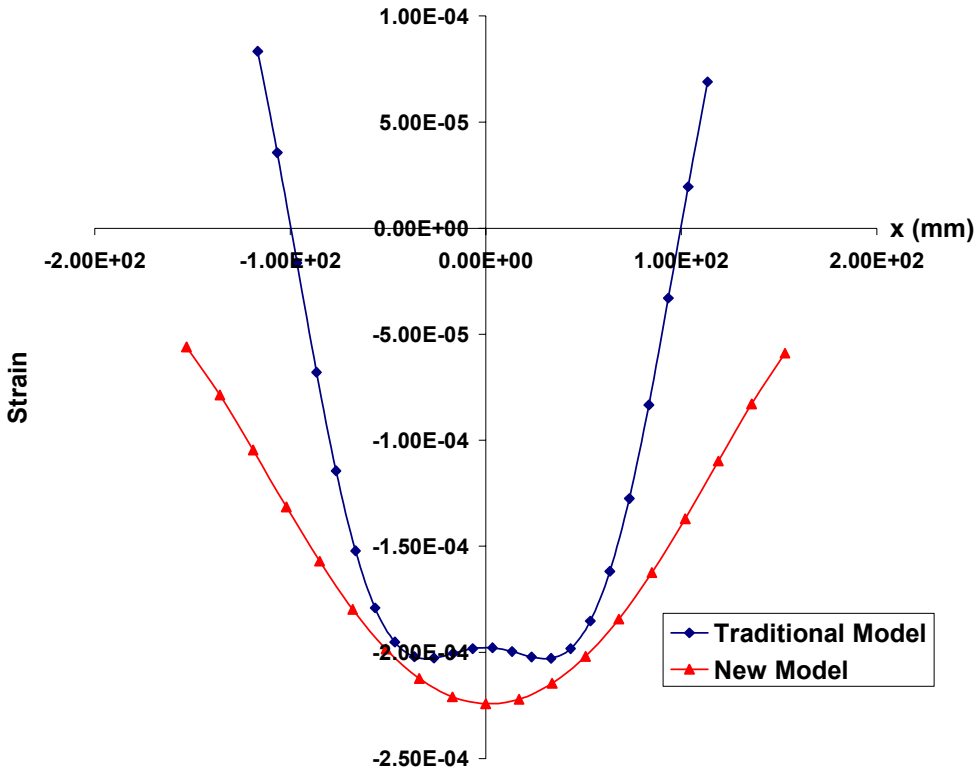
(b) ϵ_{yy}



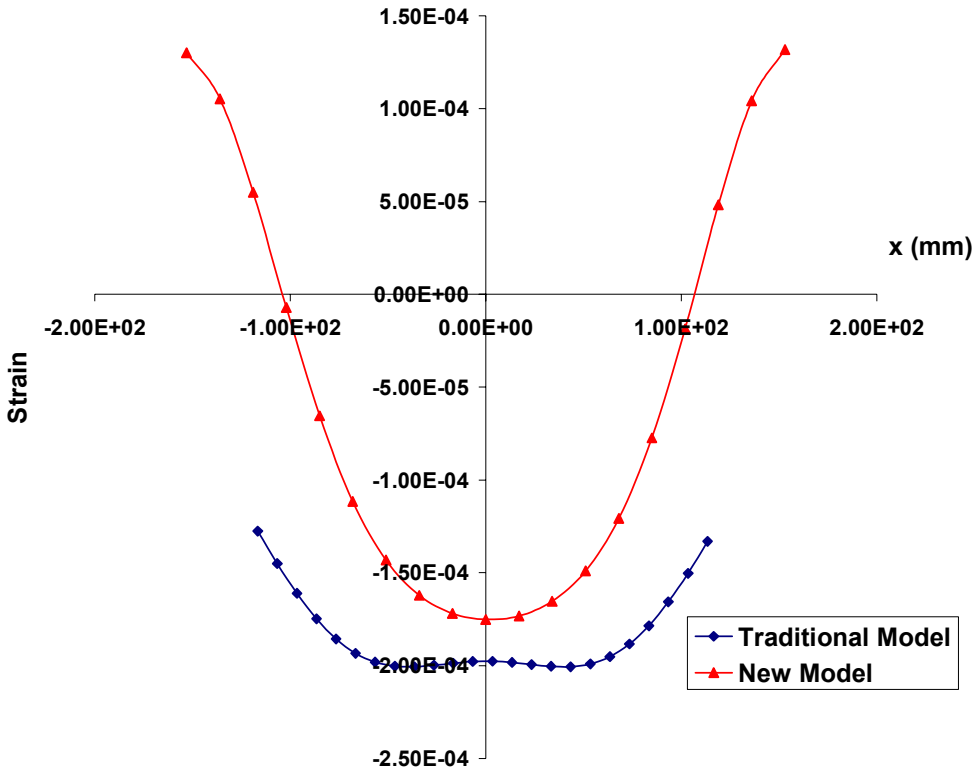
(c) ϵ_{czz}

Appendix 6: Strain Comparison in LTEX014 (L=28.3 kN, P=793 kPa)

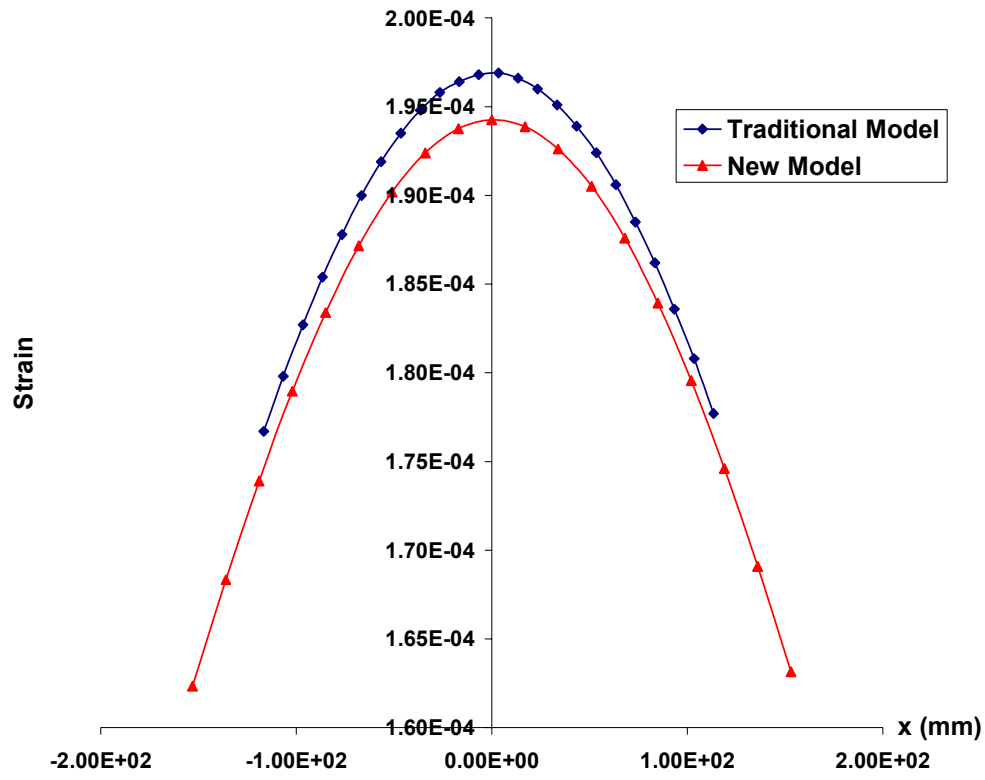
A. Pavement 1



(a) ϵ_{txx}

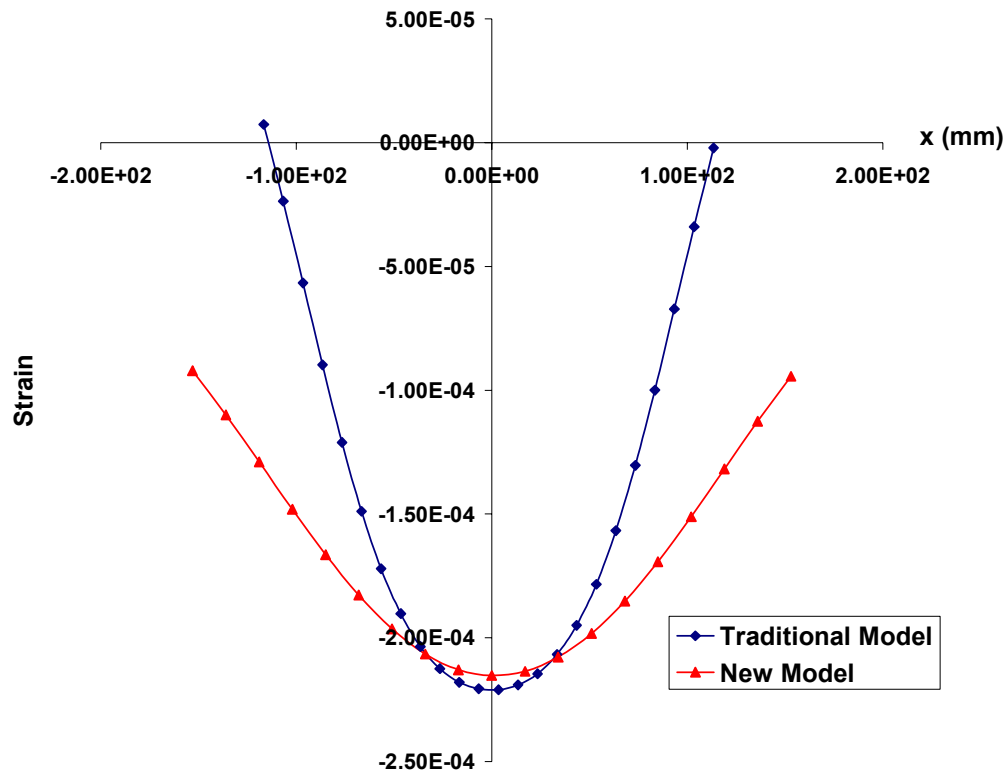


(b) ϵ_{yy}

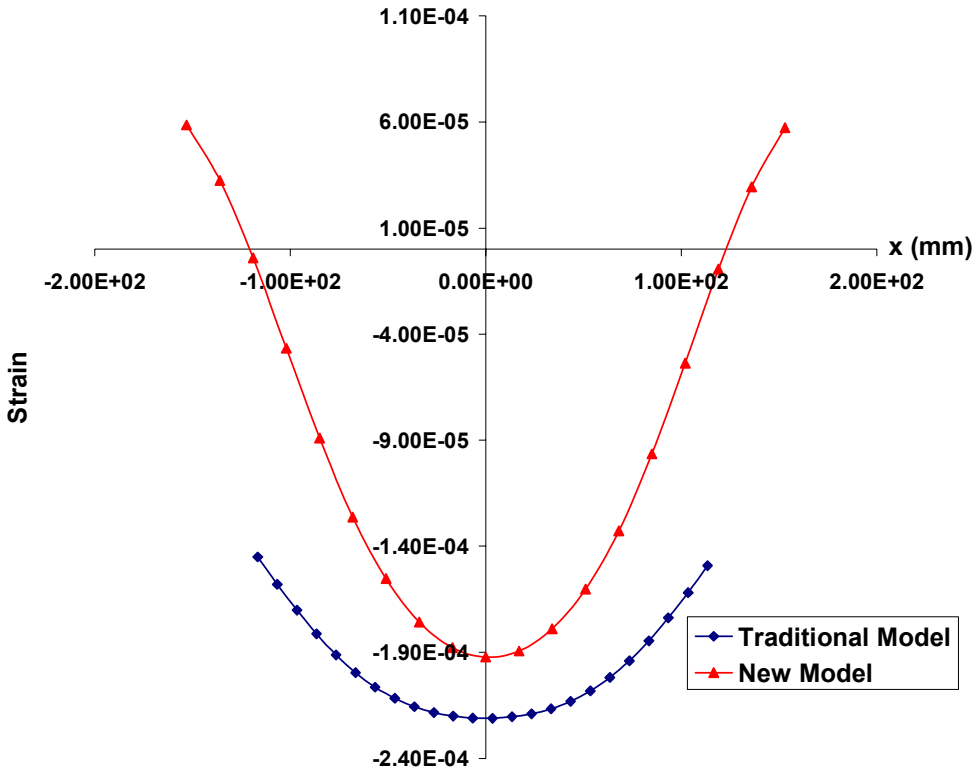


(c) ϵ_{czz}

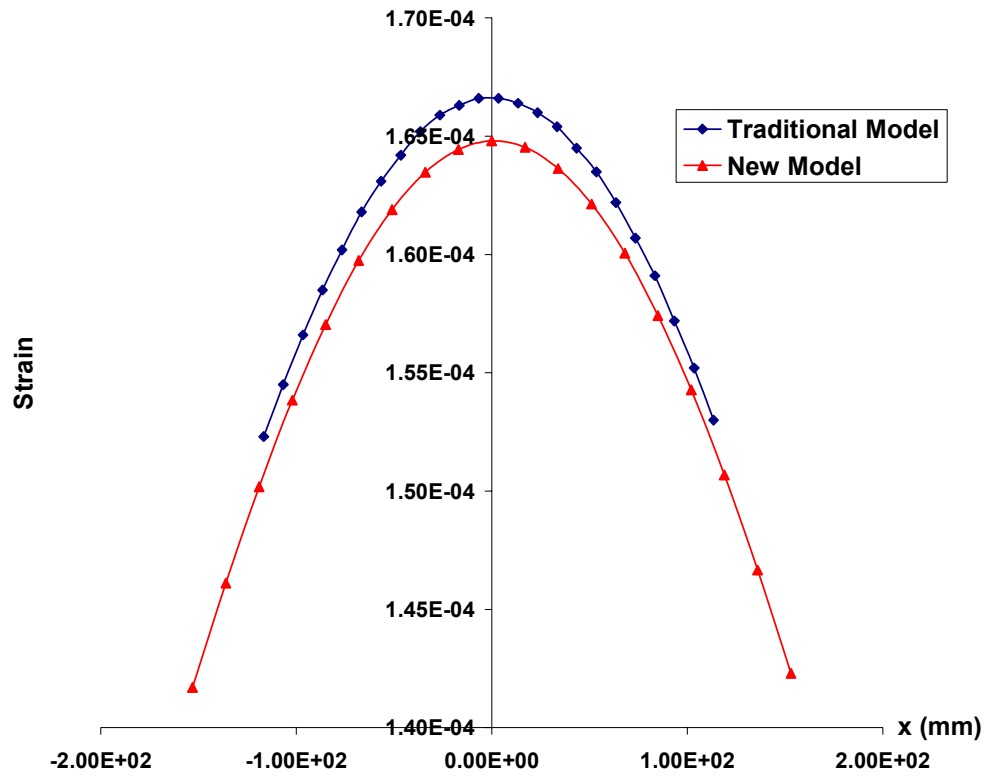
B. Pavement 2



(a) ϵ_{txx}

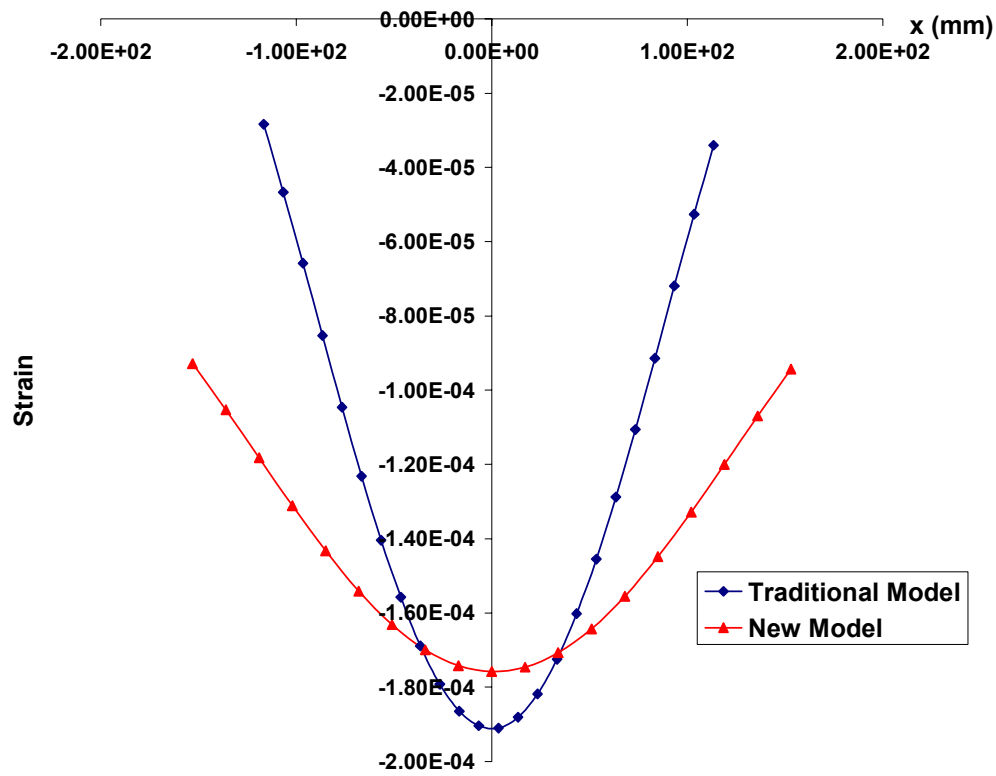


(b) ϵ_{yy}

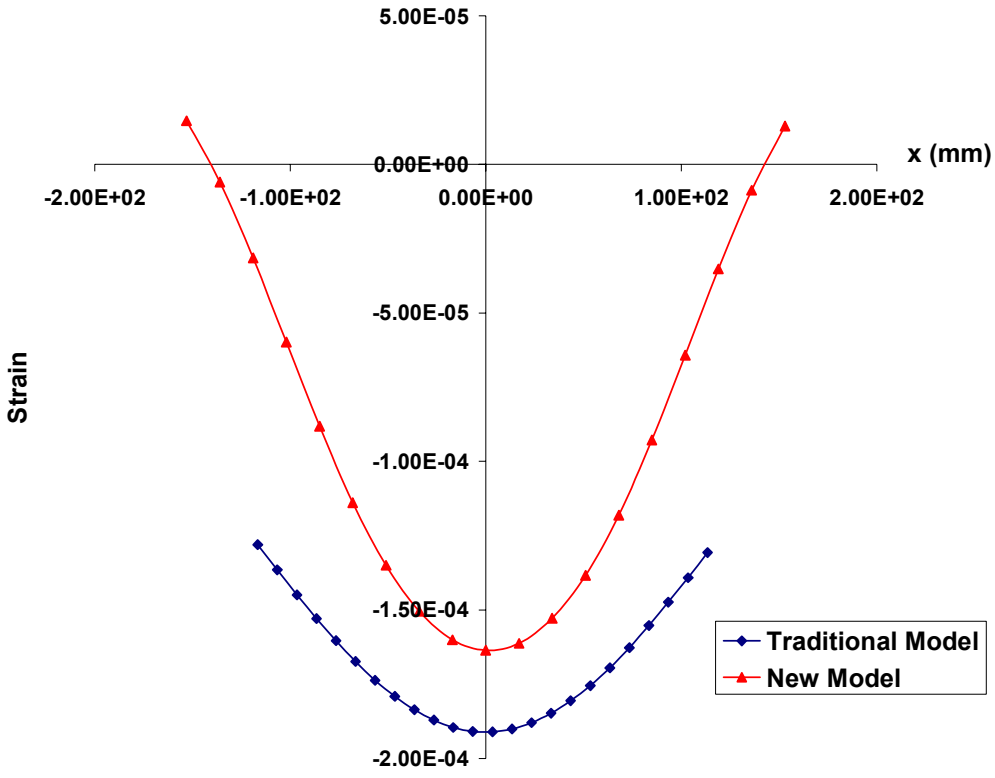


(c) ϵ_{czz}

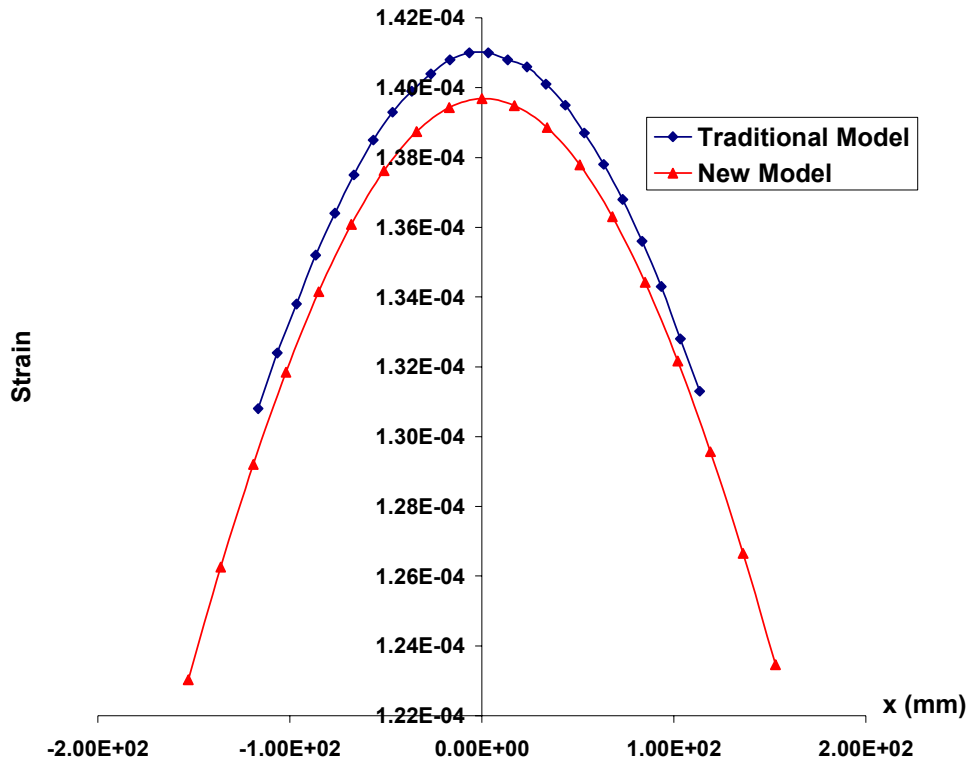
C. Pavement 3



(a) ϵ_{txx}

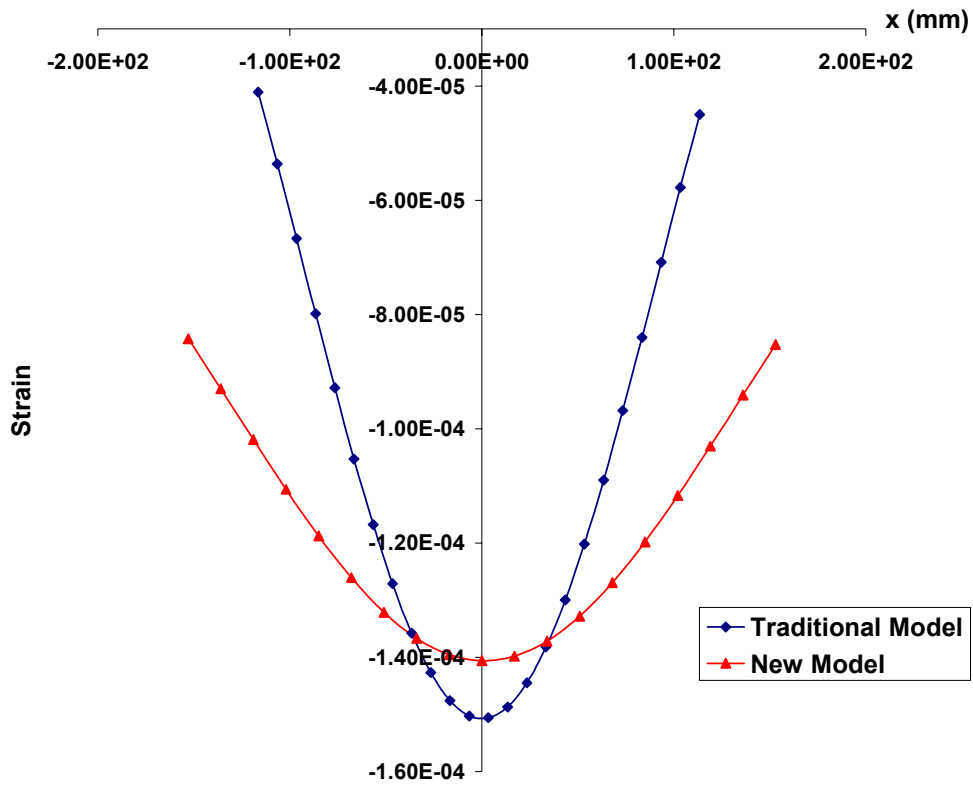


(b) ϵ_{yy}

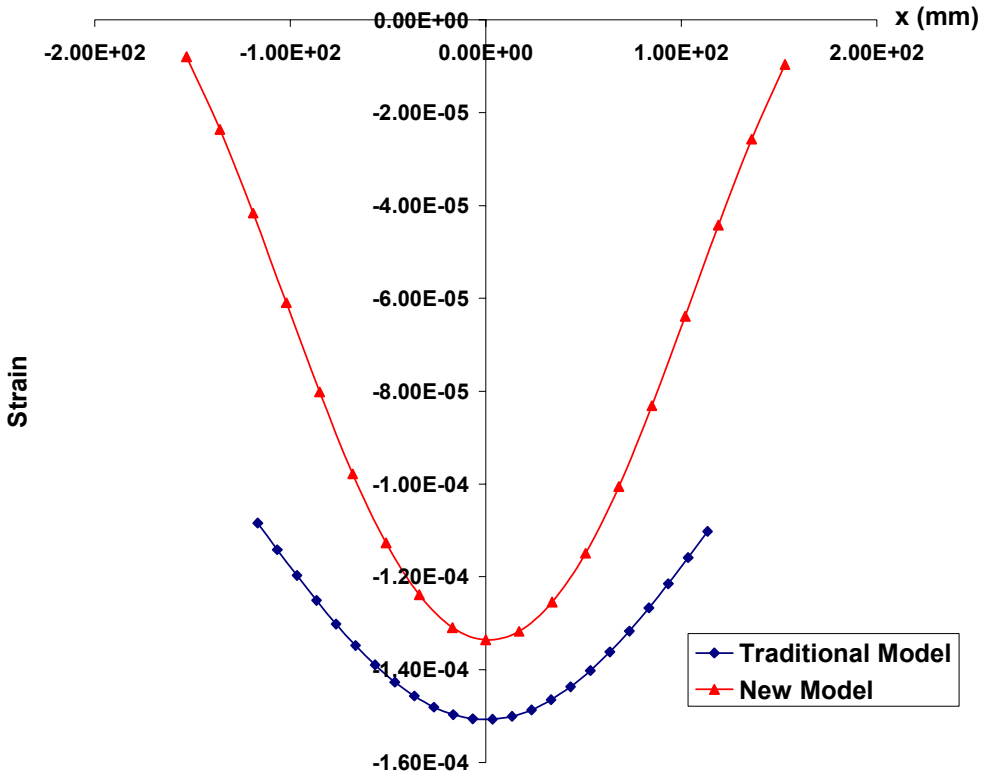


(c) ϵ_{czz}

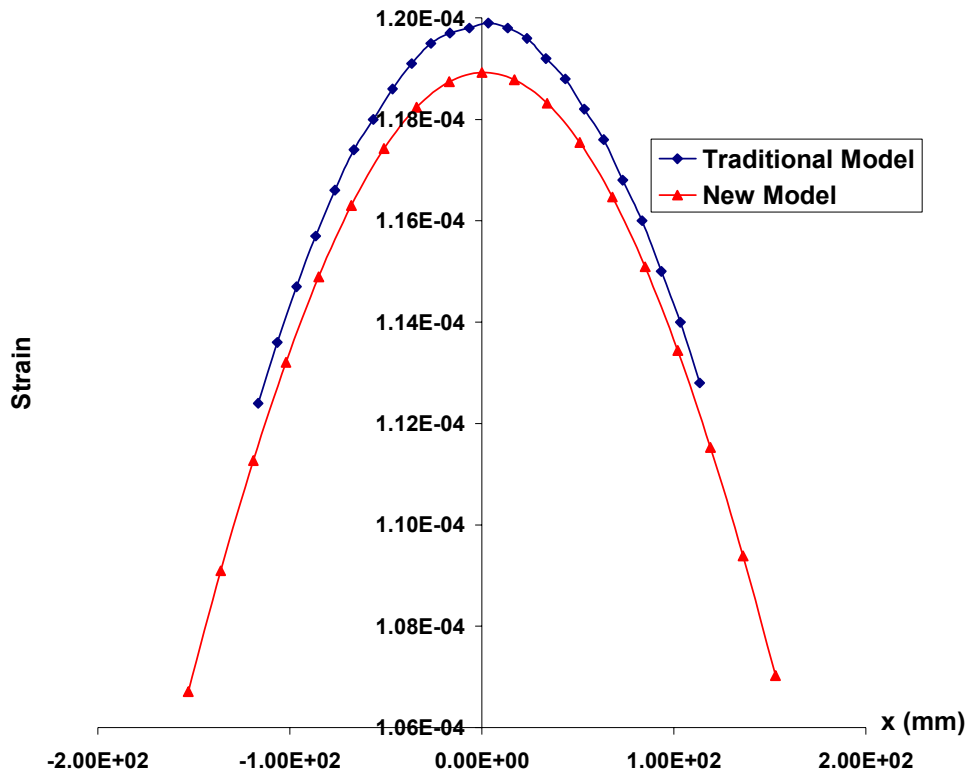
D. Pavement 4



(a) ϵ_{txx}



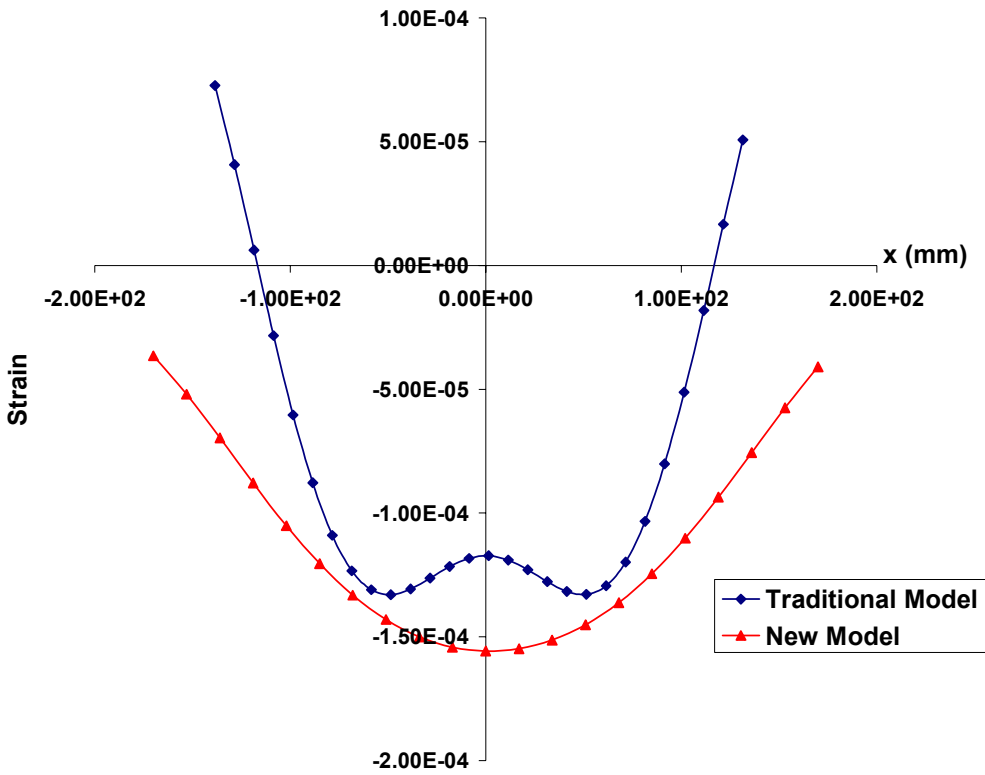
(b) ϵ_{yy}



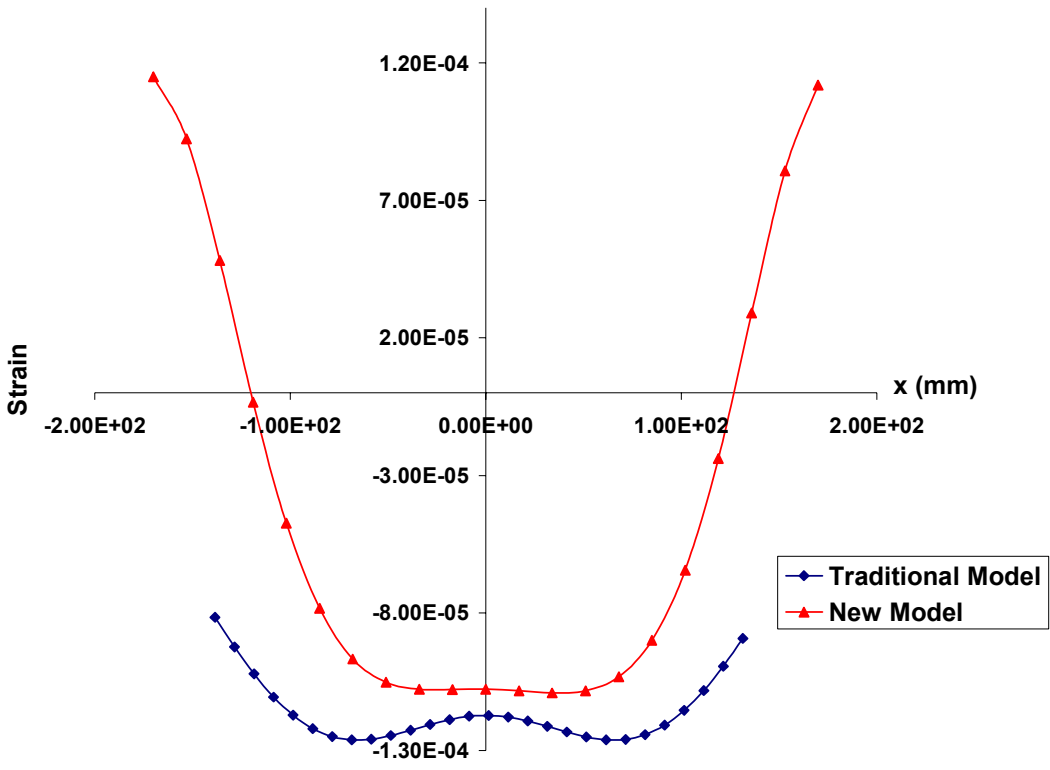
(c) ϵ_{czz}

Appendix 7: Strain Comparison in LTEX017 (L=30.4 kN, P=586 kPa)

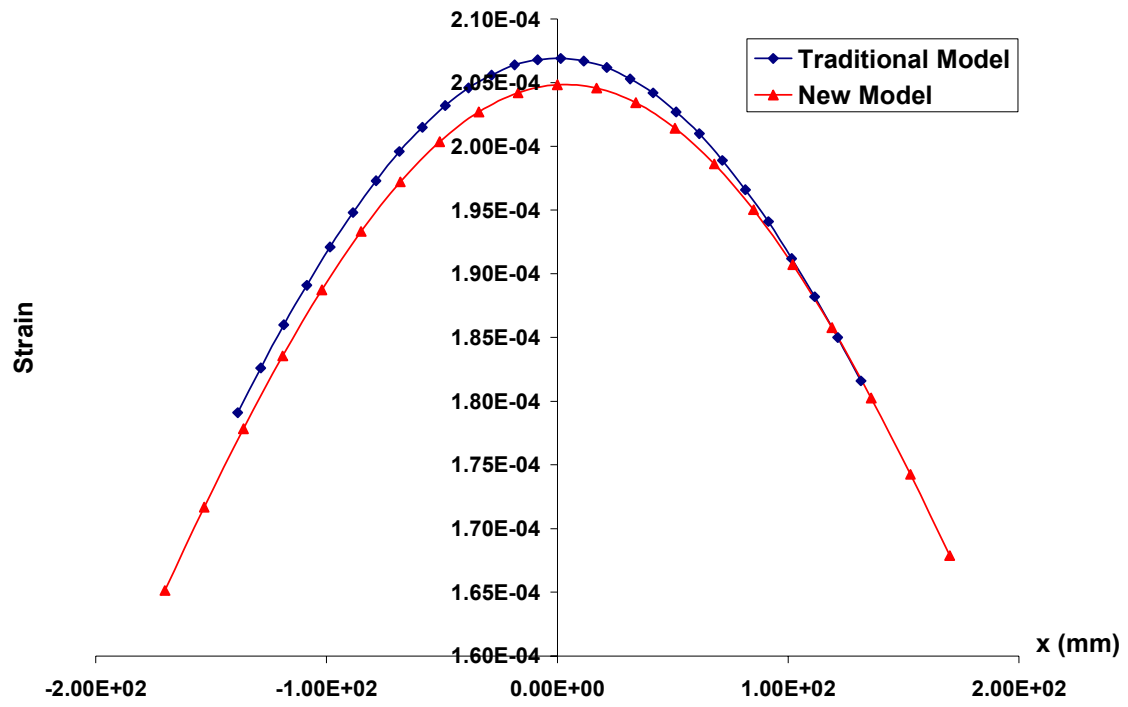
A. Pavement 1



(a) ϵ_{txx}

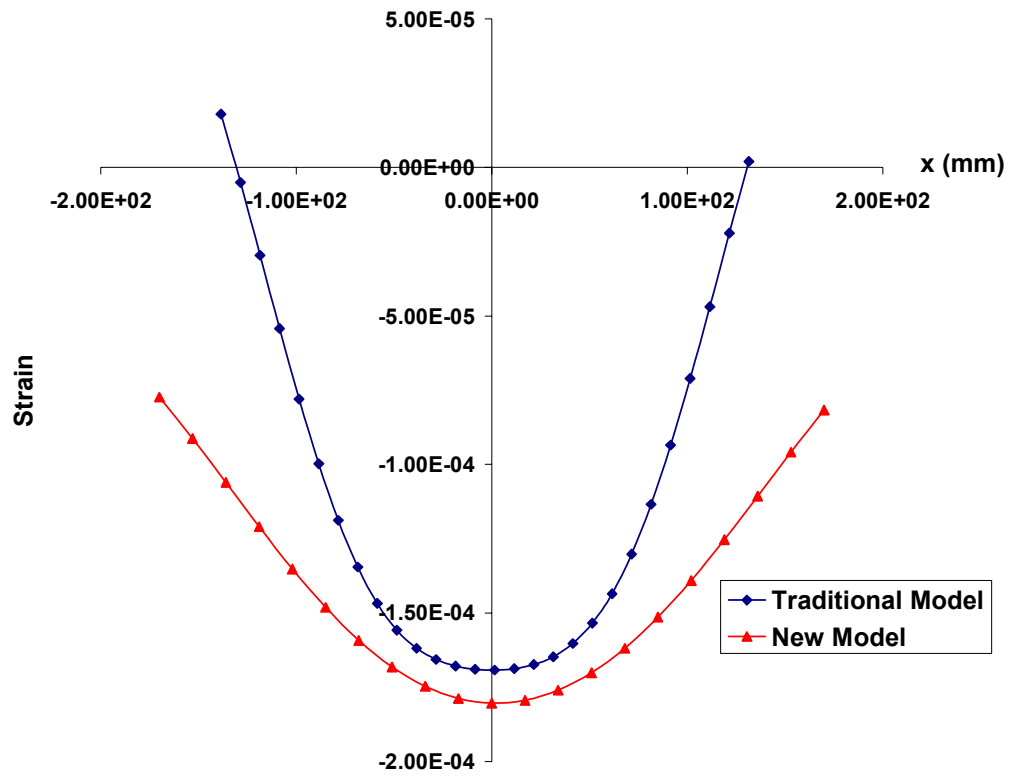


(b) ϵ_{yy}

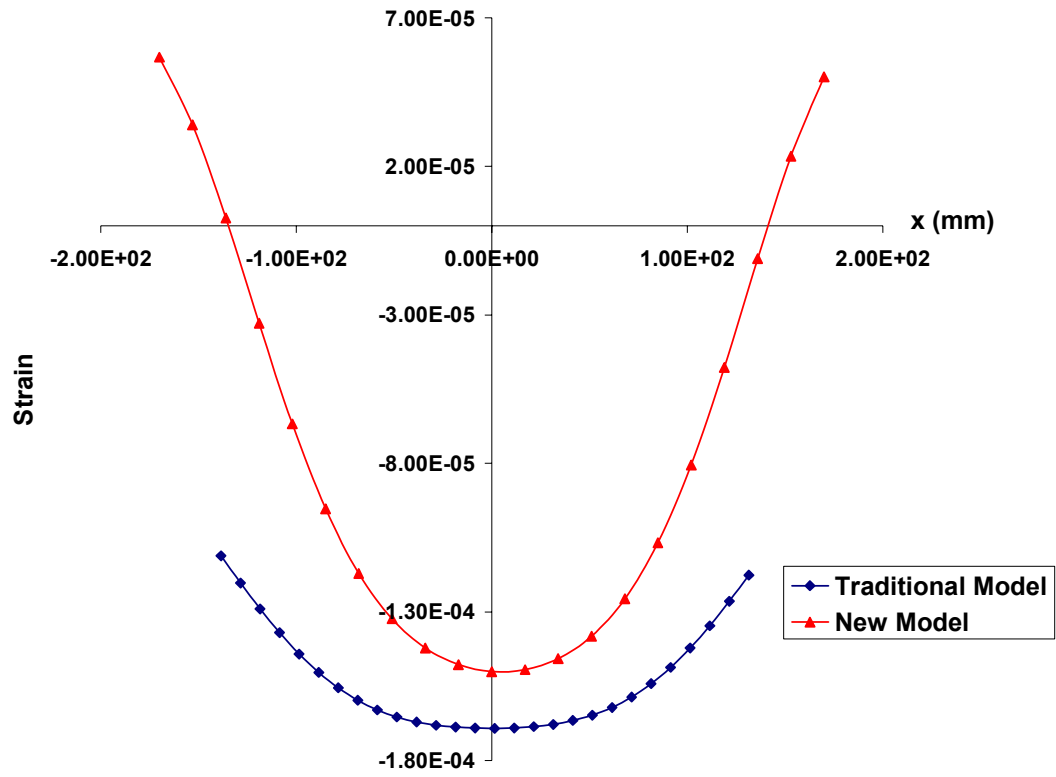


(c) ϵ_{czz}

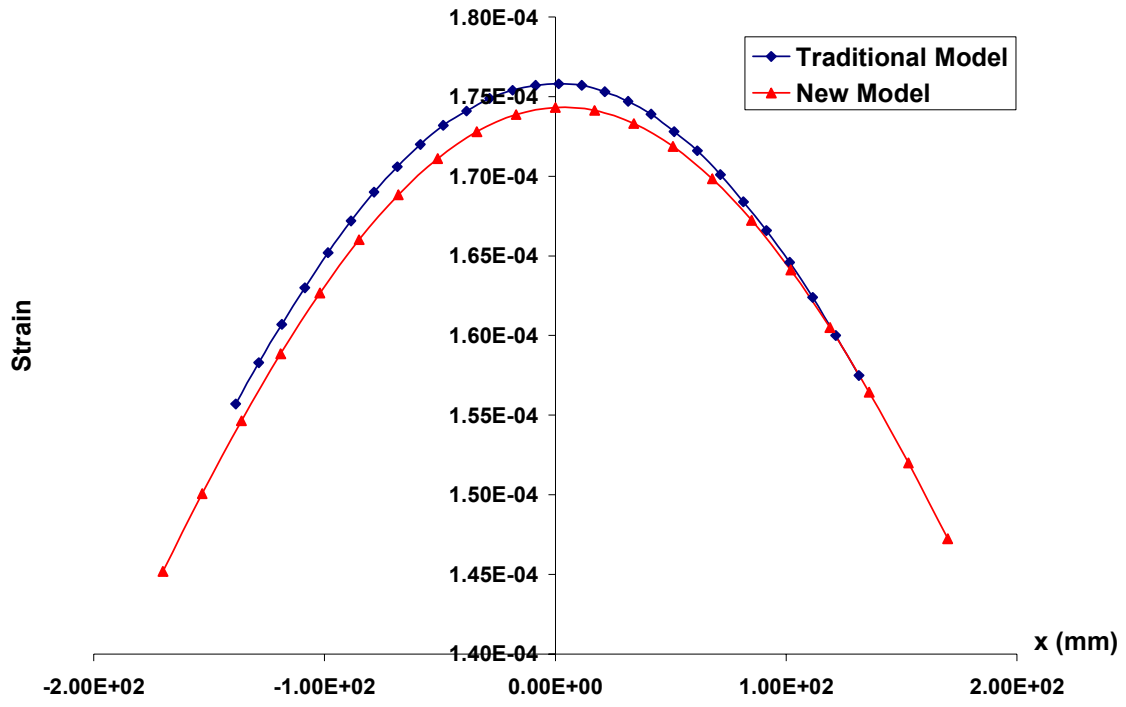
B. Pavement 2



(a) ϵ_{txx}

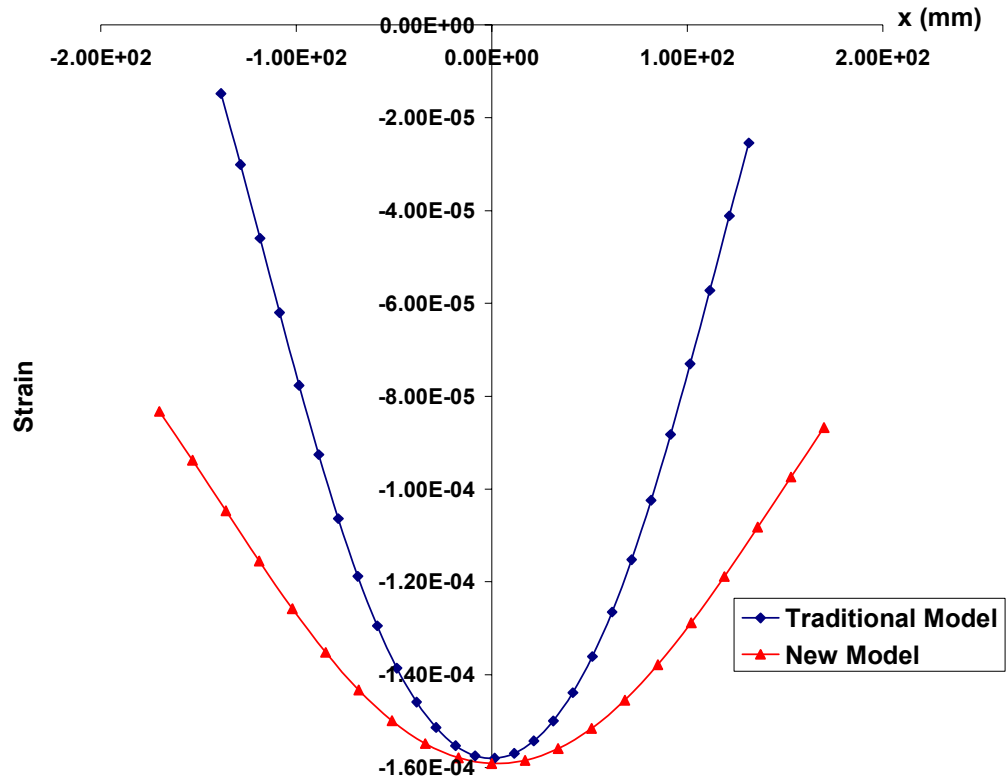


(b) ϵ_{yy}

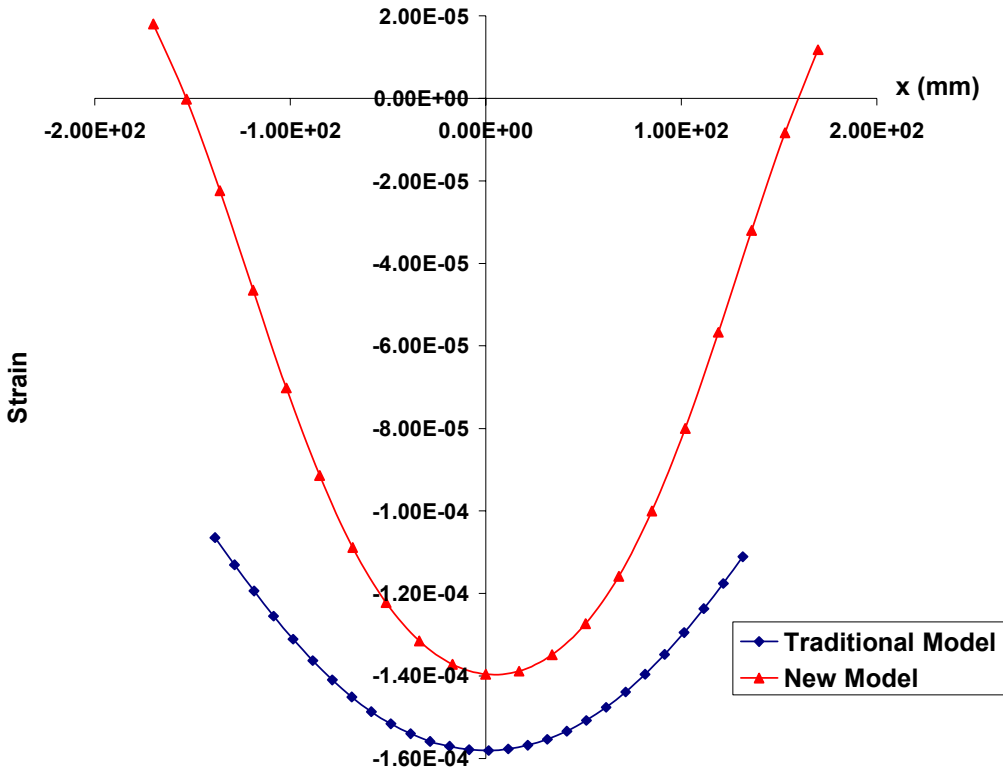


(c) ϵ_{czz}

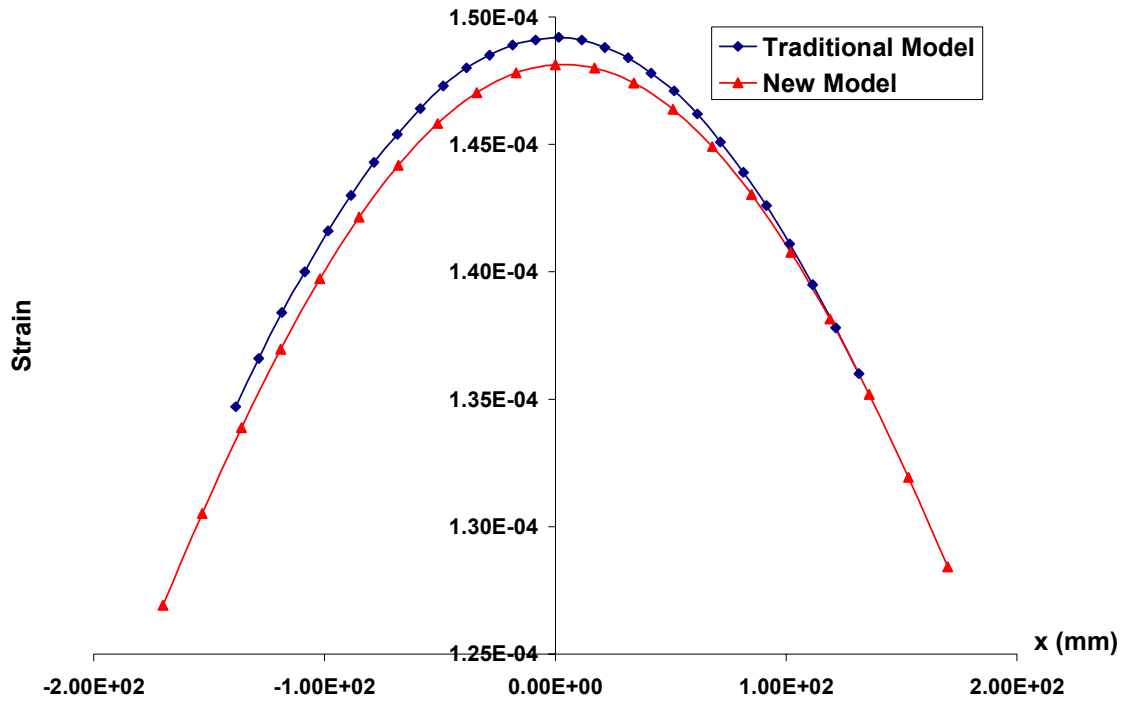
C. Pavement 3



(a) ϵ_{txx}

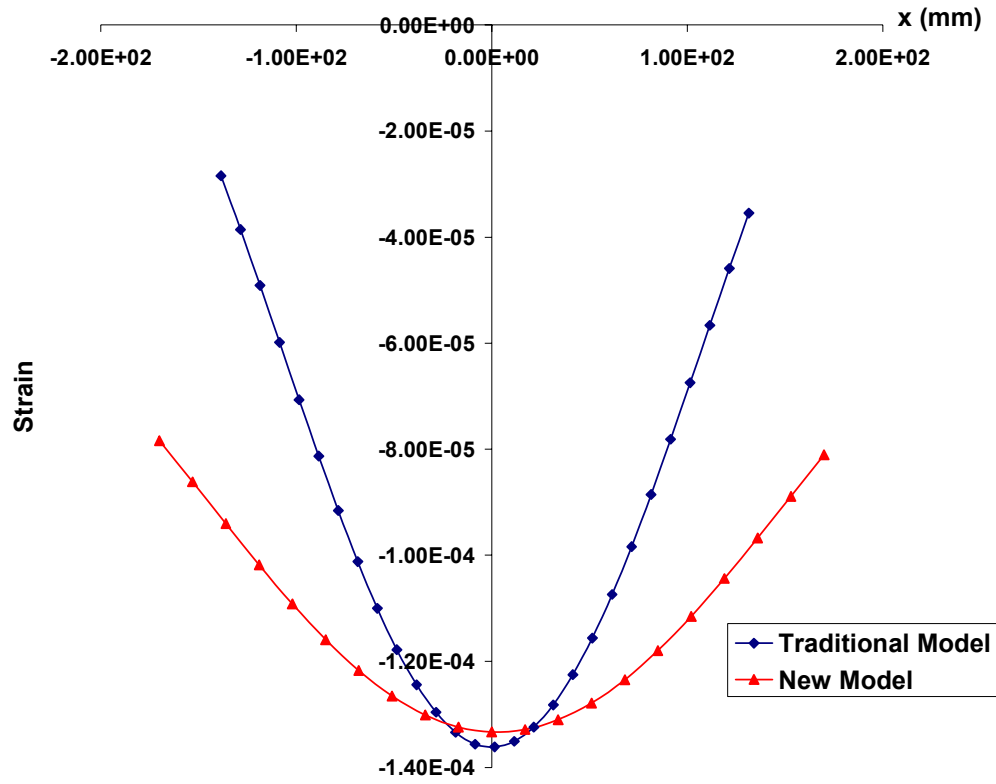


(b) ϵ_{yy}

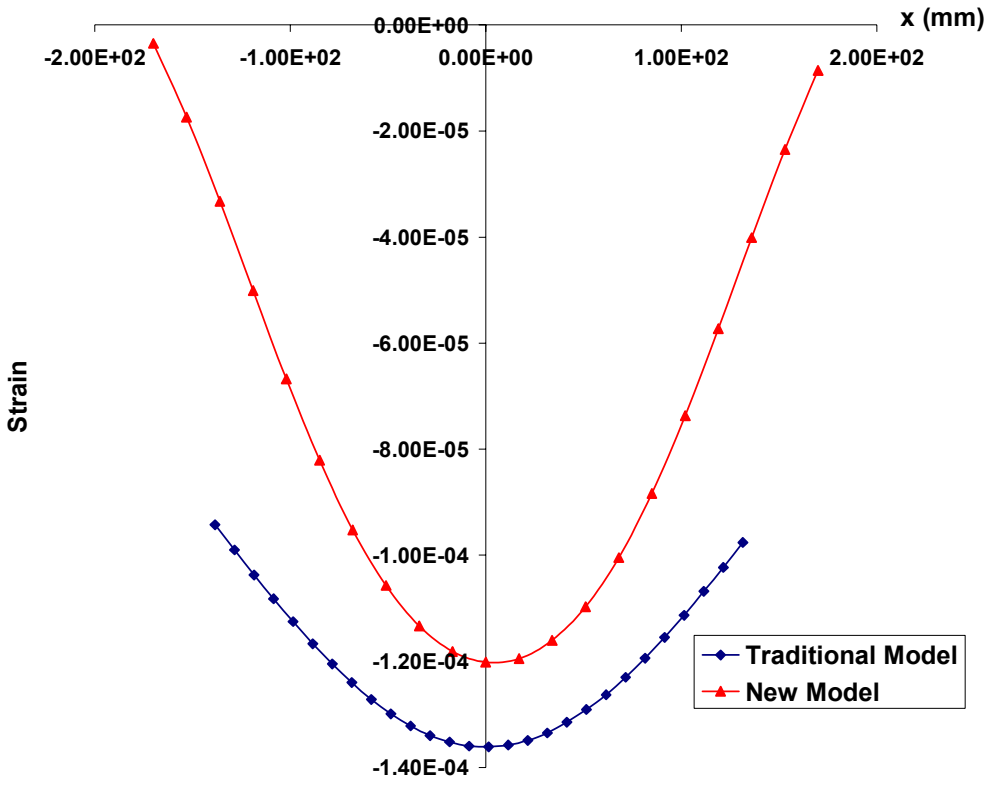


(c) ϵ_{czz}

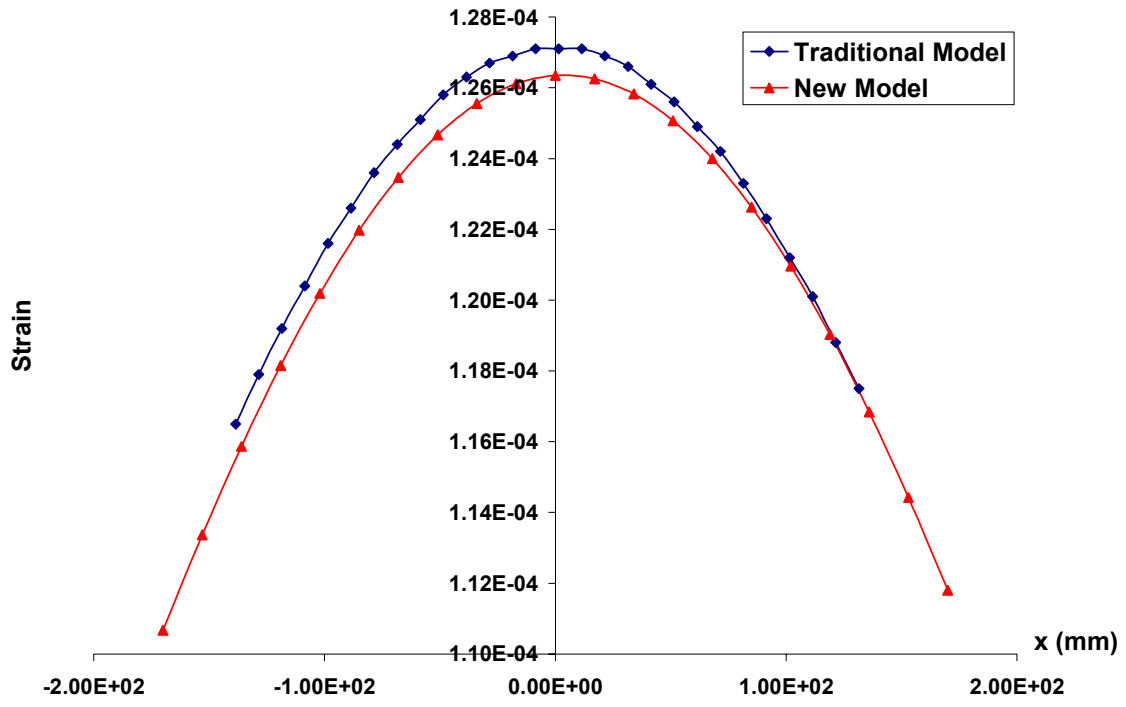
D. Pavement 4



(a) ϵ_{txx}



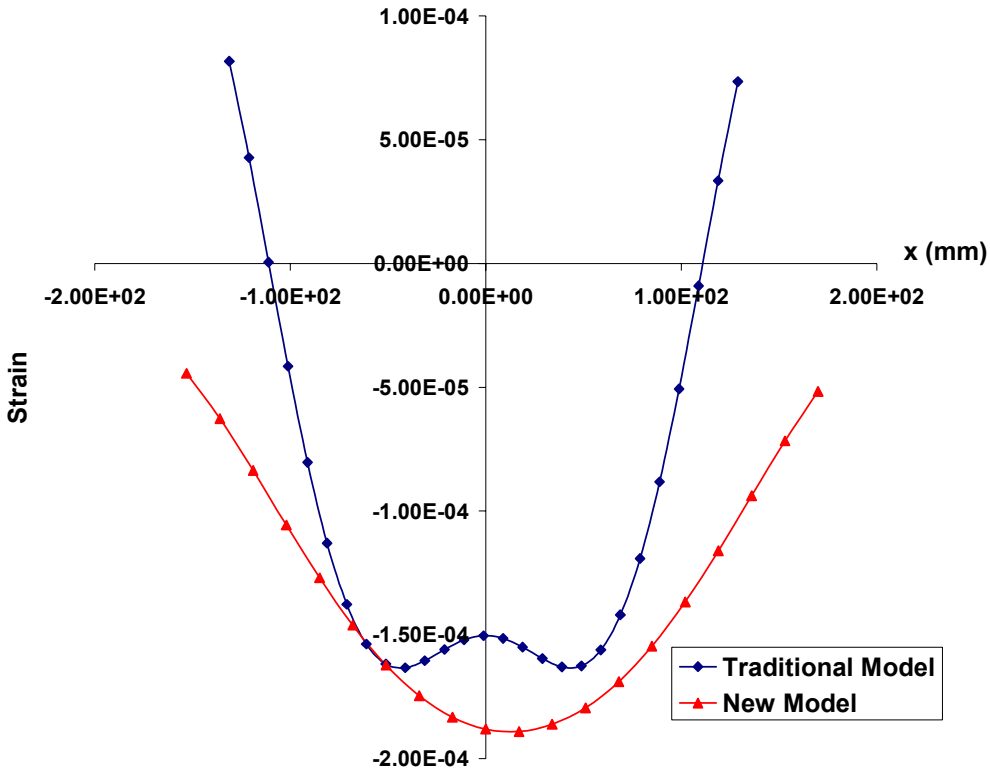
(b) ϵ_{yy}



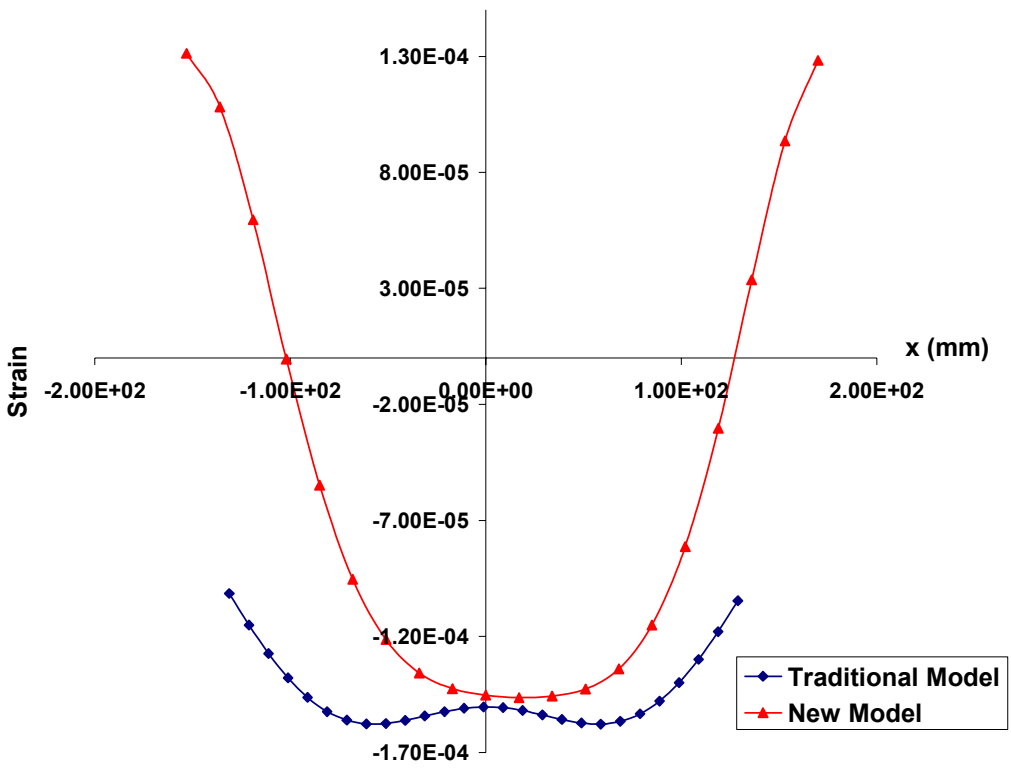
(c) ϵ_{czz}

Appendix 8: Strain Comparison in LTEX018 (L=31.8 kN, P=690 kPa)

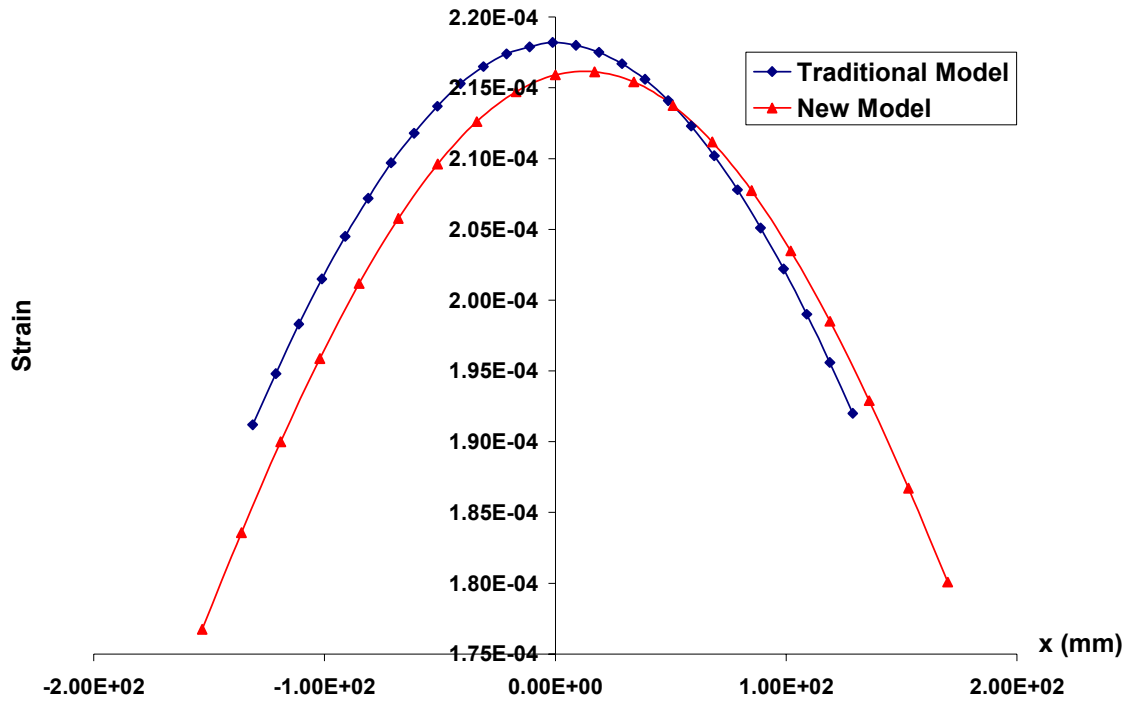
A. Pavement 1



(a) ϵ_{txx}

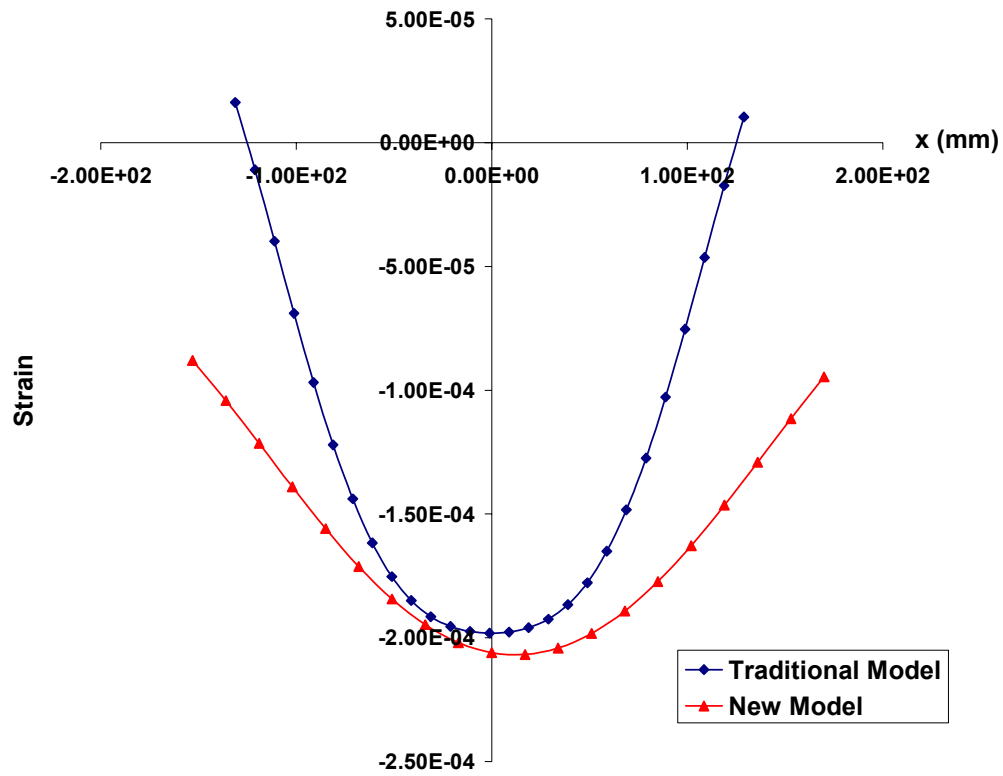


(b) ϵ_{yy}

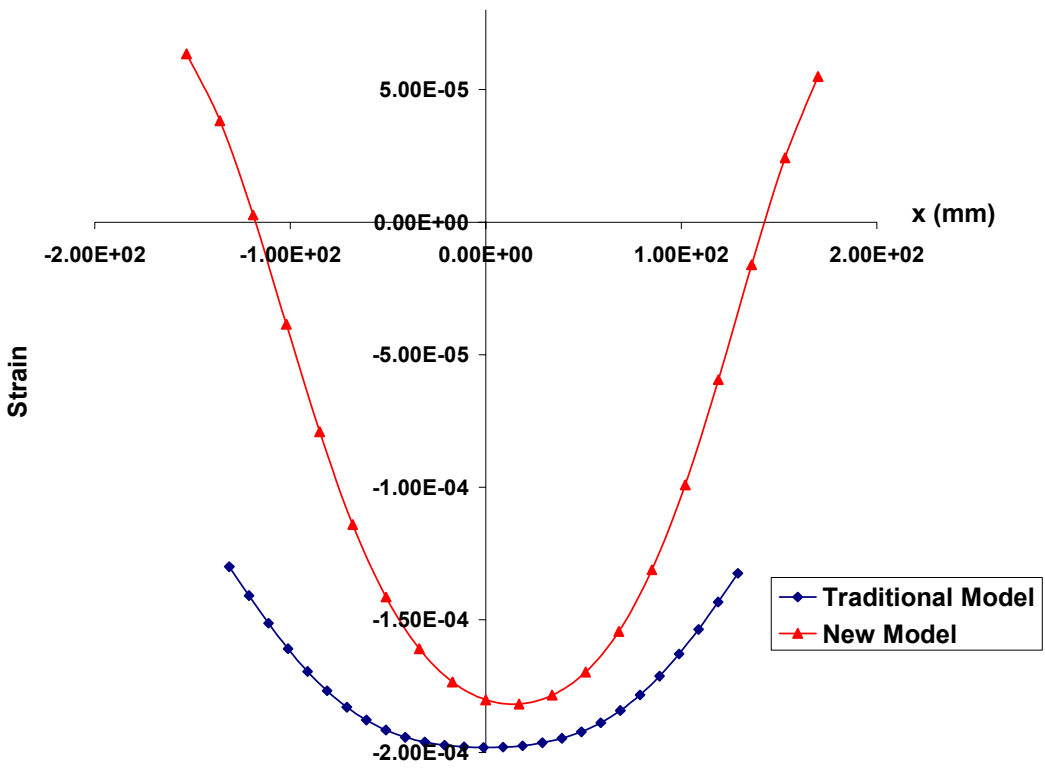


(c) ϵ_{czz}

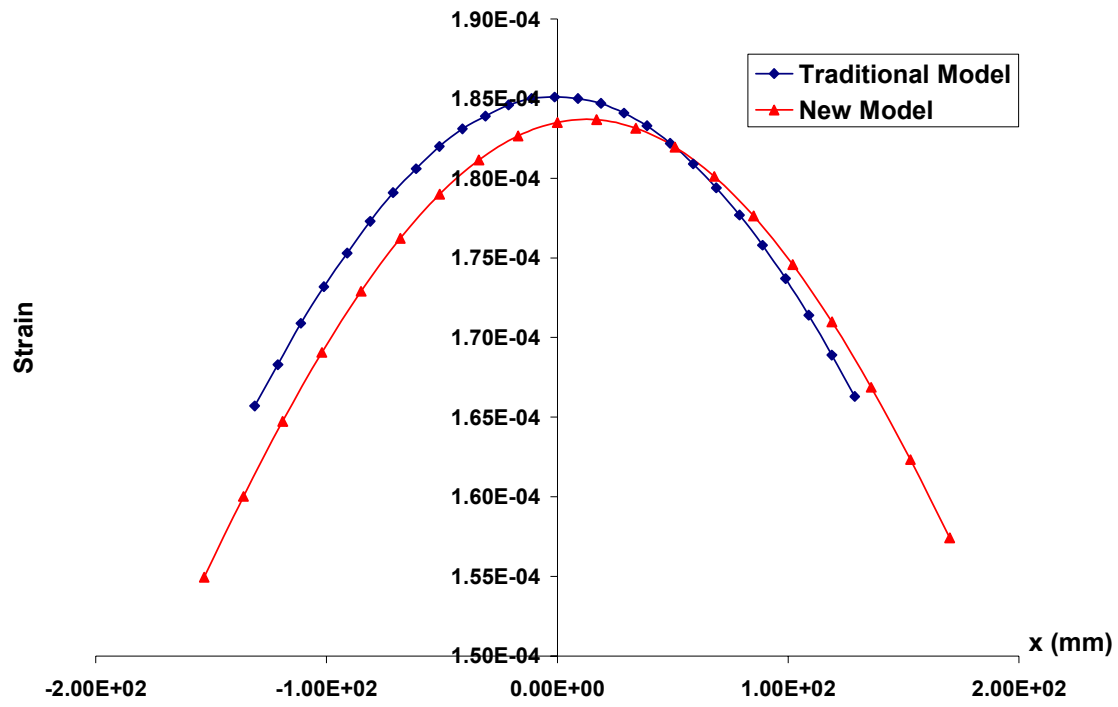
B. Pavement 2



(a) ϵ_{txx}

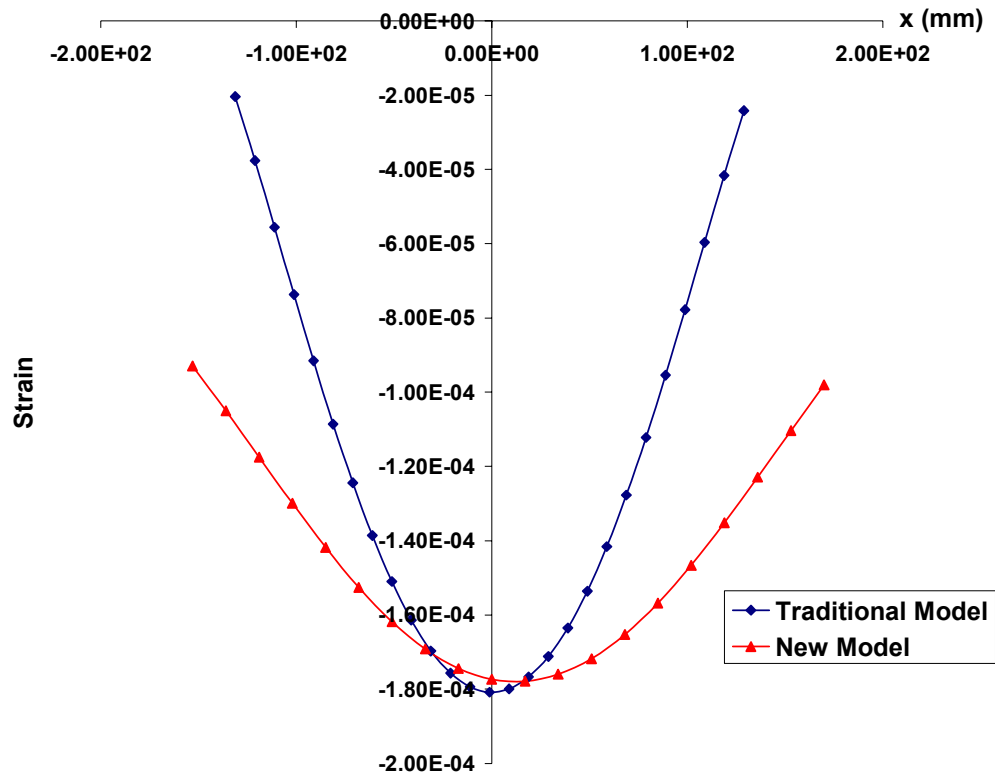


(b) ϵ_{yy}

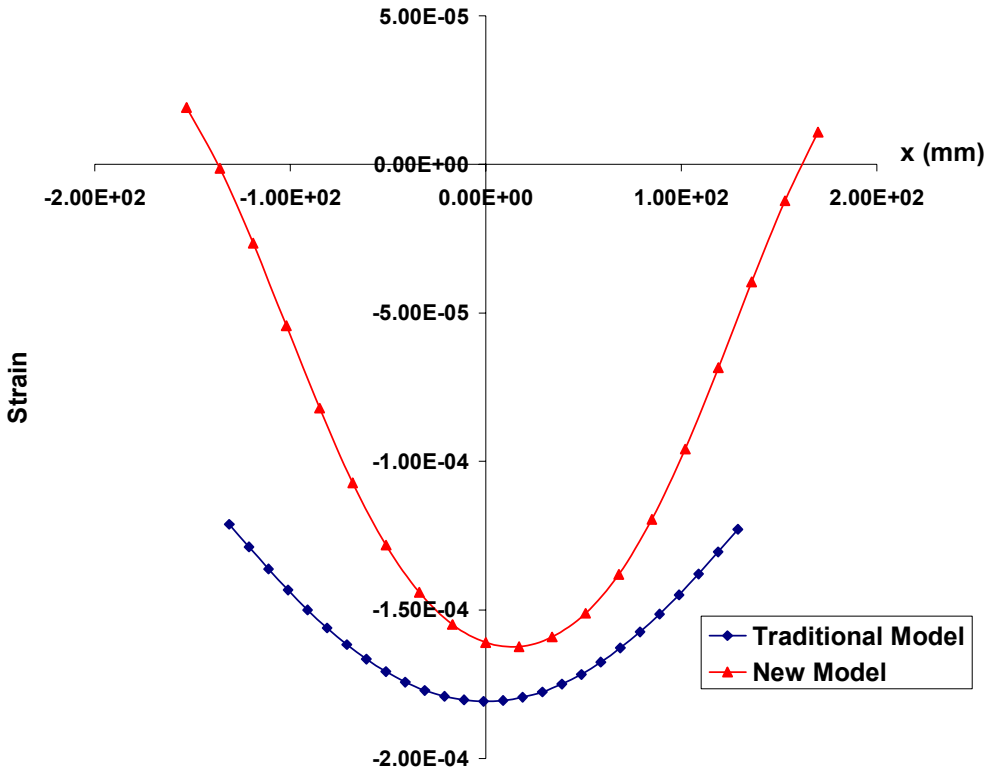


(c) ϵ_{czz}

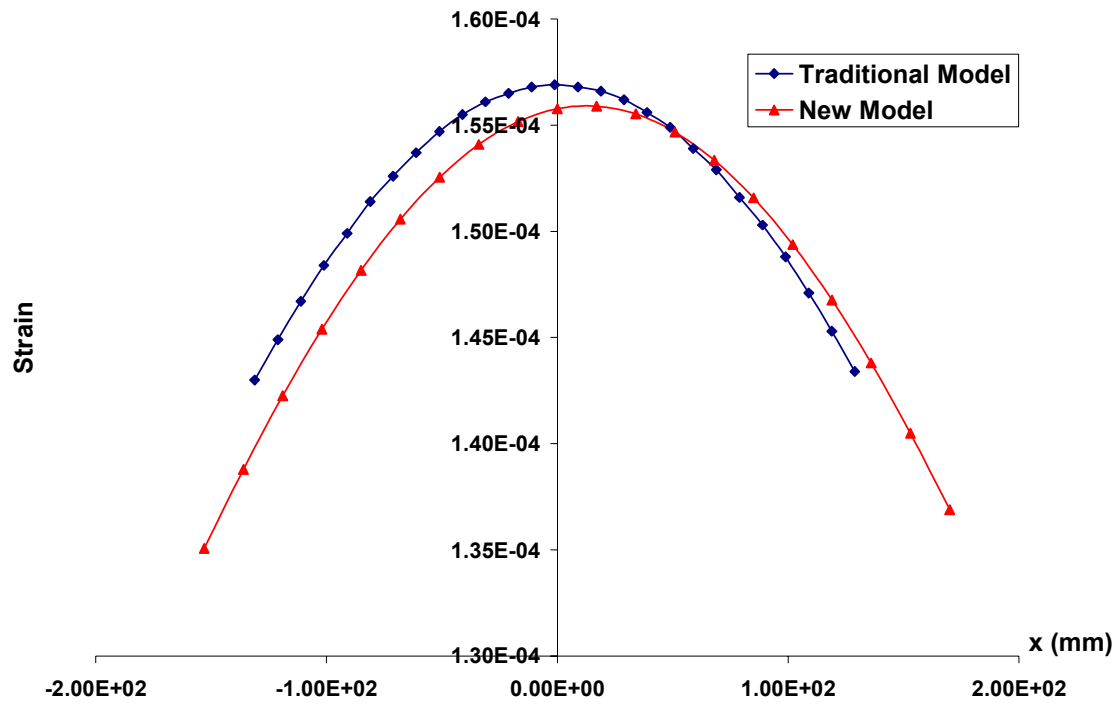
C. Pavement 3



(a) ϵ_{txx}

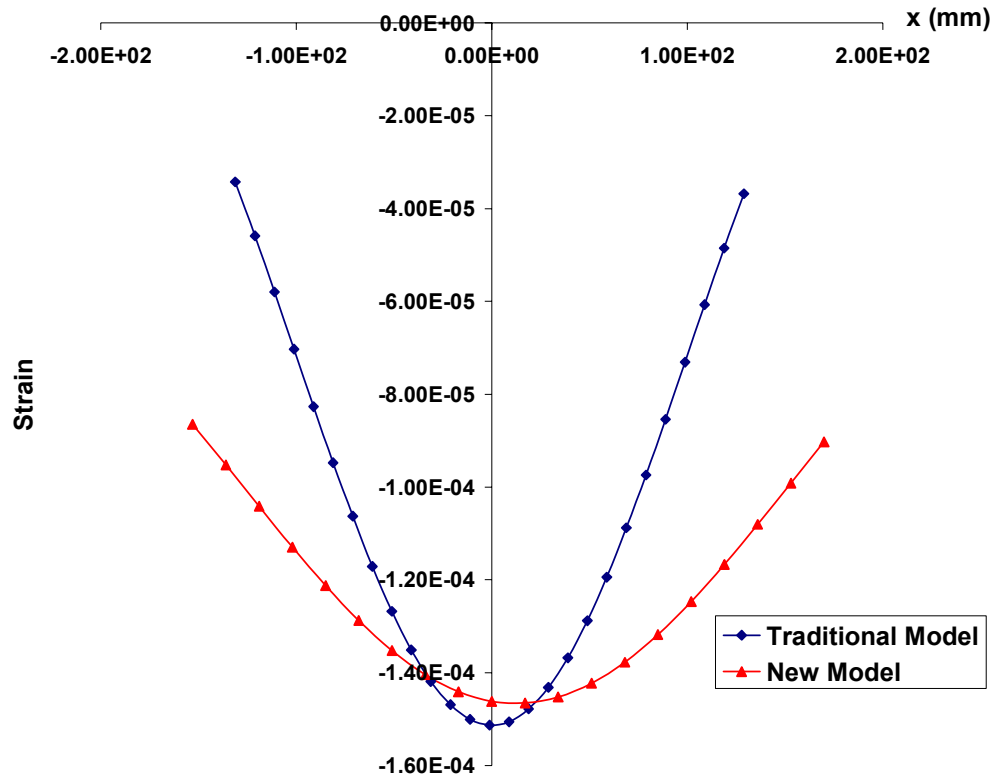


(b) ϵ_{yy}

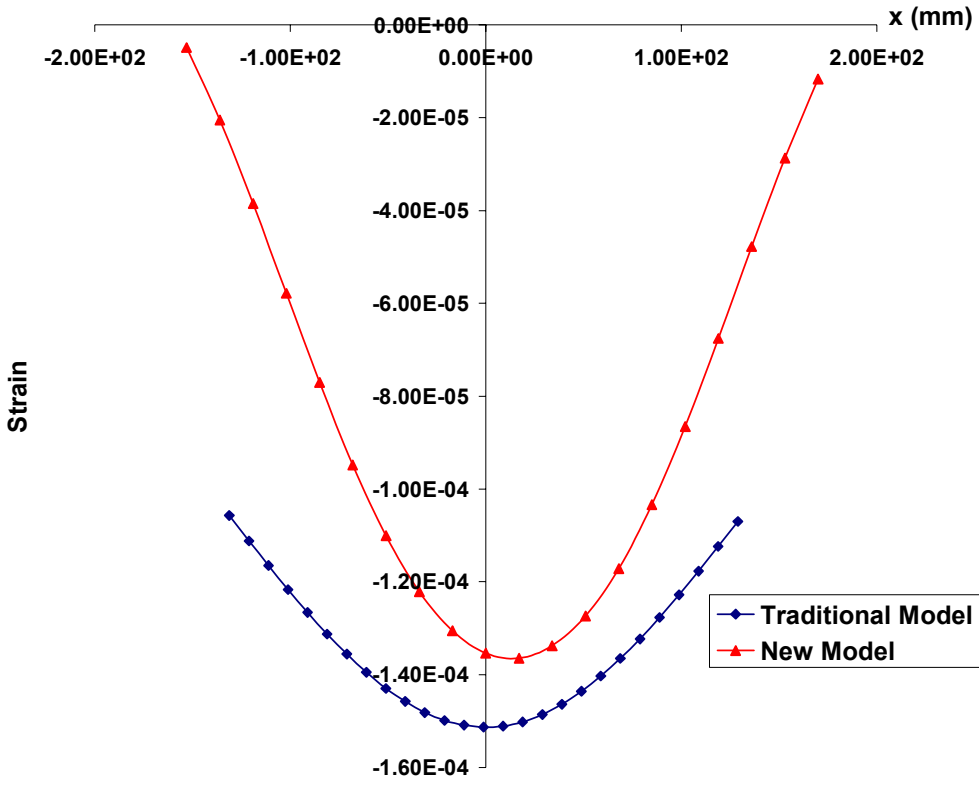


(c) ϵ_{czz}

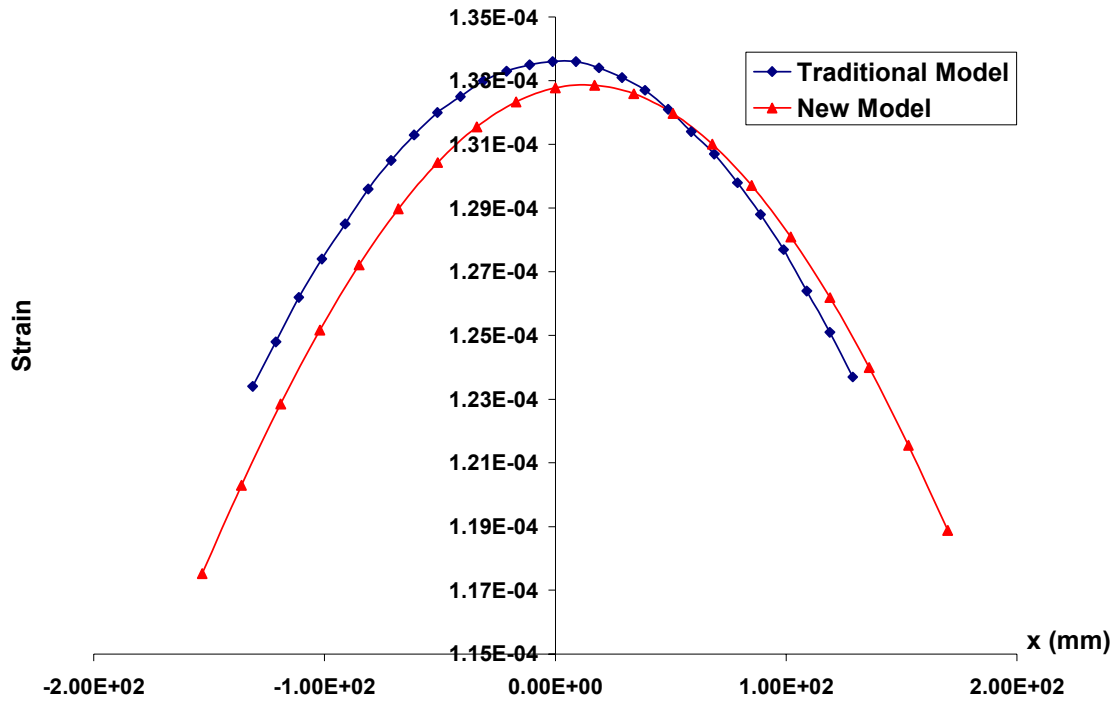
D. Pavement 4



(a) ϵ_{txx}



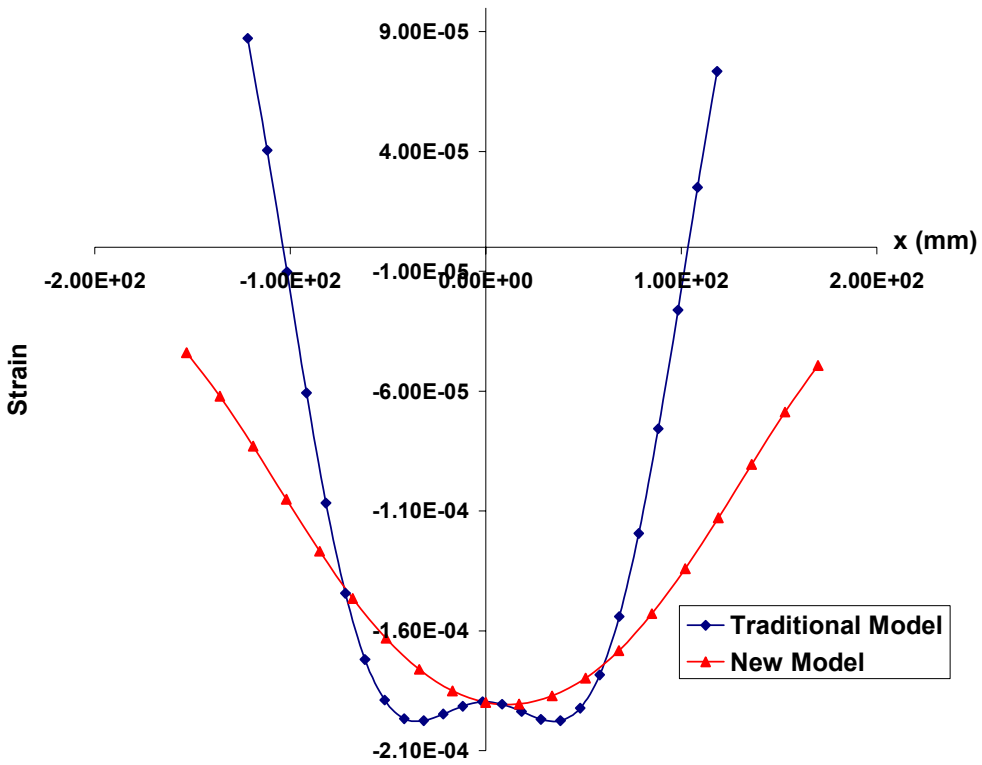
(b) ϵ_{yy}



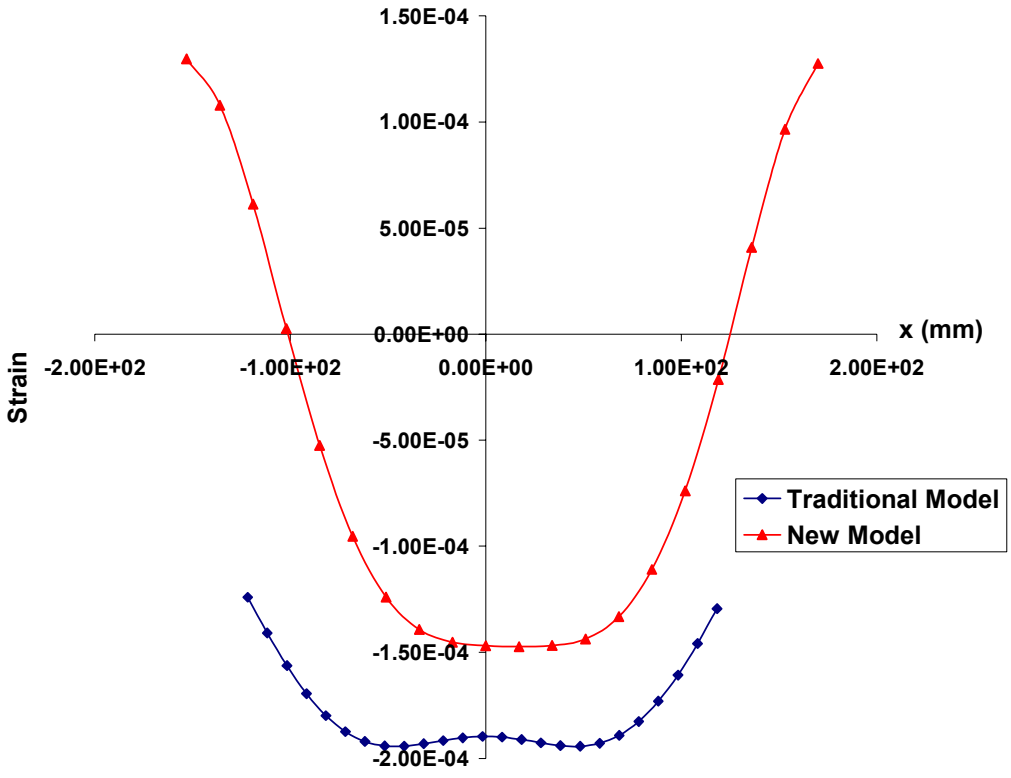
(c) ϵ_{czz}

Appendix 9: Strain Comparison in LTEX019 (L=31.1 kN, P=793 kPa)

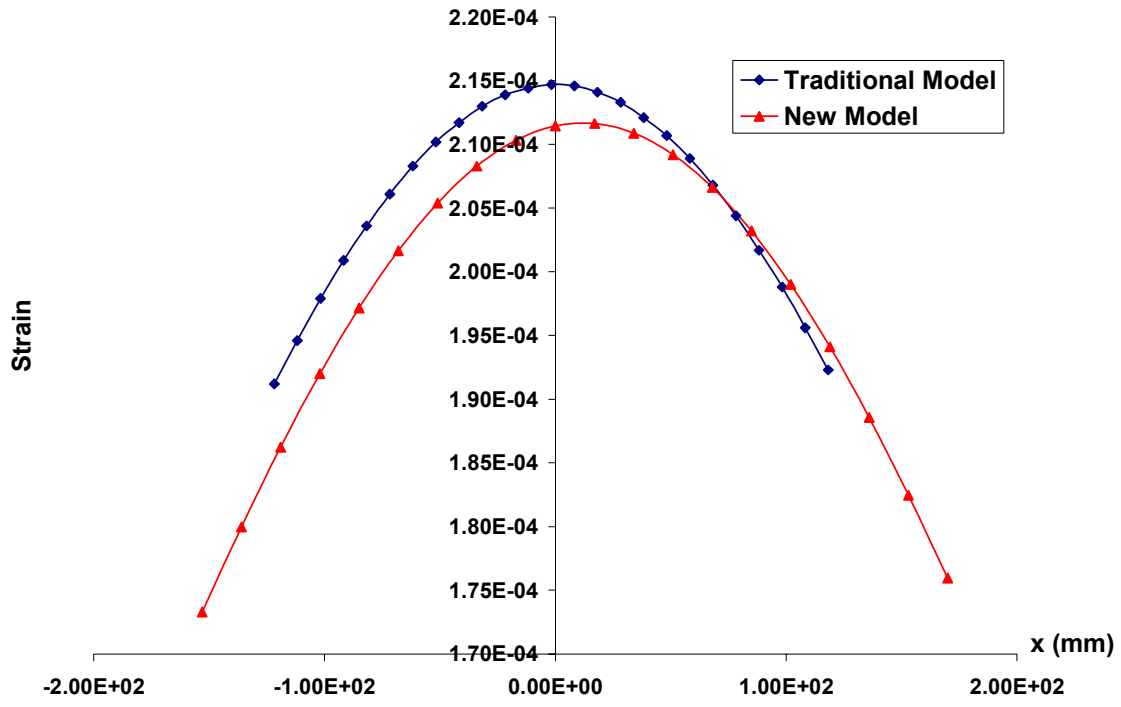
A. Pavement 1



(a) ϵ_{txx}

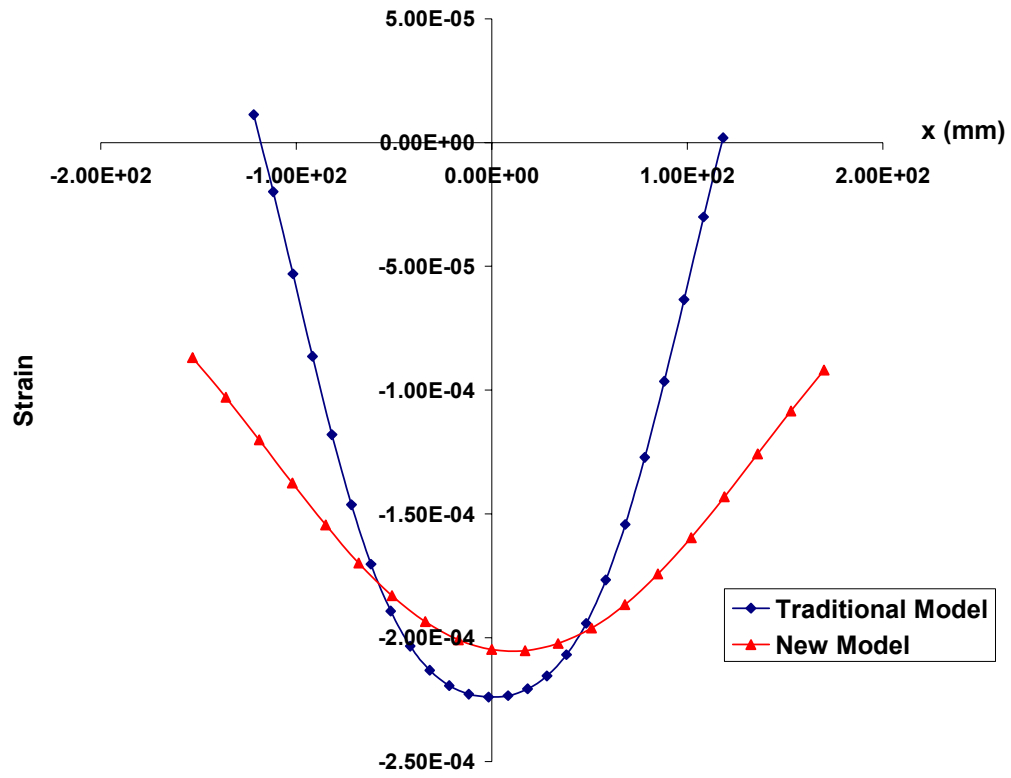


(b) ϵ_{yy}

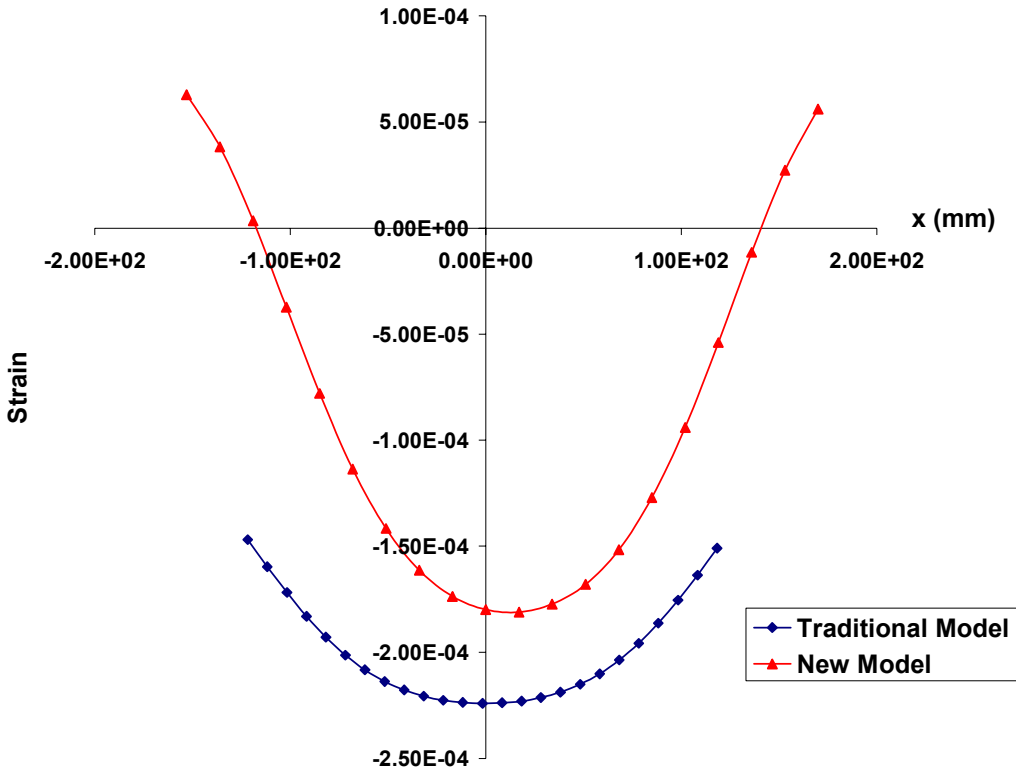


(c) ϵ_{czz}

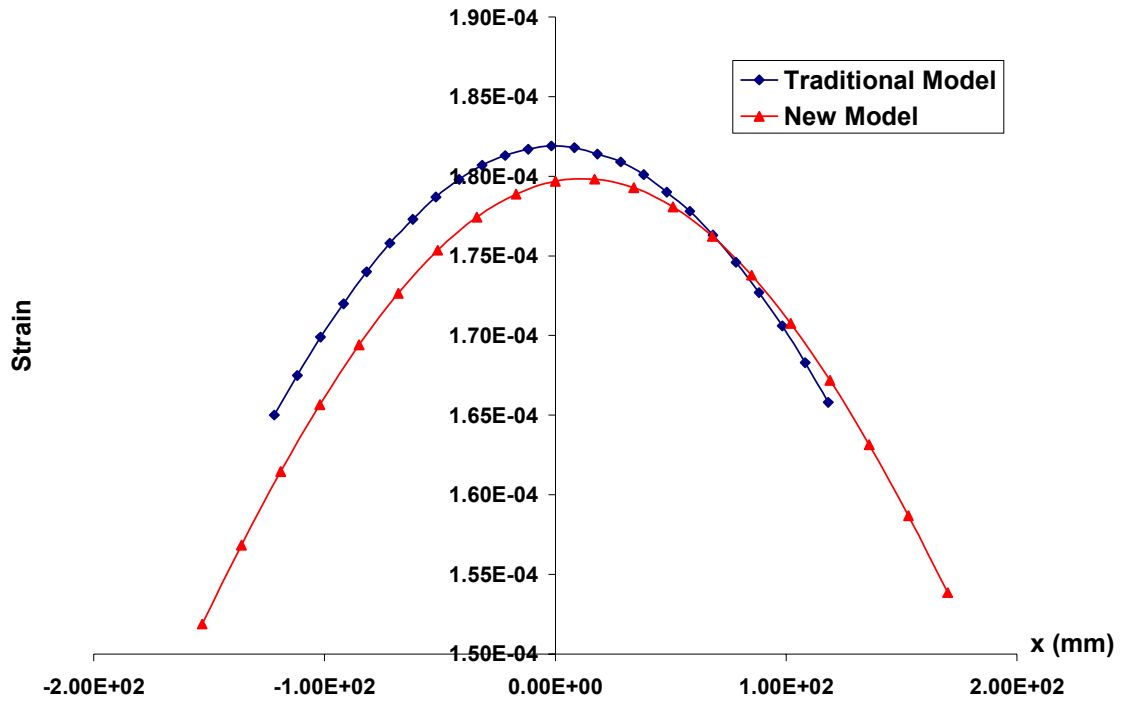
B. Pavement 2



(a) ϵ_{txx}

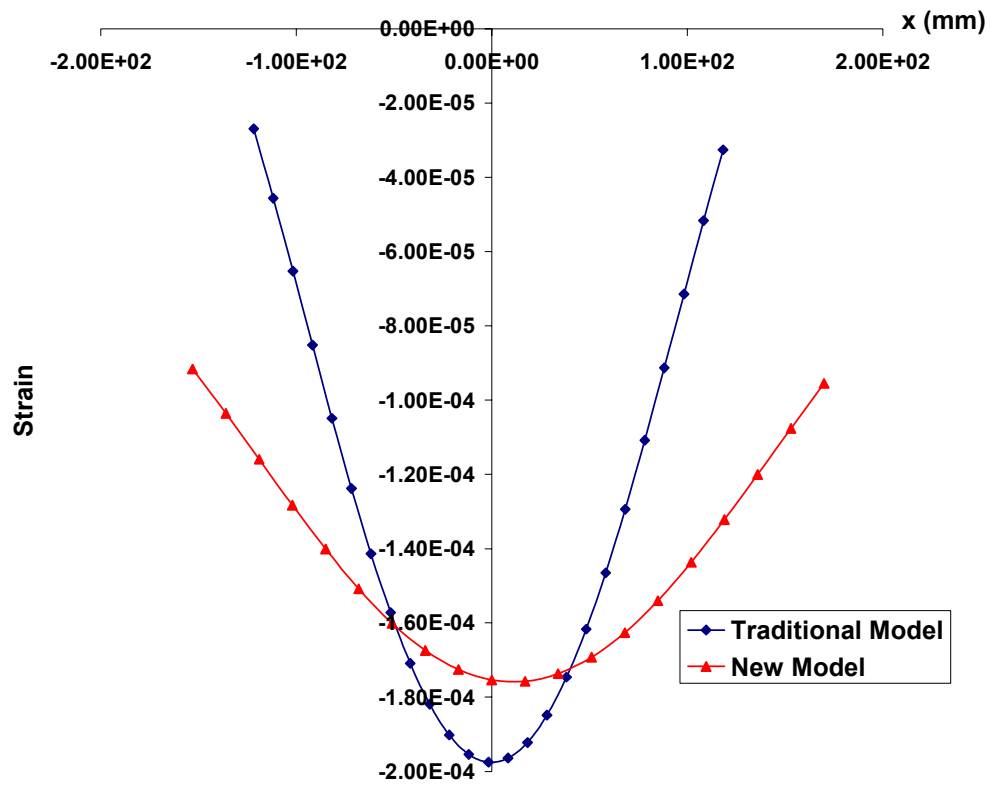


(b) ϵ_{yy}

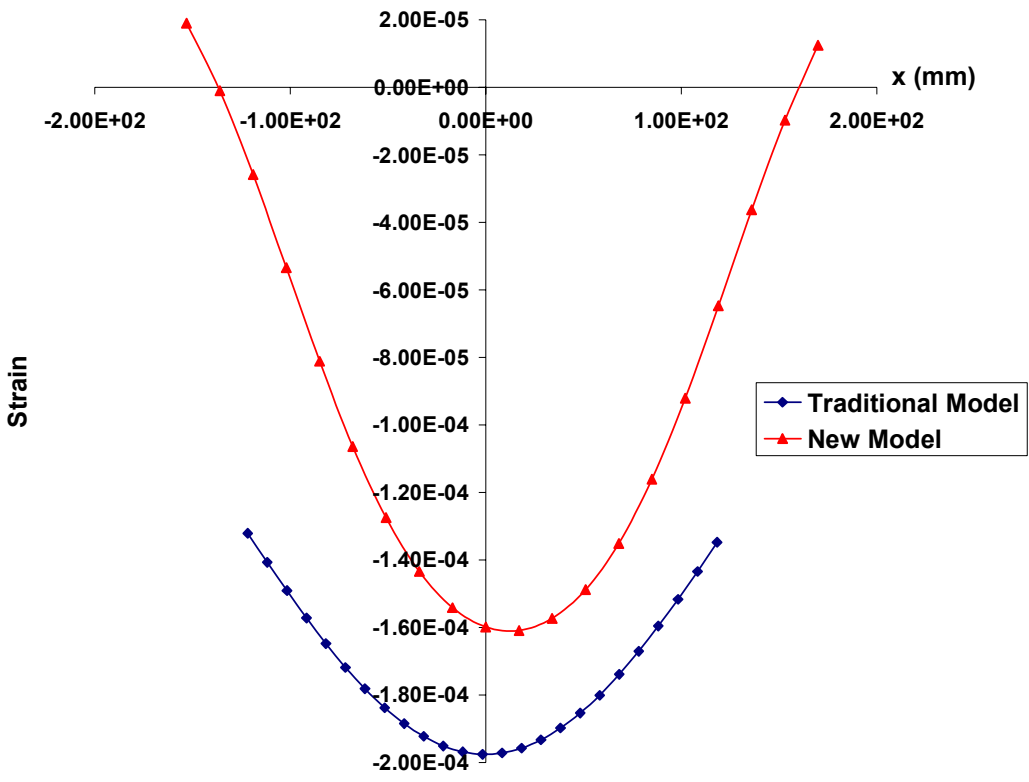


(c) ϵ_{czz}

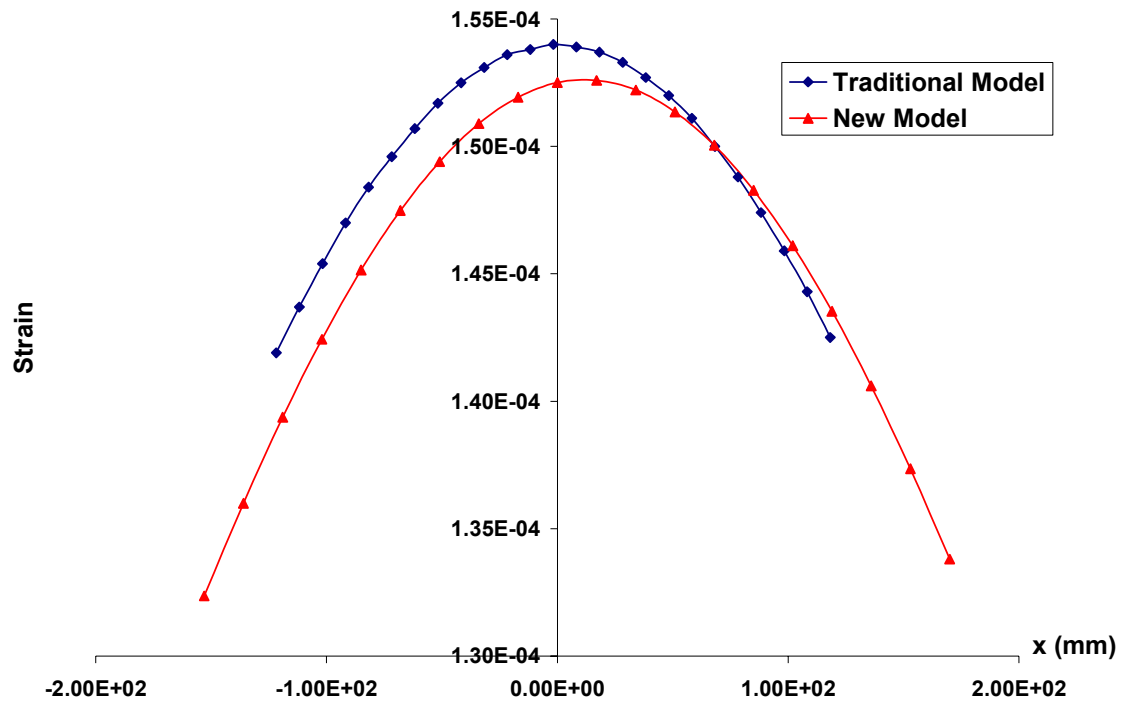
C. Pavement 3



(a) ϵ_{txx}

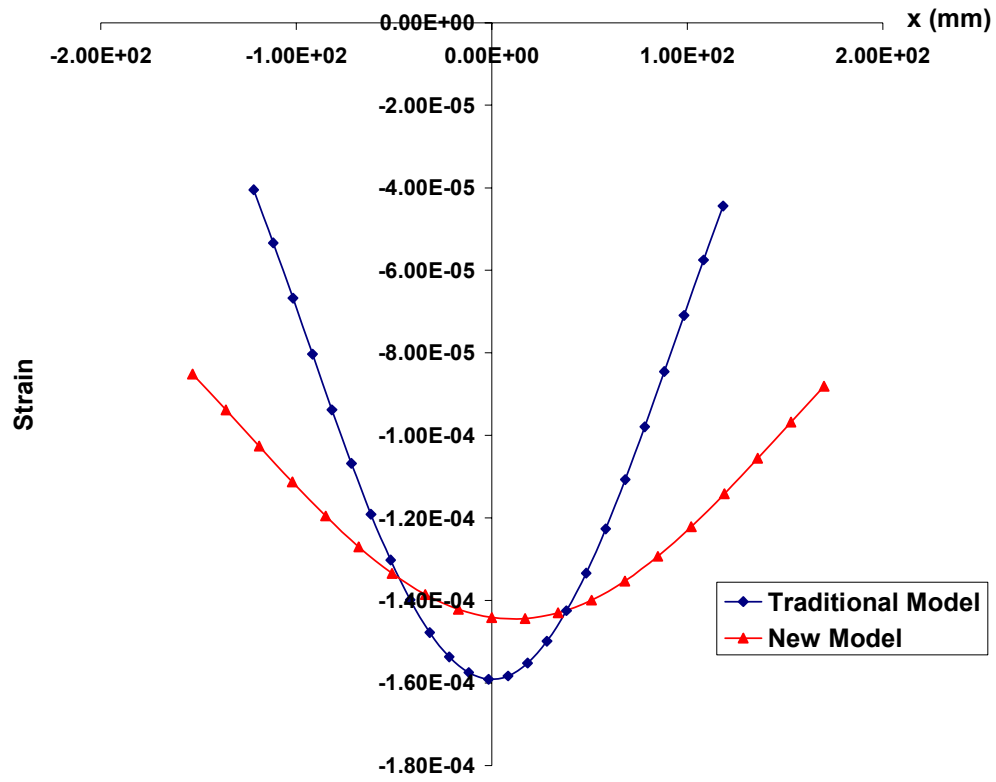


(b) ϵ_{yy}

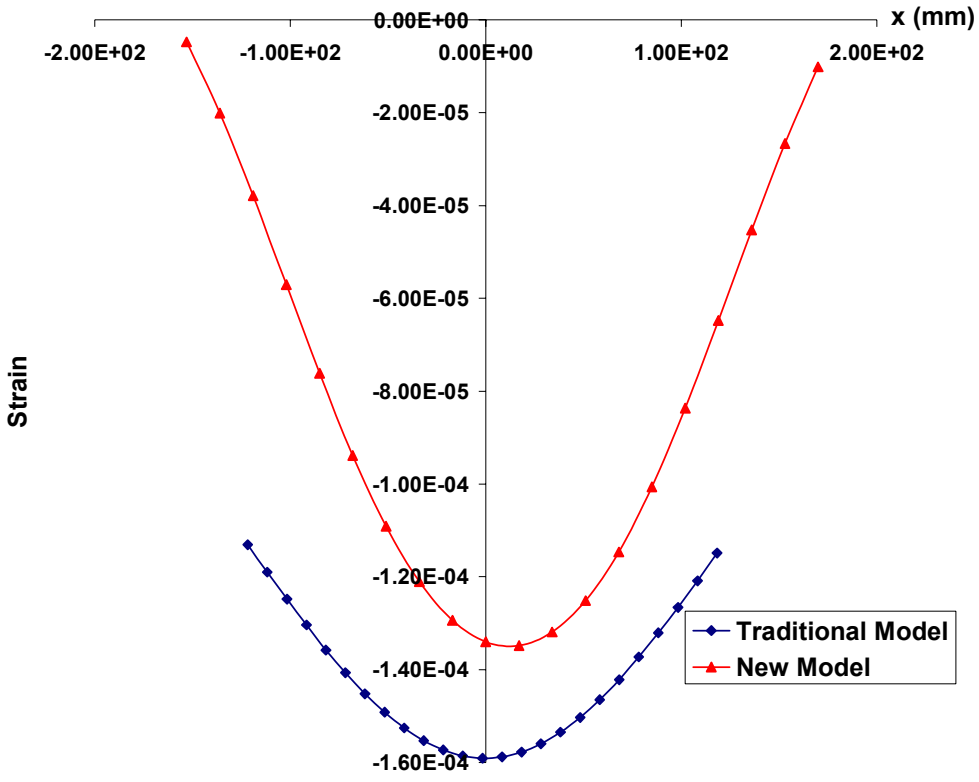


(c) ϵ_{czz}

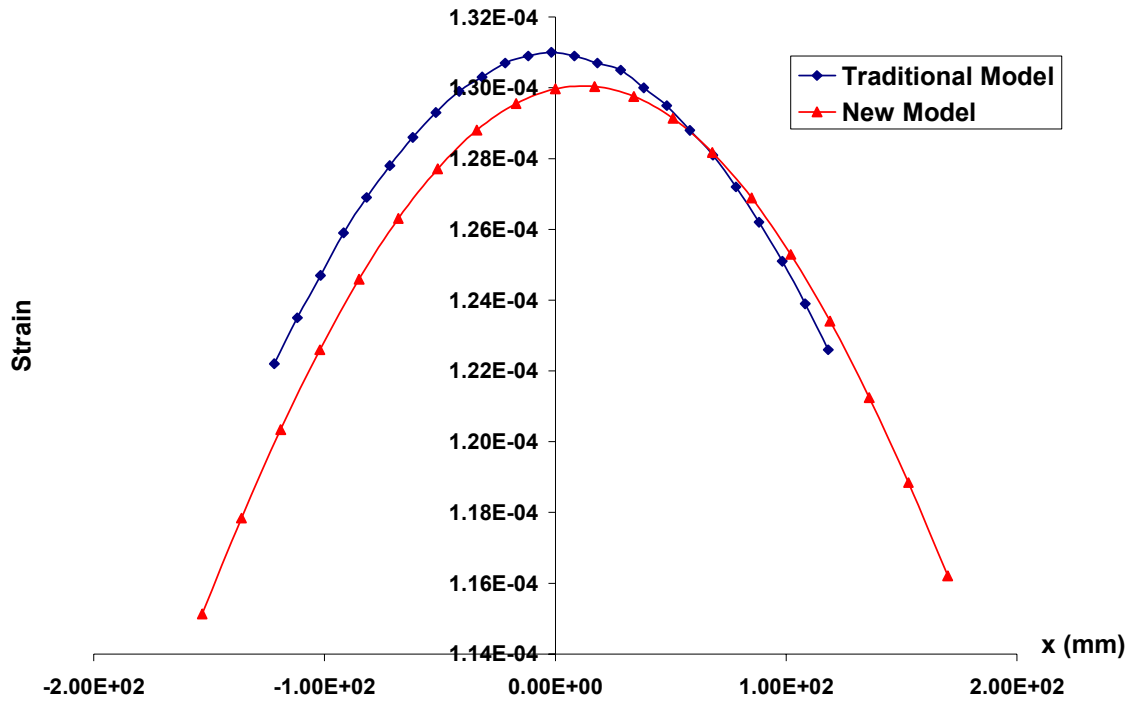
D. Pavement 4



(a) ϵ_{txx}



(b) ϵ_{yy}



(c) ϵ_{czz}